Some problems in strong interation dynamics

R. C. Johnson

THESIS

Submitted to the University of Durham

by

R. C. Johnson

for the Degree of Doctor of Philosophy

August 1968

PREFACE

The work described here was performed under the supervision of Dr. Peter Collins, to whom I am greatly indebted for his friendly help and patient guidance.

I have benefitted also from discussions with many people, in particular Dr. Philip Burke (who made available several useful computer programmes), Graham Ross, Professor Euan Squires and Dr. Peter Watson.

The help of Mrs. Q. M. Johnson in the preparation of this thesis is very gratefully acknowledged.

The work was supported by a Science Research Council Research Studentship.

C O N T E N T S.

C H A P T E R O N E

S-Matrix Theory

1. Introduction.

Our approach to the problem of strong interaction dynamics follows the S-matrix point of view, as emphasised in recent years by notably Chew and his collaborators[1]. That is, we attempt to understand the properties of hadrons as members of a "nuclear democracy" [2] in terms of assumption of analyticity, unitarity, crossing symmetry and Regge[3] asymptotic behaviour of strong interaction scattering amplitudes, without making any reference to an underlying field concept.

In this introductory Chapter, we outline our basic hypotheses, and develop some of the formalism necessary for their testing. This provides the foundation for the dynamical calculations presented in the following Chapters.

We begin with a brief summary of the general principles of dynamical S-matrix theory [4], (such as they are understood at present), and then go on to discuss their implications for two-particle to two-particle reactions.

The hypothesis that the scattering amplitude is analytic, unitary and crossing symmetric is embodied in an integral representation, which is unique up to possible arbitrary subtraction constants that express unknown high energy behaviour. An analytic continuation

hypothesis removes this uncertainty, and Regge poles appear as the subtraction terms, giving dynamical content to the theory[5].

A means of calculation is to write down an analytic, crossing symmetric amplitude whose high energy behaviour is governed by Regge poles, and to enforce unitarity upon it. We describe the N/D method[6] as a way of doing this.

2. General Principles.

Taking a typical hadronic mass to be 1 GeV, and assuming that Yukawa[2] forces operate, one expects strong interactions to be characterised by decay times $\sim 10^{-24}$ seconds and by interaction ranges $\sim 10^{-13}$ cms. These estimates are consistent with experiment[8]. Because of the very short range of the strong forces, it is possible to define asymptotic initial and final states containing only free stable hadrons on their mass shells. (Electromagnetic, weak and gravitational forces are neglected unless explicitly stated). These physical configurations are described by the usual quantum mechanical state vectors[9], labelled by the particle momenta and spin orientations - the experimental observables. We assume that the set of physical states obey the superposition principle[10], are orthonormalisable and are complete.

Then we define an operator in the space of physical states by

$$S = \sum_m |m,in\rangle\langle m,out| \quad , \tag{1.1}$$

where the summation runs over particle configurations. Taking matrix elements, it is immediately found that the assumptions of orthonormality and completeness imply that S is unitary,

$$SS^+ = S^+S = 1 \, . \tag{1.2}$$

The matrix elements of S satisfy

$$\langle b,in|S|a,in\rangle = \langle b,out|a,in\rangle = \langle b,out|S|a,out\rangle \, , \tag{1.3}$$

corresponding to the usual definition of S-matrix elements, namely

$$S_{ba} = \langle b,out|a,in\rangle \, . \tag{1.4}$$

Because momentum measurements are experimentally possible[11], the asymptotic states will be taken to be momentum eigenstates. We shall deal here with physical states containing only structureless bosons. The complications of spin[12] are in general not negligible[13], but for simplicity will be ignored since they do not affect our conclusions in this section. A single particle state will be written $|p\rangle$ where p_μ is its four-momentum[14]. The "in" and "out" labels are dropped, as permitted by equation (1.3).

We use single particle states with invariant normalisation, viz.,

$$\langle p'|p\rangle = (2\pi)^3 2p_0 \, \delta^{(3)}(p'-p) \, , \tag{1.5}$$

where the corresponding phase space volume element is

$$\frac{d^3p}{(2\pi)^3 2p_0} \qquad (1.6)$$

Multiparticle states are simply direct products of single particle ones, and their corresponding space volume element is the product of the single particle ones (divided by appropriate products of factorials to take account of any identical particles in the intermediate state in question[15].

Expression (1.6) may be replaced by

$$(2\pi)^{-3}\,\delta(p^2-m^2)\;\theta(p_0)\;d^4p \quad , \qquad (1.7)$$

using the elementary properties of the delta-function[16], so that manifest invariance under proper Lorentz transformations is displayed. The unitarity relation (1.2) may then be written in terms of general multiparticle S-matrix elements as

$$\sum_{n=1}^{\infty}(2\pi)^{-3n}\int\prod_{i=1}^{n}d^4q_i\;\delta(q_i^2-m_i^2)\;\theta(q_{ic})\,\langle p_1'\cdots p_m'|S|q_1\cdots q_n\rangle\;\times \qquad (1.8)$$

$$\times\,\langle q_1\cdots q_n|S^+|p_1\cdots p_m\rangle \;=\; \langle p_1'\cdots p_m'|\,p_1\cdots p_m\rangle \quad ,$$

(where identical particles are neglected for simplicity).

The relationship between the S-matrix defined above and a spatial description of a scattering process requires some care [17], and we shall not enter into details, except to say that the appearance of Planck's

constant in the Fourier transforms which take S from momentum space to configuration space provide the necessary statement that the theory deals with microscopic phenomena. The transformations of the physical observables from one inertial space-time frame to another are proper Lorentz transformations, under which the S-matrix elements are assumed to be invariant, as we have already implied.

Among the consequences of Lorentz invariance is the presence on the right hand side of equation (1.4) of delta-functions of energy-momentum conservation. Because strong interactions have a very short range, an S-matrix element consists of "connected parts"(18), each corresponding to one of the possible reactions which may occur between all, some, or none of the initial particles. Energy and momentum are conserved overall, and by each connected part.

For example, the (two-particle)→ (two-particle) S-matrix element breaks up as

$$S(p_3, p_4; p_1, p_2) = \langle p_3, p_4 | p_1, p_2 \rangle + i(2\pi)^4 \delta^{(4)}(p_1+p_2+p_3+p_4) \langle p_3, p_4 | A | p_1, p_2 \rangle , \tag{1.9}$$

corresponding to the particles proceeding unaffected or scattering. The factor $i(2\pi)^4$ is conventional, and we have chosen to label all the external four-momenta as

incoming. The A-matrix element is the "four-line connected part", that is, the scattering amplitude.

The assumptions introduced so far may be summarised thus:

(i) The superposition principle of quantum mechanics holds.

(ii) A unitary S-matrix exists.

(iii) The S-matrix is Lorentz invariant.

(iv) The S-matrix has a disconnected structure.

These postulates are relatively incontroversial, and are almost certain to be features of any successful theory of hadrons. Of more debatable standing are two postulates which give dynamical content to S-matrix theory, and which underly the work presented here.

They are (using Chew's nomenclature[1]), (a) Maximal analyticity of the first kind (hereafter abbreviated to MAFK). This is the postulate that the only singularities in the complex energy variables of the invariant amplitudes derived from the connected parts of the S-matrix are the poles corresponding to stable or unstable particles, and further singularities generated from these poles by unitarity and crossing. (b) Maximal analyticity of the second kind (MASK). This is the postulate that the S-matrix is continuable throughout the complex angular momentum plane, with only isolated singularities.

The first of these, MAFK, is a statement of what was loosely referred to in the Introduction as the assumption that hadron scattering amplitudes are analytic, unitary and crossing symmetric. The second, MASK, is a generalisation of the assumption that scattering amplitudes display Regge asymptotic behaviour.

It would be inappropriate to give here a lengthy discussion of the implications and theoretical justification for these two postulates for arbitrary scattering processes. Detailed reviews are given by Chew[1], by Eden[4] et. al., and by Collins & Squires[5], who give references to the original work. Instead, we shall consider only their implications for the four-line connected part, where their consequences are brought out most clearly, and where the work of later Chapters is concentrated.

3. The Four-line Connected Part.

The four-line connected part is both experimentally accessible - in simple cases - and theoretically tractable, because of its small number of degrees of freedom. Therefore its study has been, and will continue to be, one of the most fruitful testing-grounds of theories of strong interactions.

Most of the calculations described in the following Chapters will be concerned with the elastic scattering of equal-mass spinless particles, and therefore

the formulae developed here will be confined to this simple case, and later extended if necessary.

In the absence of spin, it is well-known[19] that Lorentz invariance and the mass shell condition confine the independent variables of an n-line connected part to a set of 3n-10 invariants formed from the n external four-moments. For the four-line connected part we define as usual the three invariants s, t and u to be, (see Fig. 1.1),

$$\begin{aligned} s &= (p_1 + p_2)^2 \\ t &= (p_1 + p_3)^2 \\ u &= (p_1 + p_4)^2. \end{aligned} \tag{1.10}$$

The equation relating these variables is

$$s + t + u = 4m^2, \tag{1.11}$$

where m is the external mass.

We write the amplitude corresponding to the connected part of Fig.1.1 as A(s,t,u), to emphasise its crossing symmetry, which has not been proved in S-matrix theory (as it has in quantum field theory)[20], but is a part of the postulate of MAFK.

Because of the CPT theorem[21], and crossing, the amplitude of Fig.1 describes the six processes

$$1 + 2 \longrightarrow \bar{3} + \bar{4}: \quad 3 + 4 \longrightarrow \bar{1} + \bar{2} \quad (1)$$

$$1 + 3 \longrightarrow \bar{2} + \bar{4}: \quad 2 + 4 \longrightarrow \bar{1} + \bar{3} \quad (2)$$

$$1 + 4 \longrightarrow \bar{3} + \bar{2}: \quad 3 + 2 \longrightarrow \bar{1} + \bar{4}, \quad (3)$$

but with (1), (2) and (3) as physically permitted in different regions of the s, t and u variables. For process (1) we find from (1.10) that

$$\begin{aligned} s &= (\text{centre of mass total energy})^2 \\ &= 4(m^2 + q_s^2), \end{aligned} \tag{1.12}$$

thus defining q_s, the centre of mass three-momentum. Also we find

$$\begin{aligned} t &= -(\text{centre of mass momentum transfer})^2 \\ &= 2q_s^2(1 - z_s), \end{aligned} \tag{1.13}$$

where $z = \cos\theta_s$ and θ_s is the centre of mass scattering angle. Thus u is given from (1.11), (1.12) and (1.13) as

$$u = -2q_s(1 + z_s). \tag{1.14}$$

Processes (1) are referred to as s-channel processes, and are respectively physically allowable if $\pm q_s > 0$ while $-1 \leq z_s \leq 1$.

Similarly, it follows from (1.10) that for (2) and (3) the energy and momentum transfer variables are (t,s) and (u,t) respectively, and correspondingly (q_t, z_t) and (q_u, z_u) are defined. These are called the t- and u- channel processes, and are physical for $(\pm q_t > 0,\ -1 \leq z_t \leq 1)$ and

$$(\pm q_u > 0,\ -1 \leq z_u \leq 1)$$

respectively. The three physical regions are shown on the symmetrical Mandelstam diagram[22], Fig.1.2.

MAFK asserts that a connected part has only those singularities in the (complex) energy variables which are forced upon it by unitarity in the channels it links by crossing. For a general process, the nature and location of these singularities can be found by using Landau's rules[23] and Cutkosky's rules[24]. For the four-line connected part, it is intuitively reasonable that singularities must occur in the energy variables as a new process becomes allowed by energy and other conservation laws - i.e., at the threshhold of each "communicating channel"[1] - where the amplitude suddenly acquires new degrees of freedom. Also it is natural to carry over from (e.g.) field theory the correspondence between poles and particles, and to suppose that multiparticle threshold singularities should be branch points because a continuum of final-state configurations are possible.

These conjectures are born out by detailed analysis, (reviewed in ref. 4), and we take without further comment the particle-pole correspondence. The appearance of threshold branch points comes directly from unitarity as follows. Writing for the S-matrix $S_{if} = 1 + i T_{if}$ (corresponding to (1.9)), we find from (1.2) that

$$T_{if} - T_{if}^{+} = 2i \sum_{n}' T_{in}^{+} T_{nf} \qquad (1.15)$$

(T^{+} is the Hermitian conjugate of T). Since T

conserves four-momentum, the right hand side is non-zero above the lowest threshold and changes discontinuously at each higher one, corresponding to the presence of more allowed intermediate states in the matrix product.

Equation (1.15) expresses the discontinuity across the unitarity cut, drawn from threshold to $+\infty$, but it is very difficult to handle except in the elastic or quasi-elastic region where only two-body intermediate states are retained. In this case, taking matrix elements of (1.2) and using (1.9) and (1.8), we find after a little algebra[25], that the discontinuity associated with the (quasi-)elastic channel n in the transition $a \to b$ can be written

$$A^{ab}(s_+,t) - A^{ab}(s_-,t) = \frac{i q_{sn}}{16\pi^2\sqrt{s}} \int A^{bn}(s_+,t') A^{na}(s_-,t'')\, d\Omega_n(t',t''), \qquad (1.16)$$

q_{sn} being the momentum in state n. We shall discuss this equation in more detail below; here we merely remark that it may be shown that for physical s-channel processes, ($t < 0$), the integral of (1.16) contains no singularities which change the square root nature of the threshold branch point, implied by the factor q_{sn}, so that all two-body normal thresholds are two-sheeted[26].

MAFK further asserts that A(s,t,u) has a "physical sheet" on which the analytic continuation necessary to achieve crossing can be carried out. On this sheet there are no complex singularities, and

the physical amplitude is reached by continuation to the appropriate energy value from just above the threshold branch cuts (according to the $+i\varepsilon$ prescription[4]). All the physical sheet singularities of A(s,t,u) therefore appear on the diagram of Fig.1.2, and equation (1.16) relates the amplitude evaluated above (s_+) and below (s_-) the two-body cut.

At fixed s, the t-plane physical sheet has a series of right-hand branch points at the t-channel physical thresholds, a series of left-hand branch points from the u-channel thresholds, and possibly some bound state poles. (Resonance poles are excluded from the physical sheet by unitarity, (equation (1.15)); they must be near the physical region, therefore they lie on the first unphysical sheet just below the real axis. Such a position corresponds to a wave function written as $\psi \propto \exp(-iE_R t)$, where the resonant energy E_R has a negative imaginary part and the $+i\varepsilon$ prescription dictates the choice of phase if the state is to decay).

If A(s,t,u) is expressed as a Cauchy integral in the t-plane, MAFK defines the positions of all the singularities of which the path of integration must take account. If this contour is specified to run along the upper and lower lips of both cuts, closing with semicircles at infinity, and if A goes to zero as $|t|$

goes to infinity, then the distant circle does not contribute and a dispersion relation[27] follows in the usual way,

$$A(s,t,u) = \sum \text{poles} + \frac{1}{\pi}\int \frac{D_u(s,t,u')}{u'-u}\,du' + \frac{1}{\pi}\int \frac{D_t(s,t',u)}{t'-t}\,dt' , \tag{1.17}$$

In this expression

$$D_t \equiv \frac{1}{2i}\left[A(s,t_+,u) - A(s,t_-,u)\right] ; \tag{1.18}$$

D_u is defined analogously.

Returning to (1.15), we have

$$T_{if} - T_{fi}^* = 2i \sum_n T_{ni}^* T_{nf} , \tag{1.19}$$

and with time reversal invariance this becomes

$$\mathrm{Im}\, T_{if} = \sum_n T_{ni}^* T_{nf} . \tag{1.20}$$

That is, for real s and u,

$$D_t(s,t,u) = \mathrm{Im}\, A(s,t_+,u) , \tag{1.21}$$

because (1.20) continued below the first physical threshold, implies that A(s,t,u) is real analytic in t. Similar results hold in the other two channels[28].

From (1.20) we can deduce the optical theorem,

$$\mathrm{Im}\, T_{ii} = \sum_n |T_{in}|^2 \propto \sigma_{TOT} , \tag{1.22}$$

which makes dispersion relations like (1.17) accessible to experimental verification. At present, the dispersion relations are found to be in complete agreement with experiment[29], and this constitutes an important check of our analyticity assumptions, at

least to the extent that complex singularities on the physical sheet, if present, are weak.

In practice it is found[30] that for all processes

$$\sigma_{TOT} \sim \frac{1}{t} Im\, A(s=0, t_+) \longrightarrow \text{constant}$$

as t becomes large, so that apparently (1.17) has to be written for a modified function $(t-t_1)^{-1}(t-t_2)^{-1}A(s,t,u)$, and hence arbitrary constants appear in the "twice subtracted" dispersion relation. (Fortunately, in cases of interest, these can be eliminated or fixed by experiment[31]). In general, so long as

$$A \xrightarrow[|t| \to \infty]{} \text{constant} \times t^{N-\varepsilon}, \quad (\varepsilon > 0), \tag{1.23}$$

an N-times subtracted version of (1.17) holds.

We shall assume that the amplitude is indeed bounded by a finite power of t, and in fact take N = 0, deferring further discussion for the moment.

The discontinuities D_s, D_t and D_u are defined by equations like (1.18), and in the elastic region explicit expressions for them are of the form (1.16). The right hand side of the latter equation certainly has t and u singularities, and in fact MAFK requires D_s to have only branch points at real values of these invariants. Because of this, we can write simple dispersion relations for the D's. Defining

$$\rho_{st}(s,t) = \frac{1}{2i}\left[D_t(s_+) - D_t(s_-)\right] \tag{1.24}$$

and

$$\rho_{ut}(s,t) = \frac{1}{2i}\left[D_t(u_+) - D_t(u_-)\right] , \tag{1.25}$$

we can write

$$D_t(s,t,u) = \frac{1}{\pi}\int \frac{\rho_{st}(s',t)}{s'-s}\,ds' + \frac{1}{\pi}\int \frac{\rho_{ut}(u',t)}{u'-u}\,du' . \tag{1.26}$$

In an exactly analogous way we can define $\rho_{su}(s,u)$ and $\rho_{tu}(t,u)$, and obtain

$$D_u(s,t,u) = \frac{1}{\pi}\int \frac{\rho_{su}(s',u)}{s'-s}\,ds' + \frac{1}{\pi}\int \frac{\rho_{tu}(t',u)}{t'-t}\,dt' . \tag{1.27}$$

The integrations in (1.26) and (1.27) extend over the regions where the "double spectral functions", ρ , are non-zero. The boundaries of the various double spectral functions will be determined when we discuss the implications of eq.(1.16), and the calculation of the elastic pieces of double spectral function.

Substituting (1.26) and (1.27) into (1.17), we obtain

$$A(s,t,u) = \frac{1}{\pi^2}\iint \frac{\rho_{su}(s',u'')}{(s'-s)(u''-u)}\,ds'du'' + \frac{1}{\pi^2}\iint \frac{\rho_{tu}(t',u'')}{(t'-t'')(u''-u)}\,dt'du''$$

$$+ \frac{1}{\pi^2}\iint \frac{\rho_{st}(s',t'')}{(s'-s)(t''-t)}\,ds'dt'' + \frac{1}{\pi^2}\iint \frac{\rho_{ut}(u',t'')}{(u'-u'')(t''-t)}\,du'dt'' , \tag{1.28}$$

neglecting bound state poles for simplicity.

Here we have remembered that (1.17) is written at fixed s, and that the relation

$$s + t' + u' = s + t'' + u'' = 4m^2 \tag{1.29}$$

holds. Interchanging the primes on the second and fourth terms of (1.28), and using crossing symmetry we get

$$\frac{1}{\pi^2}\iint \rho_{tu}(t',u'')\left\{\frac{1}{(t'-t')(u''-u)} + \frac{1}{(u''-u')(t'-t)}\right\} dt'\,du''$$

which simplifies, using (1.29), to

$$\frac{1}{\pi^2}\iint \rho_{tu}(t',u'')\,\frac{dt'\,du''}{(t'-t)(u''-u)} .$$

Therefore we obtain the Mandelstam representation[22,32] for the scattering amplitude,

$$\begin{aligned} A(s,t,u) &= \frac{1}{\pi^2}\iint \frac{\rho_{st}(s',t'')}{(s'-s)(t''-t)}\,ds'\,dt'' \\ &+ \frac{1}{\pi^2}\iint \frac{\rho_{tu}(t',u'')}{(t'-t)(u''-u)}\,dt'\,du'' \\ &+ \frac{1}{\pi^2}\iint \frac{\rho_{us}(u',s'')}{(u'-u)(s''-s)}\,du'\,ds'' , \end{aligned} \tag{1.30}$$

as a consequence of the postulate of MAFK for the four line connected part. We have assumed the absence of

subtractions - N=0 in eq.(1.23) - and poles have been excluded for simplicity. However, both will appear in general. The existence of a Mandelstam representation for the four-line connected part has been established for a class of potential problems[33], but, although some progress has been made[4], a comprehensive proof is lacking[34] in particle physics.

The number of subtractions necessary to make the integrals in (1.30) converge limits the dynamical content given to this theory by MAFK. Froissart[35] has used unitarity to show that if equations like (1.30) exist, then only two subtractions are needed. (Further, Martin[36] has used crossing to show that (under specific circumstances) even these are fixed.) Our second dynamical postulate, MASK, which will be discussed in the next Section, has the effect of removing arbitrariness in a particularly satisfactory way. Before turning to this, however, we discuss the calculation of the double spectral functions in the region where (1.16) is applicable, by explicitly taking the t-discontinuity of the $D_s(s,t)$ so defined.

Re-writing (1.16) for elastic intermediate states, we have,

$$D_s(s,t) = \frac{q_s}{32\pi^2\sqrt{s}} \int A(s_+,t')\, A(s_-,t'')\, d\mu(t',t''), \qquad (1.31)$$

where $t'=t'(z',s)$, $z'=\cos\theta_{nf}$, corresponding to the centre of mass angle between the intermediate and final particles, and $t''=t''(z'',s)$, $z''=\cos\theta_{in}$. These angles are related to that corresponding to $t=t(z_s,s)$, $z_s=\cos\theta_{if}$, by, (see Fig.1.3),

$$z'' = z_s z' + \sqrt{(1-z_s^2)(1-z'^2)}\,.\cos\phi\,. \tag{1.32}$$

Also

$$d\Omega = dz'\,d\phi\,. \tag{1.33}$$

If we now substitute fixed-s dispersion relations, (1.17), for the two amplitudes on the right-hand side of (1.31), and change their variables of integration from t, u, and t_2, u_2 respectively to the corresponding scattering angle cosines z_1 and z_2, we obtain

$$D_s(s,t) = \frac{q_s}{32\pi^4\sqrt{s}}\int_{-1}^{1} dz' \int_0^{2\pi} d\phi \left[\int \frac{D_t(s_1,t_1)\,dz_1(t_1)}{z_1(t_1)-z''} \right. \tag{1.34}$$

$$\left. + \int \frac{D_u(s_1,u_1)\,dz_1(u_1)}{z_1(u_1)-z''} \right] \quad \times$$

$$\times \left[\int \frac{D_t(s_2,t_2)\,dz_2(t_2)}{z_2(t_2)-z'} + \int \frac{D_u(s_2,u_2)\,dz_2(u_2)}{z_2(u_2)-z'} \right] .$$

Interchanging orders of integration, we obtain the angular integration

$$\int_{-1}^{1} dz' \int_{0}^{2\pi} \frac{d\phi}{(z_1 - z'')(z_2 - z')} .$$

Substituting for $z''(z_s, z', \phi)$ from (1.32), and doing the ϕ integration first, a straightforward calculation gives

$$\frac{2\pi}{k^{1/2}} \ln \left\{ \frac{z_s - z_1 z_2 + k^{1/2}}{z_s - z_1 z_2 - k^{1/2}} \right\} ,$$

where

$$k(z_1, z_2, z_s) = z_s^2 + z_1^2 + z_2^2 - z_s z_1 z_2 - 1,$$

and the branch of the logarithm which is real must be taken for $-1 < z_s < 1$.

Converting back to the t variables, and remembering that we are dealing with elastic scattering, we find

$$D_s(s,t) = (32\pi^3 q_s \sqrt{s})^{-1} \int dt_1 \int dt_2 \left[D_t(s_+, t_1) + D_u(s_+, t_1) \right] \times$$

$$\times \left[D_t(s_-, t_2) + D_u(s_-, t_2) \right] K^{-1/2}(s, t, t_1, t_2) \times \qquad (1.35)$$

$$\times \ln \left\{ \frac{t - t_1 - t_2 - \frac{t_1 t_2}{2q_s^2} + K^{1/2}}{t - t_1 - t_2 - \frac{t_1 t_2}{2q_s^2} - K^{1/2}} \right\} ,$$

where

$$K(s, t, t_1, t_2) = t^2 + t_1^2 + t_2^2 - 2(t t_1 + t_1 t_2 + t_2 t) - \frac{t t_1 t_2}{q_s^2} . \qquad (1.36)$$

The double spectral functions $\rho_{st}(s,t)$ and $\rho_{su}(s,u)$ are the t-discontinuities of (1.35). To simplify matters we shall neglect the u-channel discontinuities for the present and consider

$$D_s(s,t) = \frac{1}{\pi}\int_{b(s)}^{\infty} \frac{\rho_{st}(s,t')}{t'-t}\,dt'$$

$$= (32\pi^3 q_s\sqrt{s})^{-1}\int_{t_0}^{\infty} dt_1 \int_{t_0}^{\infty} dt_2 \frac{D_t(s_t,t_1)\,D_t(s,t_2)}{K^{1/2}(t,t_1,t_2,s)}\,\ln\{\cdots\}\,. \qquad (1.37)$$

Here we explicitly show t_0, the t-channel threshold, and b(s), the boundary of the double spectral function.

The t-discontinuity of the right-hand side of (1.37) arises when K=0. The smallest values of t_1 and t_2 in the integration are $t_1=t_2=t_0$, when

$$K(s,t,t_0,t_0)=t(t-4t_0-t_0^2/q_s^2).$$

The point t=o corresponds to $z_s=1$ which is not a singularity of the product $K^{-1/2}(s,t,t_1,t_2)\ln\{\cdots\}$, therefore we deduce

$$b(s)\equiv t=4t_0(1+t_0/4q_s^2). \qquad (1.38)$$

For a given q_s^2, higher values of t_1 and t_2 cause K to vanish for a higher t-value. Therefore we have for the elastic double spectral function the expression

$$\rho_{st}(s,t) = (16\pi^2 q_s\sqrt{s})^{-1}\int_{t_0}^{K=0} dt_1 \int_{t_0} dt_2 \frac{D_t(s_t,t_1)\,D_t(s_t,t_2)}{K^{1/2}(s,t,t_1,t_2)}\,. \qquad (1.39)$$

If we had kept the u-channel terms, we would have found the product $D_t D_t^*$ to be replaced by $D_t D_t^* + D_u D_u^*$, and have derived an expression for ρ_{su} containing the products $D_t D_u^* + D_t^* D_u$.

The three regions of non-zero double spectral function are marked on Fig.1.2, for the exactly symmetric case of the scattering of scalar bosons. (Because the elastic threshold is the lowest, the boundary of the elastic double spectral function is the boundary of it all).

The fact that eq.(1.39) contains only finite integrations will be found important for developing an approximation scheme for the calculation of strong interaction scattering amplitudes, as we shall discuss in Chapter Two.

4. Partial Wave Amplitudes and Regge Poles.

In the previous Section we discussed some implications of the postulate of MAFK for the four-line connected part, and wrote down the resulting Mandelstam representation, eq.(1.30). In this Section we shall discuss continuation in angular momentum and show how the postulate of MASK removes the necessity for arbitrary subtractions in eq.(1.30), and so gives dynamical content to the theory. In particular, the Regge pole concept will lead to the formulation of a bootstrap hypothesis[2].

The amplitude A(s,t,u) can be expanded on any basis of orthogonal function, but a convenient choice is the set of angular momentum eigenfunctions in one of the channels, because the conservation law leads to considerable simplifications. (For example, a resonance has definite angular momentum, and therefore a corresponding pole will occur in just one angular momentum partial wave). An s-channel partial wave amplitude is defined by the projection.

$$A_\ell(s) = (32\pi)^{-1} \int_{-1}^{1} A(s,t(s,z_s))\, P_\ell(z_s)\, dz_s \qquad (1.40)$$

for $\ell = 0, 1, 2 \ldots$, where $P_\ell(z_s)$ is a Legendre polynomial of the first kind(37). The corresponding partial wave series is

$$A(s,t,u) = 16\pi \sum_{\ell=0}^{\infty} (2\ell+1)\, A_\ell(s)\, P_\ell(z_s)\,. \qquad (1.41)$$

(The factor (16π) is needed to simplify the unitarity expression for the $A_\ell(s)$). Because $P_\ell(z_s)$ is an entire function of z_s(37), it can have no singularities in t or u. Therefore we note that the series (1.41) cannot represent the amplitude over the whole s-t-u plane,(Fig.1.2), but must diverge at the nearest t or u singularity(22).

We shall see later that a unique continuation in ℓ is not possible for the $A_\ell(s)$ defined by eq.(1.40); instead we have to deal with "amplitudes of definite signature". Re-writing eq.(1.17) (neglecting poles) as

$$A(s,t,u) = A_R(s,t) + A_L(s,t), \qquad (1.42)$$

we define amplitudes of definite signature by

$$A^{\pm}(s,t) = A_R(s,t(z_s,s)) \pm A_L(s,t(-z_s,s)), \tag{1.43}$$

each of which has only right-hand singularities in t.

In fact we can write

$$A^{\pm}(s,t) = \frac{1}{\pi}\int_{t_0}^{\infty} \frac{D_t^{\pm}(s,t')}{t'-t}\,dt' , \tag{1.44}$$

and so the analogue of (1.30) is found to be

$$A^{\pm}(s,t) = \frac{1}{\pi^2}\iint \frac{\rho_{st}(s',t'') \pm \rho_{su}(s',t'')}{(s'-s)(t''-t)}\,ds'dt'' \tag{1.45}$$

$$+ \frac{1}{\pi^2}\iint \frac{\rho_{tu}(t'',u') \pm \rho_{tu}(u',t'')}{(u'-u)(t''-t)}\,du'dt'' ,$$

where we note the lack of symmetry in s,t and u. (The derivation of eq.(1.45) is given in the Appendix).

The partial wave expansion of this amplitude is

$$A^{\pm}(s,t) = 16\pi\sum_{l=0}^{\infty}(2l+1)A_l^{\pm}(s)P_l(z_s(s,t)) , \tag{1.46}$$

and the projection is

$$A_l^{\pm}(s) = (32\pi)^{-1}\int_{-1}^{1} A^{\pm}(s,t)P_l(z_s(s,t))\,dz_s . \tag{1.47}$$

The formula of Neumann[37]

$$Q_l(z) = \frac{1}{2}\int_{-1}^{1}\frac{dz'}{z-z'}P_l(z') , \quad l=0,1,2\ldots \tag{1.48}$$

allows us to insert (1.44) into (1.47), and, if the former integral converges, reverse the order of integration to obtain

$$A_\ell^{\pm}(s) = (16\pi^2)^{-1} \int_{z_s(s,t_0)}^{\infty} \mathcal{D}_t^{\pm}(s,t(z_s))\, Q_\ell(z_s)\, dz_s \,. \tag{1.49}$$

The situation when (1.44) requires subtractions will be dealt with below, and will lead directly to the postulate of MASK. Eq.(1.49) is called the Froissart-Gribov formula[38]. Because of (1.48), expressions (1.47) and (1.49) can be written in the combined form

$$A_\ell^{\pm}(s) = (32\pi^2 i)^{-1} \int_{C_1 \text{ or } C_2} Q_\ell(z_s)\, A^{\pm}(s,t(z_s))\, dz_s \tag{1.50}$$

for $\ell = 0,1,2\ldots$, where the contours C_1 and C_2 are defined in Fig.1.4a.

We note that (1.43) implies that $A^+(s,t)(A^-(s,t))$ contains the even (odd) part in z_s of the amplitude, although in general not even (odd) itself. Because $P_\ell(-z) = (-1)^\ell P_\ell(z)$ for $\ell = 0,1,2\ldots$, we deduce

$$A^+_\ell(s) = A_\ell(s) \text{ for even } \ell,$$
$$A^-_\ell(s) = A_\ell(s) \text{ for odd } \ell,$$

These are the "physical signature" partial waves.

The singularities of partial wave amplitudes derived from the Mandelstam representation are as follows[5]. In the s-plane, $A_\ell^{\pm}(s)$ has the same right-hand singularities as $A^{\pm}(s,t)$, and a series of

left-hand singularities generated by branch points in t of $A^{\pm}(s,t)$ "pinching"[4] with the singularities at $z=\pm 1$ of $Q_\ell(z)$. If MAFK holds, these lie on the real axis. We note that because $z_s=1+t/2q_s^2$, (for equal mass kinematics), using [37]

$$Q_\ell(z) \xrightarrow[z\to\infty]{} \text{const.}\ z^{-\ell-1} \tag{1.52}$$

gives, from (1.49)

$$A_\ell(s) \xrightarrow[q_s^2\to 0]{} \text{const.}\ q_s^{2\ell}\ , \tag{1.53}$$

if the Froissart-Gribov projection converges. It is usually conjectured[1] that this will hold in general, as it does in non-relativistic scattering from well-behaved potentials [1,41]. Therefore, when $A_\ell^{\pm}(s)$ is defined for non-integer ℓ, the extra kinematical branch point (1.53) must be taken into account.

The dispersion relation (1.44) for $A^{\pm}(s,t)$ may not converge as it stands, but if $D_t^{\pm}$ is power bounded, i.e.

$$D_t^{\pm}(s,t) \xrightarrow[|z_s|\to\infty]{} \text{const.}\ z_s^{N(s)-\varepsilon(s)}\ , \tag{1.54}$$

where N(s) is integral and $0<\varepsilon(s)<1$, we can make N subtractions at $z_s=0$ to give the convergent expression

$$A(s,t) = F_{N-1}(s,z_s) + \frac{z_s^N}{\pi}\int_{z_s(s,t_0)}^{\infty} \frac{D_t^{\pm}(s,t(z_s'))}{(z_s'-z_s)\cdot z_s'^{\,N}}\,dz_s'\ , \tag{1.55}$$

where F_{N-1} is a polynomial of degree N-1 in z_s. Inserting this expression into the projection (1.47),

and using $\int_{-1}^{1} P_\ell(x)\, x^M dx = 0$ for $\ell > M$, the first term vanishes for $\ell + 1 > N$. Writing $(z_s/z_s')^N = (1+\frac{z_s - z_s'}{z_s'})^N$ and expanding in powers of $(z_s - z_s')/z_s'$, we find the integral

$$\frac{1}{2}\int_{-1}^{1} P_\ell(z_s)\left(\frac{z_s}{z_s'}\right)^N \frac{dz_s}{z_s' - z_s}$$

$$= \frac{1}{2}\int_{-1}^{1} \frac{P_\ell(z_s)\,dz_s}{z_s' - z_s} + \frac{1}{2}\int_{-1}^{1} P_\ell(z_s)\left[-\frac{z_s^{N-1}}{z_s'^{N}} + \cdots\right] dz_s$$

$$= Q_\ell(z_s') \qquad \text{for } \ell \geq N(s).$$

So the Froissart Gribov projection (1.49) exists as it stands for $\ell \geq N(s)$ because of the asymptotic behaviour of the Q-function, eq.(1.52). This means that provided the Mandelstam representation is power bounded, the higher partial waves $A_\ell^{\pm}(s)$ for $\ell \geq N(s)$ are completely determined by the double spectral functions, and only the lower ones need subtractions.

The postulate of MASK is essentially that the $A_\ell^{\pm}(s)$ defined by the Froissart Gribov projection can be continued to $\ell < N(s)$ to eliminate all remaining arbitrariness. This will become more explicit when we discuss Regge poles. We note that because of the asymptotic behaviour[37]

$$Q_\ell(z) \xrightarrow[|\ell| \to \infty]{} \text{const.}\, \frac{e^{-(\ell+\frac{1}{2})\xi(z)}}{\sqrt{\ell}} \qquad (1.56)$$

where $\xi(z) = \ln\left(z+\sqrt{z^2-1}\right)$, the $A_\ell^{\pm}(s)$ defined by (1.50) satisfies the conditions for Carlson's theorem[39] to be applied, and so defines a unique continuation to arbitrary ℓ. It is apparent that because the Froissart-Gribov projection for the unsignatured amplitude $A_\ell(s)$ involves an integral over negative z_s, (i.e. the u-channel cut), and because $Q_\ell(-z)=e^{-i\pi\ell}Q_\ell(z)$[37], Carlson's Theorem excludes the possibility of using it to continue meaningfully in ℓ. Also the poor asymptotic behaviour of $P_\ell(z)$ at large ℓ excludes projections like (1.40) and (1.47). For non-integer ℓ, the Q_ℓ function has a cut which gives rise to the singularity structure shown in Fig.1.4b for the integrand in (1.50), and the contour C_2 must be extended accordingly.

As we have already mentioned, Froissart has used unitarity, and analyticity of the amplitude in a small region of the z_s plane, to obtain the following bounds:

$$|A(s,t(z_s\neq\pm1))| < \text{const.}\ s(\ln s)^2, \qquad (1.57)$$

and

$$|A(s,t(z_s\neq\pm1))| < \text{const.}\ s^{3/4}(\ln s)^{3/2}, \qquad (1.58)$$

at large s. A simple version of his proof is given by Chew[1,5]. By crossing symmetry, for $s\leq 0$ we have $N(s)\leq 1$ in eq.(1.54). So that for negative s only the S and P waves are undetermined by

the Froissart-Gribov projection, and have to be defined by some outside means.

According to the postulate of MASK, $A_\ell^{\pm}(s)$ is an analytic function of ℓ apart from isolated singularities, at least in the right-half ℓ-plane[1], so that continuation to $\ell < N(s)$ gives the physical partial waves at the lower integers. This allows us to write a representation of the partial wave series (1.46) which can not only be used outside the latter's limited region of convergence, but the isolated singularities which may be present will give contributions to this expression which can be identified with the subtraction terms in the Mandelstam representation.

Eq.(1.46) is re-written as[40]

$$A^{\pm}(s,t) = 8\pi i \int_{C_1} (2\ell+1)\, A_\ell^{\pm}(s) \frac{P_\ell(-z_s(s,t))}{\sin \pi\ell}\, d\ell \quad , \tag{1.59}$$

where the contour C_1 is chosen to encircle clockwise all the integers $\ell = 0,1,2\ldots$ and avoid the singularities of $A_\ell^{\pm}(s)$. (See Fig.1.5a). Using Cauchy's Theorem, it is easy to see that (1.59) and (1.46) are equivalent. If the contour is deformed in the usual way[41], (see Fig.1.5b), to include a line parallel to the imaginary axis at $\mathrm{Re}\,\ell = L$, and close via a loop at infinity, as L is decreased below $\mathrm{Re}\,\ell = N(s)$ the singularities responsible for the non-convergence of the Mandelstam

representation are exposed. According to the postulate of MASK these are isolated poles and branch points, called Regge[3] poles and cuts. Hereafter we ignore cuts for simplicity, unless the possibility of their presence is particularly relevant. Eq.(1.59) becomes

$$A^{\pm}(s,t) = 8\pi i \int_{\substack{L-i\infty \\ \text{via } C_2}}^{L+i\infty} (2l+1)\, A_l^{\pm}(s)\, \frac{P_l(-z_s)}{\sin \pi l}\, dl$$

$$- 16\pi^2 \sum_i (2\alpha_i(s)+1)\, \beta_i(s)\, \frac{P_{\alpha_i(s)}(-z_s)}{\sin \pi \alpha_i(s)} \quad , \tag{1.60}$$

where $\alpha_i(s)$ is the position of the i^{th} Regge pole, and $\beta_i(s)$ is its residue in $A_l^{\pm}(s)$. Because[37]

$$P_\alpha(z) \xrightarrow[z\to\infty]{} \frac{1}{\sqrt{\pi}} \frac{\Gamma(\alpha+\frac{1}{2})}{\Gamma(\alpha+1)} (2z)^\alpha \tag{1.61}$$

we deduce

$$A^{\pm}(s,t) \xrightarrow[z_s\to\infty]{} \text{const.}\ z_s^{\alpha_1(s)} \tag{1.62}$$

where $\alpha_1(s)$ is the Regge pole furthest to the right in the l-plane. The first term in eq.(1.60) is minimised by taking $L=-\frac{1}{2}$ $\left(P_l(z) = P_{-l-1}(z)\right)$[37], and the second term, which dominates at high t (αs_s), is an

explicit statement of the power bound, and the subtraction terms necessary to make the Mandelstam representation converge. We note that the Froissart bound (1.57) sets a condition on all the "trajectory functions" $\alpha(s)$: $Re\alpha(s) \leq 1$ for $s \leq 0$.

The Regge poles in eq.(1.60) give rise to poles in $A^{\pm}(s,t)$ at $s=s_R$ where $\alpha(s_R)$ is an integer, and these are identified with dynamical bound states and resonances. This parallels the situation in potential scattering where the partial waves are meromorphic in ℓ and MASK is established.(42)

The partial wave projection of a Regge pole term in (1.60) is found by using(37)

$$\int_{-1}^{1} P_\alpha(-z) P_\ell(z)\, dz = \frac{2}{\pi} \frac{\sin \pi\alpha}{(\alpha-\ell)(\alpha+\ell+1)} \tag{1.63}$$

to be

$$A_\ell^{\pm}(s) = \frac{\beta(s)\left(2\alpha(s)+1\right)}{\left(\ell-\alpha(s)\right)\left(\ell+\alpha(s)+1\right)} \,. \tag{1.64}$$

Assuming MAFK, the functions $\alpha(s)$ and $\beta(s)/q_s^{2\alpha(s)}$ can be shown(44) to be real analytic in s cut from the physical threshold to infinity. Unitarity will not permit $Im\,\alpha(s) = 0$, and causality requires $Im\,\alpha(s) > 0$. If we choose $s \approx m^2$ and assume $Im\,\alpha'(s) \ll Re\,\alpha'(s)$, eq.(1.64) becomes

$$A_\ell^{\pm}(s) = \frac{-\beta(m^2)}{Re\alpha'(m^2)(s-m^2) + i\,Im\alpha(m^2)}, \quad Re\alpha(m^2) = \ell, \tag{1.66}$$

which for $\mathrm{Im}\,\beta(m^2)$ small corresponds to a Breit-Wigner resonance of mass m and full width at half height $\Gamma = \mathrm{Im}\,\alpha(m^2) \Big/ m \cdot \mathrm{Re}\,\alpha'(m^2)$. Each trajectory is then expected to give rise to a series of bound states and resonances spaced apart by two units of angular momentum, (remembering eq.(1.51)). Evidently all poles of the S-matrix must be Regge poles - if they were not they would be Kronecker delta singularities in ℓ, contrary to MASK.

The postulate of MAFK states that given a set of particle poles, unitarity determines the singularity structure of the amplitude completely - i.e., the double spectral functions. The postulate of MASK states that these in turn enable a complete determination of the particle poles, which must be Regge poles. In the face of this violently non-linear situation, the hypothesis of Chew and Frautschi[1,2] is now a natural one: the only set of particles consistent with MAFK and MASK is the set observed in nature. Each particle is a composite of all others; they "bootstrap" themselves.

In this thesis we shall present some calculations designed to test whether these hypotheses are likely to give an adequate description of strong interactions. Of course, anything approaching a complete treatment of the infinite set of coupled non-linear equations simplified by maximal analyticity is impossible at present. In

the next Chapter we shall approach the problem of constructing an amplitude for a simple (two-particle) $\longrightarrow$ (two-particle) process which is analytic, crossing symmetric, and displays Regge asymptotic behaviour. A dynamical calculation will then consist of enforcing unitarity upon it, and seeing if the result corresponds to experiment. In the last Section of this Chapter we describe the N/D method, which gives one way of carrying out such a procedure.

5. The N/D Method.

It is simple to verify that the quasi-elastic unitarity condition (1.16) is satisfied in the same form by the signatured amplitudes, $A^{\pm}(s,t)$. Taking into account all two-body channels open at a given energy it becomes

$$A^{ab\pm}(s_+,t) - A^{ab\pm}(s_-,t)$$

$$= \frac{i}{16\pi^2\sqrt{s}} \sum_n q_{sn} \int A^{bn\pm}(s_+,t') A^{na\pm}(s_-,t'') \, d\Omega_n(t',t'') \,. \qquad (1.67)$$

Expressing the amplitudes as partial wave sums, eq.(1.47) and using the addition theorem for Legendre functions[37], the integral in (1.67) can be carried out to yield the unitarity condition for partial wave amplitudes.

$$A_\ell^{ab\pm}(s)_+ - A_\ell^{ab\pm}(s)_- = \frac{4i}{\sqrt{s}} \sum_n A_\ell^{bn\pm}(s_+) q_{sn} A_\ell^{na\pm}(s_-) \,. \qquad (1.68)$$

It is clearly far easier to impose unitarity upon individual partial waves with eq.(1.68) than to deal with the full amplitude using the more complicated expression (1.67). We note that, in accordance with MASK, if a unitary partial wave amplitude can be constructed for one positive ℓ-value, the rest of the series can be found by analytic continuation.

Because we wish to consider non-integral ℓ, it is better to use the "reduced" partial wave amplitude

$$B_\ell^\pm(s) = q_s^{-2\ell} A_\ell^\pm(s) \quad , \tag{1.69}$$

which from eq.(1.53) has no kinematical branch point at threshold. The elastic unitarity equation, (i=n=f in (1.68), for this amplitude is

$$\mathrm{Im}\, B_\ell(s) = \rho_\ell(s) \left| B_\ell(s) \right|^2 \quad , \tag{1.70}$$

where

$$\rho_\ell(s) = \frac{2}{\sqrt{s}} q_s^{2\ell+1} \quad . \tag{1.71}$$

The superscript ± has been dropped and is to be understood hereafter unless otherwise specified.

Eq.(1.70) can be linearised by the decomposition

$$B_\ell(s) = N_\ell(s) \Big/ D_\ell(s) \quad , \tag{1.72}$$

where the N-function carries the left-hand singularities of $B_\ell(s)$, and the D-function carries its right-hand singularities. Both N and D are real-analytic in s, and can be normalised

$$N_\ell(s) \xrightarrow[|s|\to\infty]{} 0 \tag{1.73a}$$

$$D_\ell(s) \xrightarrow[|s|\to\infty]{} 1 \,. \tag{1.73b}$$

Elastic unitarity, eq.(1.70) gives

$$\mathrm{Im}\, D_\ell(s)\Big|_{R.H.\ cut} = -\rho_\ell(s)\, N_\ell(s) \,, \tag{1.74}$$

so that

$$D_\ell(s) = 1 - \frac{1}{\pi}\int_{s_0}^{\infty} \frac{\rho_\ell(s')\, N_\ell(s')\, ds'}{s'-s} \,. \tag{1.75}$$

We now introduce

$$B_\ell^L(s) = B_\ell(s) - \frac{1}{\pi}\int_{s_0}^{\infty} \frac{\mathrm{Im}\, B_\ell(s')}{s'-s}\, ds' \,, \tag{1.76}$$

which has the same left-hand cut as $B_\ell(s)$. Therefore the combination $N_\ell(s) - B_\ell^L(s)\, D_\ell(s)$ has only a right-hand cut, and so, using (1.74), we have

$$N_\ell(s) = B_\ell^L(s) D_\ell(s) + \frac{1}{\pi}\int_{s_0}^{\infty} \frac{B_\ell^L(s')\, \rho_\ell(s')\, N_\ell(s')}{s'-s}\, ds' \,. \tag{1.77}$$

Substituting for $D_\ell(s)$ from (1.75) we obtain the standard[45] equation

$$N_\ell(s) = B_\ell^L(s) + \frac{1}{\pi}\int_{s_0}^{\infty} \frac{B_\ell^L(s') - B_\ell^L(s)}{s' - s}\, \rho_\ell(s')\, N_\ell(s')\, ds' . \qquad (1.78)$$

This is a Fredholm equation if its kernel is square-integrable. That is, given a suitably behaved "potential function" $B_\ell^L(s)$, it may be solved for $N_\ell(s)$ by standard means. $D_\ell(s)$ is then found from eq.(1.75).

We note that with a well-behaved potential function, $N_\ell(s)$ is regular at threshold. Similarly $D_\ell(s)$ is regular at threshold, and so is $B_\ell(s)$. Therefore, from eq.(1.69), $A_\ell(s)$ always has correct threshold behaviour. Had we written N/D equation for $A_\ell(s)$ directly, with phase space factor $\rho(s) = 2q_s/\sqrt{s}$ there would be no guarantee that the correct threshold behaviour would result, unless the potential function were constrained by moment conditions[46].

Equation (1.76) for $B_\ell^L(s)$ is of little practical use, and several more convenient expressions can be written down[5]. One follows simply from the Froissart-Gribov projection, (1.50), and is

$$B_\ell^L(s) = \left(32\pi^2 q_s^{2\ell+2}\right)^{-1} \int_{-\infty}^{0} \mathrm{Im}\left\{ Q_\ell(z_s) \right\} V(s,t)\, dt \quad , \qquad (1.79)$$

where $V^{\pm}(s,t)$ is $A^{\pm}(s,t)$ less that part which contributes to the right-hand cut. Another is found by inserting into eq.(1.49) the expression, implied by eq.(1.45), for $D_t^{\pm}(s,t)$ in terms of the double spectral function. This gives

$$B_l^{\pm}(s) = (32\pi^3 q_s^{2l+2})^{-1} \iint \left\{ \frac{\rho_{st}(s',t'') \pm \rho_{us}(s',t'')}{s'-s} ds' + \frac{\rho_{tu}(t'',u') \pm \rho_{tu}(u',t'')}{u'-u''} du' \right\} Q_l(z_s(s,t'')) \, dt'' \tag{1.80}$$

The right-hand discontinuity in s is easily recognised, and removed, to give

$$B_l^{L\pm}(s) = (32\pi^3)^{-1} \iint \left\{ \frac{\rho_{st}(s',t'') \pm \rho_{us}(s',t'')}{s'-s} \right\} \times \left\{ \frac{Q_l(z_s(s,t''))}{q_s^{2l+2}} - \frac{Q_l(z_s(s',t''))}{q_{s'}^{2l+2}} \right\} ds' dt'' + (32\pi^3)^{-1} \iint \left\{ \frac{\rho_{tu}(t'',u') \pm \rho_{tu}(u',t'')}{u'-u''} \right\} Q_l(z_s(s,t'')) \, du' dt''. \tag{1.81}$$

We shall find both these forms useful.

If the partial wave contains a bound state or resonance, it will occur at $s=s_R$ where

$$D_l(s_R)=0 \tag{1.82}$$

In practice the N/D equations are solved only for real s, and so a resonance position m^2 is determined by the approximate equation

$\mathrm{Re}D_\ell(m^2)=0$. Then the (Breit-Wigner) resonance has width

$$\Gamma = -\frac{1}{m}\rho_\ell(m^2)\frac{N_\ell(m^2)}{\mathrm{Re}\,D_\ell'(m^2)}\ , \tag{1.83}$$

and residue equal to $N_\ell(m^2)/\mathrm{Re}D_\ell'(m^2)$. At $s=m^2$, we may take $\ell \approx \mathrm{Re}\alpha(s)$ where $\alpha(s)$ is the trajectory on which the state lies, because we are dealing with correctly signatured amplitudes. We note that (1.82) implies that $\alpha(s)$ has the same analyticity properties as $D_\ell(s)$. Therefore we write

$$\alpha(s) = \alpha(\infty) + \frac{1}{\pi}\int_{\text{Threshold}}^{\infty}\frac{\mathrm{Im}\,\alpha(s')}{s'-s}\,ds'\ , \tag{1.84}$$

where we assume that the integral converges. Also, a simple-minded continuation of (1.83) to threshold implies, (see eq.(1.66) etc.),

$$\mathrm{Im}\,\alpha(s) \xrightarrow[q_s^2 \to 0]{} \text{Const.}\ q_s^{2\alpha(0)+1}\ . \tag{1.85}$$

From eqs.(1.66) and (1.68), $\mathrm{Im}\alpha(s)$ cannot change sign. Therefore $\mathrm{Im}\alpha(s)$ and $\mathrm{Re}\alpha'(s)$ have the same sign, ($\Gamma > 0$ above threshold). Experimentally[5], trajectories rise through resonances, and in fact in potential scattering[42], (to which appeal is frequently

made[41] to resolve uncertainties by analogy),

$\alpha'(s) \propto |\text{Range of potential}|^2$ below threshold.

Hence $\mathrm{Im}\,\alpha(s) > 0$.

Our statements in the preceding paragraph are based at most on plausibility arguments, but all can be given rigorous proof based on MAFK[44]. Because we have assumed $\gamma(s) = \beta(s)\, q_s^{-2\alpha(s)}$ to be real at $s=m^2$, (eq.(1.66)), we cannot give similar arguments for it. But it can be shown[44] that $\gamma(s)$ is real analytic in s cut from threshold to infinity, and

$$\mathrm{Im}\,\gamma(s) \xrightarrow[q_s^2 \to 0]{} \text{const.}\; q_s^{2\alpha(0)+1} . \tag{1.86}$$

A dispersion relation like (1.85) holds for $\gamma(s)$ also.

We have assumed that the N/D equation can be continued in ℓ. This has been proved to be so by Mandelstam[47], who goes further to show that this property means that the only solution of eqs.(1.75) and (1.77) consistent with MASK is that containing no CDD[48] poles. The CDD ambiguity, of course, corresponds to the possibility of the presence of elementary particles in the theory, and is specifically excluded by MASK. (Strictly we should distinguish between one-channel and multi-channel CDD poles[50] and cuts[51], but such considerations are peripheral to the present discussion).

6. Summary.

To summarise, our dynamical postulates for the four-line connected part are:

(a) the amplitude obeys the Mandelstam representation;

(b) continuation in angular momentum removes arbitrary subtractions.

In addition, the bootstrap hypothesis states that the result is unique and describes nature.

A dynamical calculation within this framework consists of constructing an amplitude from double spectral functions which have Regge asymptotic behaviour, and enforcing unitarity upon it. The non-linearity of the unitarity equations "drives" the dynamics and allows the calculation of numbers up to a scale factor determined for example by the external masses in the problem, in much the same way as the non-linearity of current commutators allows the derivation of non-trivial sum rules. The N/D method is convenient for practical calculations because of its simplification of unitarity.

In Chapter Two we discuss the construction of a suitable form for the scattering amplitude.

Fig.(1.1). Schematic representation of the four-line connected part. The particle four-momenta are labelled p_1 to p_4, and are conventionally taken all to be ingoing.

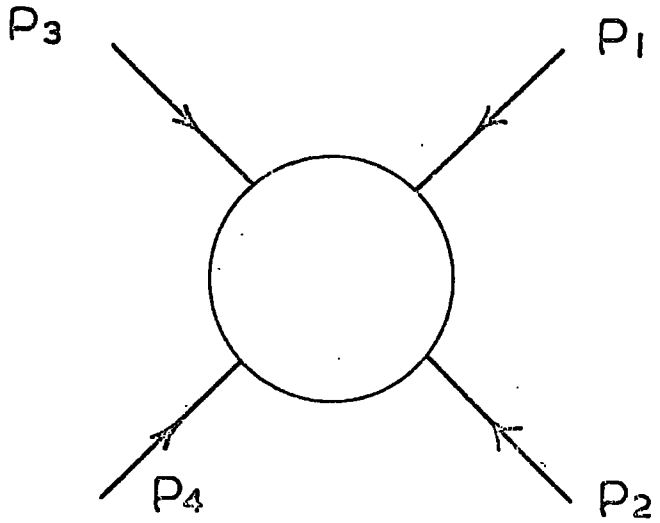

FIG. I.I

Fig.(1.2). The Mandelstam diagram for the scattering of equal mass scalar particles. The physical regions for the three channels are shown shaded, and the double spectral functions are indicated.

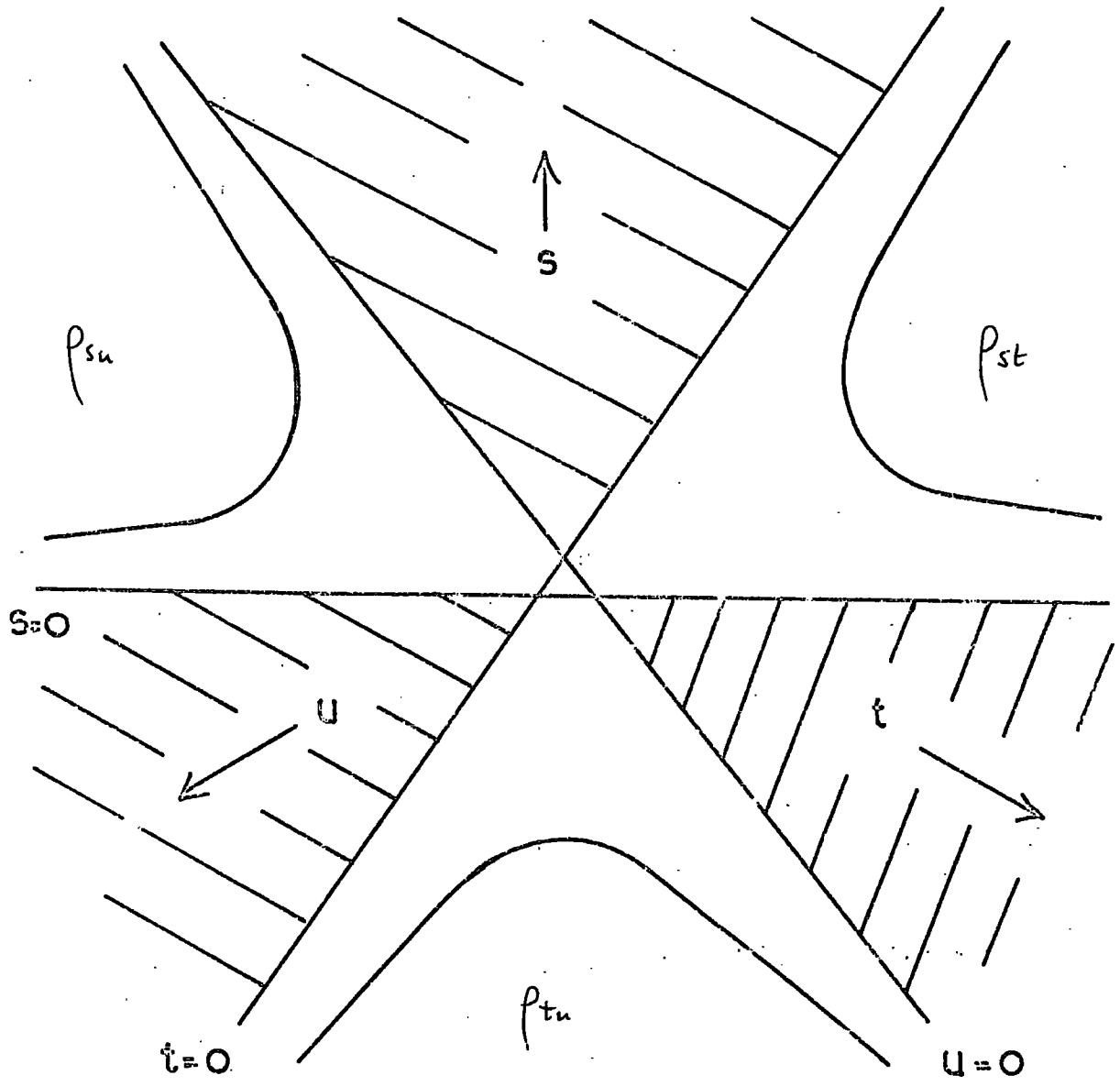

FIG. 1.2

Fig.(1.3). Diagram to define the angular variables used in eqs.(1.31) and (1.32).

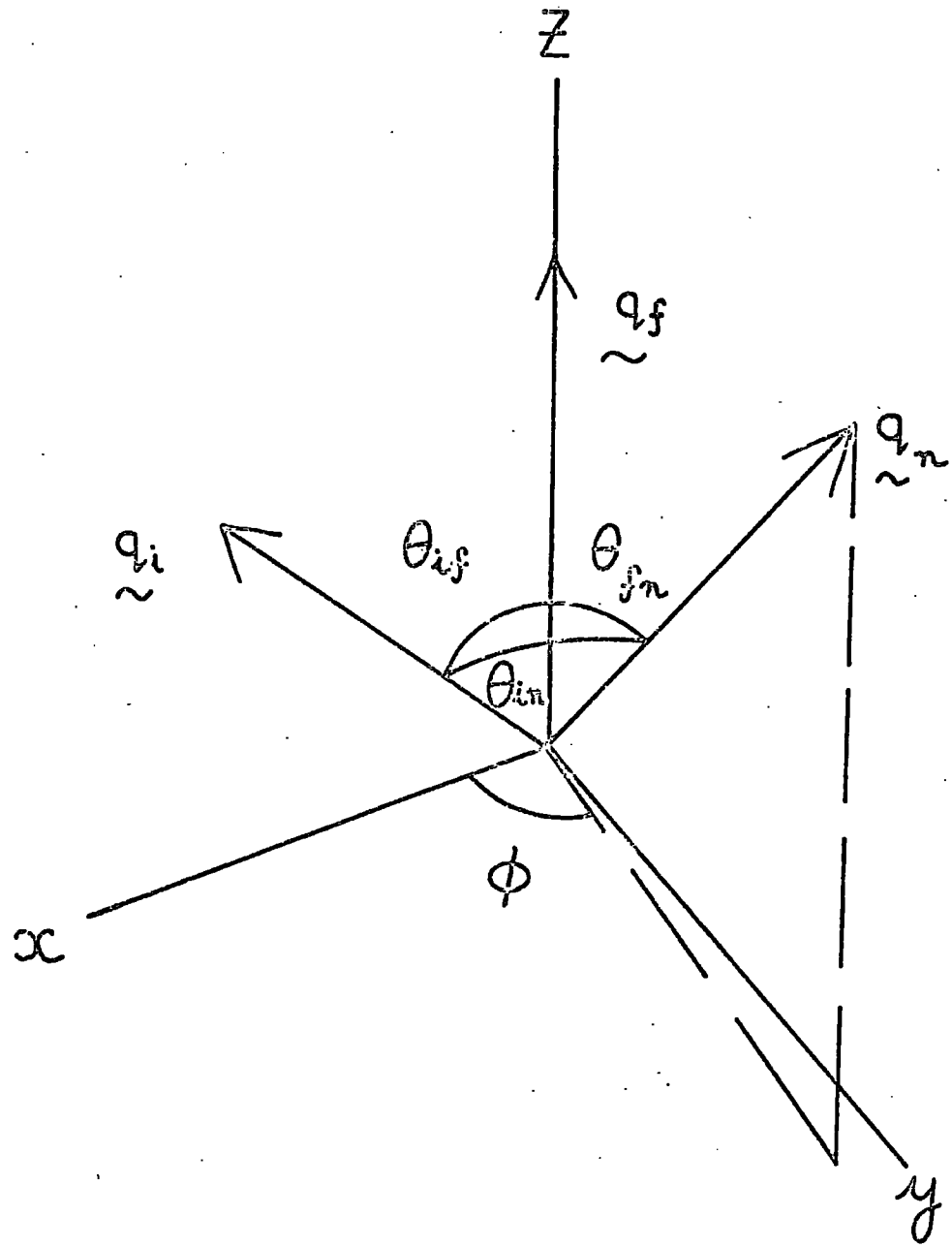

FIG. 1.3

Fig.(1.4). The s_s plane for the integrand on the right of eq.(1.50). The cuts are shown for (a) integral ℓ and (b) general ℓ, and C_1 and C_2 are the appropriate integration contours.

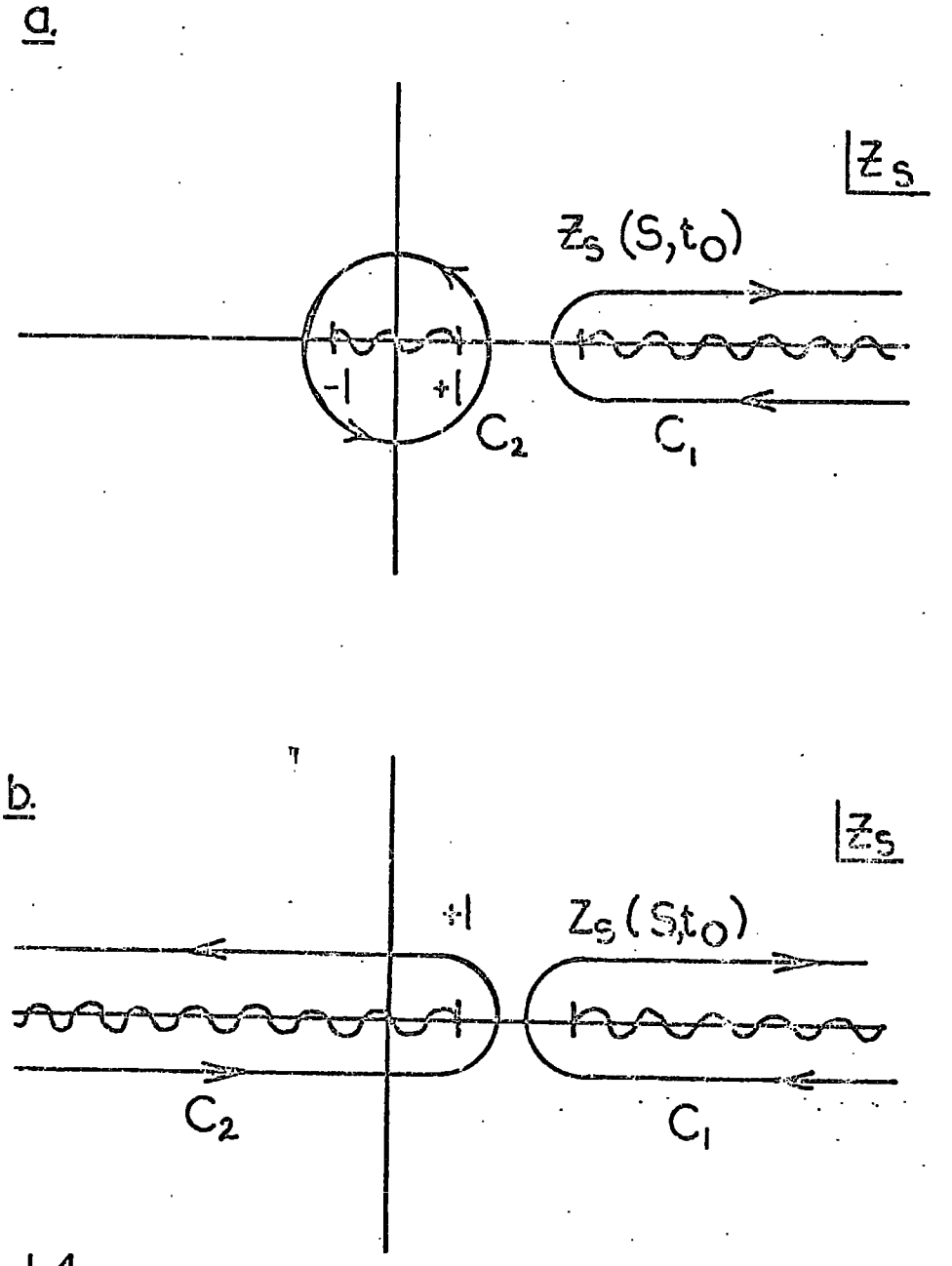

FIG. 1.4

Fig.(1.5). The ℓ-plane contours (a) C_1 (for eq.(1.59)). and (b) C_2 (for eq.(1.60)).

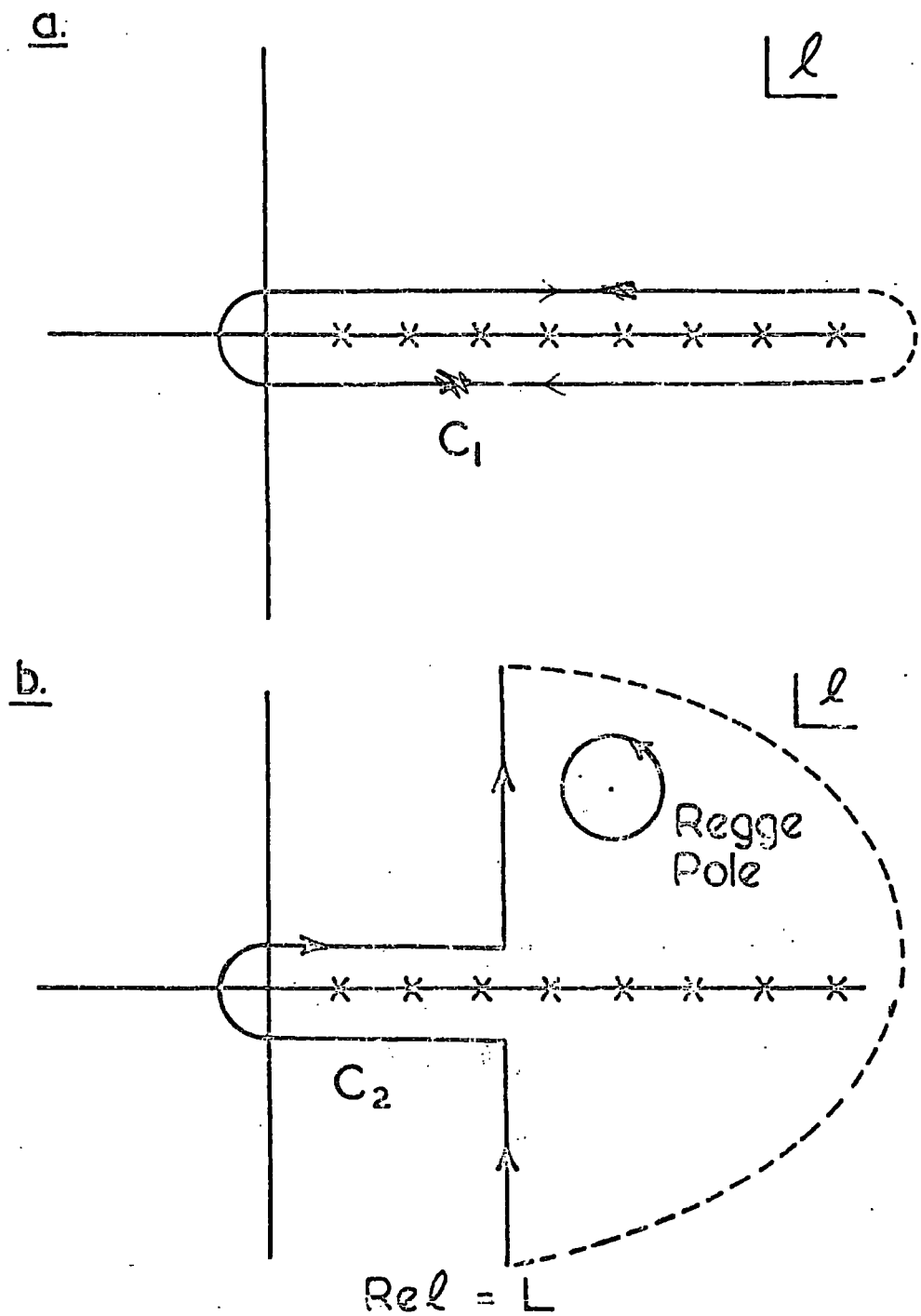

FIG. 1.5

CHAPTER TWO

A Model for the Scattering Amplitude

1. Introduction.

In this Chapter we describe a particular approximation to A(s,t,u) which displays broad features in agreement with experimental observation, and which can be cast in a form suitable for the sort of dynamical calculations we have outlined. In the next three sections we introduce the model and discuss its general validity, paying particular attention to some criticism which has recently arisen against it. In Section Five we give a mathematical formulation of the approximation and in Section Six describe some of its drawbacks which have appeared in practice, suggesting how they could be rectified.

2. The Interference Model.

In general, scattering amplitudes for two-body processes display the following prominent features:[52]

(a) At high energies, (energy $\gg$ characteristic mass involved), the amplitude is concentrated into forward and/or backward peaks;

(b) at lower energies, (energy $\sim$ characteristic mass involved), it appears to be dominated by resonance structure;

(c) the appearance of high energy peaks is correlated with the occurrence of crossed-channel particles.

The simplest approximation to the four-line connected part would be, on this basis, to write it as a direct sum of the few leading Regge poles in each channel, with analytic properties consistent with the Mandelstam representation.

A t-channel Regge trajectory $\alpha(t)$ certainly represents a series of t-channel resonances, (eq.(1.66)), and at large s gives an asymptotic behaviour proportional to $s^{\alpha(t)}$, (eq.(1.62)). So, describing at $t=t_p$ a low energy t-channel pole, the trajectory gives the amplitude nearby a behaviour roughly proportional to $(t-t_p)^{-1}$. This accounts qualitatively for the rapid variation in the s-channel close to the forward direction at high energies where the effects of direct-channel resonances have died away[53].

We shall refer to the approximation of adding the effects of the resonances in the three channels as "the interference model". It includes as a special case the model of the same name introduced[54] to parameterise pion-nucleon scattering data at intermediate energies, and generalises the peripheral model[55] ideas underlying fits to high energy date using a few crossed channel Regge poles[56].

We expect this model to be a good approximation to A(s,t,u) only in the resonance region and in the forward and backward peaks at high energy. In particular

we should not anticipate good results from it when two of the variables s,t,u are both large.

In the next two Sections we shall consider the validity of the interference model, with special attention to the question of double counting, which has recently aroused interest[57].

3. Validity of the Interference Model.

An amplitude $A(s,t,u)$ can be expressed in any one of the three channels as a background integral plus a sum of Regge pole terms. Symbolically

$$\begin{aligned} A(s,t,u) &= B^s(s,t,u) + R^s(s,t,u) \\ &= B^t(s,t,u) + R^t(s,t,u) \\ &= B^u(s,t,u) + R^u(s,t,u). \end{aligned}$$

The interference model which we contemplate sets

$$A(s,t,u) \approx R^s(s,t,u)+R^t(s,t,u)+R^u(s,t,u)+\text{possible background}. \qquad (2.1)$$

It is not clear that this is a valid procedure, for there appears to be no guarantee that all parts of the scattering amplitude are counted only once. For example, if for some values of s,t,u the background parts B in each channel were very small compared with the Regge pole parts R, then each of R^s, R^t and R^u would alone be a reasonable approximation to $A(s,t,u)$ and the representation (2.1) would break down. We contend, however, that with proper care, such

ambiguities can be avoided, and that the interference model can give a reasonably faithful representation of at least the overall features of the amplitude, as outlined in the previous Section.

First of all, we note that if in the decomposition $A=B^t+R^t$ (for example) the Regge part R^t contains a finite number of terms, then it is regular in the variables s and u, (see eq.(1.60)), and so cannot contain the crossed channel resonance poles. In this sense the replacement of B^t by R^s+R^u is not inconsistent. The question is now whether R^t contains some parts of R^s and R^u, without having necessarily the pole-like behaviour. There is no clear-cut answer to this problem at present, but it is probably true that the degree of double counting can be made negligible if the model is used judiciously.

The crucial requirement is that each term $R(s,t,u)$ must contain only the highest-lying trajectories, i.e. those with the largest value of $\mathrm{Re}\,\alpha$. Each term in R^t gives a characteristic asymptotic behaviour in the crossed channel like $s^{\alpha(t)}$, and so provided $\mathrm{Re}\,\alpha(t)$ are confined to (say) values above -1, there is a minimum chance of including effects of low energy crossed channel resonances, which, on the basis of a simple pole form, are expected to die away at least as fast as s^{-1}.

The interference model has been criticised on the grounds of calculation with finite energy sum rules[58] (FESR). A full discussion of FESR is outside our scope - details have been given by Dolen, Horn and Schmid[58] - but the basic idea is as follows. Consider an amplitude antisymmetric under s-u crossing, (i.e.-$A(s_+,t,u)=A(u_+,t,s)$), and use this property to write a fixed t dispersion relation for it as an integral over the s-discontinuity only. Then if an energy s_1 exists above which $A(s,t,u)=R^t(s,t,u)$, one can derive

$$\int^{s_1} ds \, \mathrm{Im}\, A(s_+,t,u) = \sum_i G_i(t)\, s_1^{\alpha(t)} \,. \qquad (2.2)$$

The right-hand side is the asymptotic form of R^t (see eq.(2.9) below). This equation is expected to be valid in a range of t where Regge pole exchange is a valid approximation.

The following example is quoted[60]: "consider an elastic amplitude A(s,t,u) at t=0 where the optical theorem (eq.(1.22)) constrains its imaginary part to be positive definite. Eq.(2.2) expresses the fact that for $s<s_1$ the imaginary part must average out to a curve (proportional to) $s^{\alpha(t)}$, whereas the interference model suggests that all the necessarily positive resonance contributions (R^s) should be added to $s^{\alpha(t)}$, so yielding a curve everywhere above $s^{\alpha(t)}$." This example clearly sets forth limitations for the model, but by no means demolishes it.

The first point is that at low energies the asymptotic form $s^{\alpha(t)}$ is not a unique representation of R^t. The second is that below s_1 there are important contributions to the amplitude from low-lying t-channel trajectories not included in R^t. These are buried in B^t, which we replace by R^s. (The term R^u is "folded over" into R^s by crossing symmetry in eq.(2.2)). Therefore the implications of FESR are that the Regge terms must be constructed to die away quickly at high energy in their own channel, since they replace the low-lying crossed channel Regge poles - which are to be excluded from R^s, R^t and R^u, as we have already emphasised. A reasonable practical restriction is probably that $\alpha(o)$ should exceed zero for each pole included in any R, and so this will generally describe only prominent resonances which give unmistakable structure to the cross section. However, provided that $\alpha(o)$ exceeds -1 there is probably little danger of double counting.

Recently it has been observed[61] that if R^t is decomposed into s-channel partial wave amplitudes the latter display characteristics usually associated with the presence of resonance. Therefore, it has been asserted, R^t must contain large parts of R^s, and "the interference model commits severe double counting".[61]

This criticism will be discussed at length in the next Section, and some of its interesting implications[62] for phenomenological analysis will be pointed out.

4. Regge Pole Exchange and Direct Channel Resonances.

We write

$$A_\ell(s) = \frac{\eta_\ell(s)\, e^{2i\delta_\ell(s)} - 1}{2i\rho(s)} \qquad (2.3)$$

as a formal solution to eq.(1.68), where $\delta_\ell(s)$ is a real phase shift, $\rho(s)=2q_s s^{-\frac{1}{2}}$, and $0 \leq \eta_\ell(s) \leq 1$ parameterises inelasticity. Plotting a graph of $2\rho\,\mathrm{Re}A_\ell$ versus $2\rho\,\mathrm{Im}A_\ell$ as functions of s, one obtains an Argand diagram[63] as shown in Fig.(2.1). The vector is confined inside the circle by unitarity. The presence of a resonance implies a bump in the cross-section, that is, a maximum in $\mathrm{Im}A_\ell(s)$, which is correlated by causality (a dispersion relation) with a sharp dip in $\mathrm{Re}A_\ell(s)$. Thus a typical resonance structure is a rapid (with s) anti-clockwise loop in the Argand diagram.

Schmid[61] observed that if one extrapolates to low energy the ρ-meson Regge pole exchange term which fits the process $\bar{\pi}p \to \pi^0 n$ at high energy[64], and calculates direct channel angular momentum components using

$$a_\ell(s) = \int_{-1}^{1} P_\ell(z_s)\, R_\rho^t(s,t(z_s))\, dz_s \,,$$

the Argand plot of $a_\ell(s)$ displays just this behaviour. Schmid identified his loops with well-established[65] N^* resonances.

To understand Schmid's results, we must examine the form of R^t in detail. In the preceding Chapter, we emphasised that a Regge pole couples to a signatured amplitude, each giving a contribution of the form

$$-16\pi^2(2\alpha+1)\beta\,\frac{P_\alpha(-z)}{\sin\pi\alpha}\,, \tag{2.4}$$

From (1.42) and (1.43) the physical amplitude is given by $A = \frac{1}{2}(A^+(s)+A^-(s)+A^+(-s)-A^-(-s))$, so that a t-channel Regge pole gives a contribution to the physical amplitude

$$R^t(s,t,u) = -16\pi^2(2\alpha(t)+1)\beta(t)\,\frac{P_{\alpha(t)}(-z_t) \pm P_{\alpha(t)}(z_t)}{\sin\pi\alpha(t)} \tag{2.5}$$

where a positive or negative sign is taken according to whether the pole couples to A^+ or A^-. Using[37]

$$P_\alpha(-z) = e^{-i\pi\alpha}P_\alpha(z) - \frac{2}{\pi}\sin\pi\alpha\,.\,Q_\alpha(z)\,, \tag{2.6}$$

we deduce

$$R^t = -16\pi^2(2\alpha(t)+1)\beta(t)\,\frac{1\pm e^{i\pi\alpha(t)}}{\sin\pi\alpha(t)}\,P_{\alpha(t)}(-z_t) + O\left(z_t^{-\alpha-1}\right). \tag{2.7}$$

The last term comes from the Q-function[37], and will be neglected. For elastic scattering $z_t = 1 + s/2q_t^2$, so using (1.61) we have

$$R^t \xrightarrow[s \to \infty]{} - \text{Const.}\ \beta(t) \frac{1 \pm e^{i\pi\alpha(t)}}{\sin \pi\alpha(t)} \left(-\frac{s}{q_t^2}\right)^{\alpha(t)} .$$

Introducing

$$\gamma(t) = \beta(t) \left(\frac{s_0}{q_t^2}\right)^{\alpha(t)} \tag{2.8}$$

which has no kinematical cut, and which because of the scale factor s_0 has constant dimensions, we finally have

$$R^t(s \to \infty, t, u) \propto \gamma(t) \frac{\mp 1 - e^{-i\pi\alpha(t)}}{\sin \pi\alpha(t)} \left(\frac{s}{s_0}\right)^{\alpha(t)} . \tag{2.9}$$

This is essentially the form used by Schmid[61]. We note immediately that it is an aymptotic expression and its extrapolation to low s is almost completely arbitrary[5].

A large amount of high energy small angle data can be fitted satisfactorily using the expression (2.9) for R^t, with $\alpha(t)$ linear with t[56]. Although linear trajectories are dynamically puzzling (as we shall discuss later), they are certainly consistent with observed resonances which almost always appear well-placed to be their recurrences[66]. The appearance of loops depends crucially on the (near) linearity of $\alpha(t)$

out to large negative t, as will become obvious.

We consider as an example the scattering of equal (unit) mass scalar particles, whose high energy amplitude is well represented by a single Regge pole term of the form (2.9). Projecting out s-channel partial waves we have

$$A_\ell(s) = \frac{1}{s-4}\int_{4-s}^{0} P_\ell\left(1+\frac{2t}{s-4}\right) R^t(s,t,u)\, dt . \qquad (2.10)$$

The lower limit is proportional to s, so that at a given value of this variable the linear trajectory $\alpha(t)=a+bt$ passes through proportionately many negative integers in the range of integration. At these points $\gamma(t)$ must vanish to avoid "nonsense" states in the crossed channel[67]. Therefore we could rewrite $\gamma(t)$ as $\gamma(t)/\Gamma(\alpha(t))$, but, noting that[37] $\Gamma(z)\Gamma(1-z) = \pi/\sin\pi z$ which would imply an exponential divergence of $A_\ell(s)$ at high s, we prefer to "kill the ghosts" by simply leaving out as appropriate the $\sin\pi\alpha(t)$ denomination of (2.9).

In the integral (2.10) the signature factor $\mp 1 - e^{-i\pi\alpha(t)}$ has oscillatory real and imaginary parts that interfere with the Legendre polynomial P_ℓ which changes sign ℓ times in the range of integration. As s increases the relative number of oscillations changes, and the net result is that $\mathrm{Re}A_\ell(s)$ increases from zero,

passes through a maximum, and changes sign to reach a minimum, eventually returning to zero. At the same time $\mathrm{Im}A_\ell(s)$ increases to a maximum and falls back. Thus a counterclockwise loop is induced in the Argand plane. At successively higher values of ℓ the Legendre function has more nodes in the range of integration and as a result the loops appear at higher s-values. Therefore an s-channel "Regge trajectory" is produced, and can be followed as high as we please. A number of examples, upon which these deductions are based, are given in Fig.(2.2).

The choice of ghost killing factor in the residue affects to some extent the results - if instead of a function which changes sign at its zeroes (like $1/\Gamma(\alpha(t))$ or $\sin\pi\alpha(t)$) we used one that did not, (like $\sin^2\alpha(t)\pi$) only at low ℓ do loops appear, and then rather weakly. We note that input (t-channel) and output (s-channel) trajectories always have the same slope, and that if the input trajectory is raised parallel to itself the output one is correspondingly lowered, and vice versa.

We have used the asymptotic expression (2.9) for our discussion because of its simplicity but it is found that our results remain essentially unaltered for other extrapolations to low energy.

Our general conclusion from these examples is that Schmid's loops are an inevitable result of a single Regge pole exchange amplitude, extrapolated from high energy and to wide angles. Where several poles are allowed with comparable strength and different slopes and/or signatures, interference between them may produce either no loops at all[61], or loops which execute clockwise motion and which are acausal[69].

Acausal loops are simply understood. Consider two t-channel trajectories of different slopes which contribute with opposite sign residues to $A_\ell(s)$. They each produce a counterclockwise loop, but because of their different slope these are executed at different speeds with respect to s. Because the contributions are opposite in sign, a net clockwise loop is possible. In general, a combination of different signature factors with different trajectory slopes may add to give a net function hardly resembling a simple $e^{i\pi\alpha(t)}$ at all, and so Schmid's loops are not always to be expected. Further, there is no reason to expect partial wave unitarity ($\mathrm{Im}\, A_\ell(s) \geq 0$) to be always obeyed when there are trajectories of different couplings, and indeed in a simple scalar meson model with two opposing trajectories this is the case. (Partial waves projected from fits to high energy data[71] generally obey unitarity at low energies, as they do at high energies[71]).

Turning now to the interpretation of Schmid's loops, it is at once clear that they cannot be associated with resonance poles because there are manifestly no second sheet singularities in s in eq.(2.10). Other properties of the partial waves lead one to the conclusion that indeed the loops have nothing at all to do with the presence of s-channel resonances or parts thereof. Firstly, while one partial wave has structure, the remaining ones conspire to conceal it in the total which is smoothly proportional to $s^{\alpha(t)}$. Such a correlation is most uncharacteristic of a resonance, which should appear clearly in one partial wave. Secondly, the loops depend on crossed channel quantum numbers and not on direct channel ones. The processes $\pi\pi \to \pi\pi$ and $\pi\pi \to N\bar{N}$ have the same direct channels and so should share a number of resonances. Their crossed channels differ, however, and if Schmid's loops correspond to resonances, there is no a priori reason why they should appear in the same place in each process. As Alessandrini and Squires have pointed out[68], in the processes $\pi^- p \to \pi^0 n$ and $\pi^- p \to K^+ \Sigma^-$ where the direct channels should have identical resonances with comparable strengths (if SU3 gives a reliable order of magnitude estimate), the t-channels are completely different. Neglecting the u-channels, which are roughly the same - N^*'s in one case, Y^*'s in the other - we see that the presence of the ρ in the t-channel for the charge exchange process

will give Schmid loops, whereas the absence of any known trajectory in the t-channel of the associated production process will lead to no s-channel loops at all. Finally, with a combination of several trajectories of different slopes and signatures it appears quite possible to contrive to produce acausal, clockwise loops[69], as we have already remarked.

These conclusions are at present under further investigation by explicit numerical calculation of partial wave amplitudes for the processes $pp \longrightarrow pp$ and $p\bar{p} \longrightarrow p\bar{p}$ where high energy fits with P,P' and ω trajectories exist[71]. Preliminary results are in good agreement with qualitative expectations. In particular, Schmid's loops appear in both processes, whereas if they were manifestations of resonances, they should be confined to $p\bar{p}$.

If Schmid's loops are not to be interpreted as resonances, we are led to look afresh at the criteria currently used for identification of resonances in phase shift analysis. The usual method is well summarised by Lovelace[65]: "in the present paper, I shall call a resonance anything which when . . . plotted describes a considerable part of a circle, making some allowance for distortion by background." In recent years a large number of such resonances have been identified in the πN system using this criterion[65,70],

but we now see that there is another mechanism in nature, namely the crossed channel Regge pole contribution, which has nothing to do with direct channel resonances but which is capable of generating such circles.

To explore this situation further[62] we have taken the Regge pole fit to the forward and small angle πN data at high energies from Rarita et al.[71], using the P, P' and ρ trajectories taken from solution I, and the fit to the backward data, using the N and Δ trajectories of Barger and Cline[72]. A factor $\sin\pi\alpha(t)$ was incorporated into the residue functions given by these authors in such a way as to fit smoothly onto the behaviour in the fitted ranges of t and u respectively. Therefore we were able to make a partial wave projection equivalent to (2.10) using the formalism given by, e.g., Donnachie[63] to take account of external spin and unequal mass kinematics. We find several Schmid loops, and collect the results in Table (2.1) and Fig.(2.3). Most circles occur in the $I=\frac{1}{2}$ channel, and in the $I=3/2$ channel, which differs mainly in the sign of the ρ contribution, there are fewer large circles because the contributions of the ρ and P' trajectories more or less cancel. In fact in the latter case the circles stem mainly from the baryon exchange in the backward peak.

Evidently we find loops in most of the partial waves, and some are in positions which correspond rather closely to those found in phase shift analyses[65,70]. In view of the manifest uncertainties in Regge pole fits we would certainly not jump to a conclusion that any such loop was wrongly interpreted, but we do feel that the criteria used for resonance interpretation are rather inadequate since there are clearly other mechanisms apart from resonance poles which can produce circles in the Argand diagram. Of course, where a resonance leads to a bump in some cross section (which includes our interference model), we can be reasonably confident it really does correspond to a pole on an unphysical sheet, but very inelastic resonances may be difficult to distinguish from Schmid loops reflecting the Regge nature of the amplitude's asymptotic form unless we can find processes to which they are more strongly coupled.

It is obviously desirable[78] from an S-matrix point of view to be able to distinguish between genuine resonance poles and other loops in the Argand diagram, and it is particularly important for the quark model where it is natural to correlate resonances with bound states of quark systems[74].

Our conclusions from this discussion are quite clear - Schmid's results in no way invalidate the interference model, particularly the form we shall

use for numerical work, when the trajectories will not be linear. In the next Section we describe a formulation of the model due to Chew and Jones[75] which is our starting point for a dynamical calculation.

5. The Chew-Jones Representation.

We wish to construct double spectral functions for A(s,t,u) which give the amplitude in the interference model form of eq.(2.1). We shall start with the prescription of Chew and Jones[75], who parameterised "strips" of double spectral function such that each Regge term R in eq.(2.1) is given by an expression similar to eq.(2.4). This is a first approximation to the amplitude which has been shown to be unsatisfactory in detail, and which needs augmenting if a dynamical calculation is to give satisfactory quantitative results. There is a well-defined way of doing this, as we shall discuss in the next Section, calculating extra pieces of double spectral function using the "Mandelstam iteration".[22].

The regions of double spectral function which Chew and Jones retain are shown in Fig.2.4, where each term R^s, R^t and R^u of eq.(2.1) is given by a pair of strips as indicated. Each is characteristic of the regions of the s-t-u plane dominated by the Regge poles it contains. We shall deal explicitly with $R^t(s,t,u)$

- similar results will hold for the other terms by appropriate permutation of the variables.

The prescription for the piece of double spectral function labelled R_1^t in Fig.2.4 is

$$\rho = \frac{1}{2}\,\Delta_t \left\{ \Gamma(t)\, P_{\alpha(t)}(-z_t) \right\} \theta(s-s_1)\,, \tag{2.11}$$

where $\Gamma(t) = -16\pi^2 \left(2\alpha(t)+1\right) \gamma(t) \left(-q_t^2/s_0\right)^{\alpha(t)}$, s_1

is the "strip width", and the symbol Δ_t indicates that the discontinuity with respect to t must be taken. This gives a contribution to the s-discontinuity of R^t of $\Gamma(t)\, P_{\alpha(t)}(-z_t)\, \theta(s-s_1)$ and a contribution to R^t itself of

$$-\frac{1}{2\pi}\,\Gamma(t) \int_{s_1}^{\infty} \frac{P_{\alpha(t)}\left(-z_t(s',t)\right)}{s'-s}\, ds' \,.$$

Using the formula(37)

$$P_\alpha(-z) = -\frac{\sin\pi\alpha}{\pi} \int_1^{\infty} \frac{P_\alpha(z')}{z'-z}\, dz'\,, \tag{2.12}$$

we may re-write this in an equivalent form which converges for $\alpha(t) \geq 0$ as

$$\frac{1}{2}\Gamma(t) \left\{ \frac{P_{\alpha(t)}(z_t)}{\sin\pi\alpha(t)} + \frac{1}{\pi} \int_{-4q_t^2}^{s_1} \frac{P_{\alpha(t)}(-z_t')}{s'-s}\, ds' \right\} \tag{2.13}$$

Including in a parallel way the strip R_2^t of Fig.2.3, we deduce the Chew-Jones equivalent of eq.(2.5):

$$\begin{aligned} R^t(s,t,u) &= R_1^t \pm R_2^t \\ &= \frac{1}{2}\Gamma(t) \left\{ \frac{P_{\alpha(t)}(z_t) \pm P_{\alpha(t)}(-z_t)}{\sin\pi\alpha(t)} + \frac{1}{\pi} \int_{-4q_t^2}^{s_1} P_{\alpha(t)}(-z_t') \left[\frac{1}{s'-s} \pm \frac{1}{s'-u} \right] ds' \right\}\,, \end{aligned} \tag{2.14}$$

where in the integral we have made a simplifying change of variable using $s_t=1+s/2q_t^2=-1-u/2q_t^2$. Eq.(2.14) is identical to (2.5) up to Q-functions, except that the analytic properties have been adjusted according to the strip approximation.

This representation was developed specifically within the context of N/D calculations, and a modified form of the equations set out in Chapter One are relevant. Within this framework one can draw an analogy between relativistic scattering and potential theory. The N/D equations take the place of Schroedinger's equation, and the potential is the function $B_\ell^L(s)$ derived from $R^{tu}=R^t+R^u$, with some contributions from R^s acting as a reaction to the potential. Unitarity is enforced in the strip between s_0 and s_1 which is dominated by the direct channel poles that we wish to calculate. Therefore $D_\ell(s)$ is taken to be cut only from threshold s_0 to the strip boundary s_1, and $N_\ell(s)$ carries, besides a left-hand cut, the remainder of the right-hand cut. The potential function $B_\ell^L(s)$ is equal to $B_\ell^\pm(s)$ except that the portion of the physical cut from s_0 to s_1 is removed. Equations (1.75), (1.76), (1.77) and (1.78) carry over immediately, unchanged except that the infinite upper integration limit is replaced in each case by s_1.

A slight complication arises because in general the dispersion numerators in these equations do not vanish at s_1, and so logarithmic singularities are introduced by this cutoff. It has been shown (76) that despite this the equations can be handled by straightforward means, and yield a unique solution provided that $\lambda_\ell \equiv \rho_\ell(s_1)\, Im\, B_\ell^L(s_1) \leq 1$. Other important properties of the N/D equations, such as analyticity in ℓ, have also been shown(77) to hold in the cutoff form, and all the conclusions reached previously are still valid.

The derivation of $B_\ell^L(s)$ in the Chew-Jones approximation is straightforward. Firstly, one must construct amplitudes of definite signature in the s-channel. The expression for this follows straight from eq.(1.45) giving $A^\pm(s,t)$ in terms of the double spectral functions. The function ρst is made up of the two strips R_1^s and R_1^t of Fig.2.4, ρsu contains R_2^u and R_2^s, and ρtu has R_1^u and R_2^t. These terms are of the form (2.11) with appropriate permutation of variables s, t and u (see Appendix). The portion of $A^\pm(s,t)$ which comes from $R^{tu}(s,t,u)$ by construction has no cut in s between s_0 and s_1, and so contributes unsubtracted to $B_\ell^L(s)$. The so-called "Wong projection"(78) eq.(1.79) is thus appropriate for this piece of potential, and, because it contains an integration

over only negative t-values, involves only real values of the trajectory and residue function. (The motive for extracting the factor $(-q_t^2)^{\alpha(t)}$ is thus apparent).

The direct channel poles R^s make a contribution to $B_\ell^{\pm}(s)$ in the $\int st$ and $\int su$ term of eq.(1.80) and it is clear that they give rise to a function cut in s between $-\infty$ and s_0-t, due to the s discontinuity of $q_s^{-2\ell}Q_\ell(1+t/2q_s^2)$, and also cut between s_0 and ∞ due to the s-discontinuity of the poles themselves. Therefore their contribution to $B_\ell^L(s)$ is simply calculated by expressing it as a dispersion integral over its left cut only (thus using $\alpha(s)$ and $\gamma(s)$ only where they are real), and neglecting the cut above s_0, which is expected to be small in the spirit of the model[75].

More detailed algebra is not very illuminating and therefore is set out in the Appendix for the special case of $\pi\pi$ elastic scattering, where it will be used for calculation in Chapter Four.

Jones[79] has analysed the strip approximation in detail, and demonstrated its internal consistency. He found from the form of the N/D equations that because calculated residues are given by the equation

$$\gamma(m^2) = Re\,\alpha'(m^2)\; N_\ell(m^2)/Re\,D_\ell'(m^2) \tag{2.15}$$

the asymptotic behaviour

$$\gamma(s) \xrightarrow[s\to\infty]{} Const.\; s^{\alpha(\infty)-1} \tag{2.16}$$

is forced upon them. Here $\alpha(\infty)$ is the dynamically determined asymptote of $\alpha(s)$, and provided $\alpha(\infty) \leq \frac{1}{2}$ the term R^s has high-s behaviour consistent with its being part of the t-channel background B^t. Such a restriction is obeyed in practice[80], and so this form of the interference model should commit no double counting.

6. Higher Born terms.

The Chew-Jones representation has been used for numerical calculation of pion-pion elastic scattering[80,81], with appropriate modifications to the formalism for these isospin one, odd G-parity particles. Prominent trajectories which couple to two pions[43] are the even signature P and P' of zero isospin, and the odd signature ρ meson of isospin one. A rho bootstrap[80] was successful to the extent that the input t and u channel trajectory could be reproduced in the s-channel below threshold. The output trajectory however did not pass through Re $\alpha=1$ at $s=m_\rho^2$, and although the I=1, $\ell=1$ cross section showed a peak at roughly the correct mass, it had a width above five times that seen experimentally[66]. Further, the overall slope of the self-consistent trajectory was very small, and the residues were large and in shape were not at all like those which are needed to fit high energy data[71].

In this calculation an I=0 s-channel trajectory appeared which had not been inserted in the input, and so a further investigation[81] included both P and ρ trajectories in a search for a completely self-consistent crossing symmetric amplitude. However, in this situation it was found that the attractive force coming from ρ exchange was completely swamped by a repulsion from the P. As a result, a dubious "normalisation" procedure suggested by Chew and Teplitz[82] to be used to obtain sensible results. Nevertheless, the self-consistent trajectories and residues thus calculated displayed just the same unsatisfactory features as the ρ trajectory of the first problem, because the normalised P contribution was essentially negligible.

The reason why the P gives a repulsion has been explained by Chew[83] on the basis of the Khuri-Jones[84] representation for a Regge pole. If only one trajectory α contributes to R^t, we can approximate it by a t-channel partial wave series.

$$R^t(s,t) = \sum_{l_t} (2l_t+1)\, R^t_{l_t}(t)\, P_{l_t}(z_t)\,, \tag{2.17}$$

with

$$R^t_{l_t}(t) = \frac{\gamma(t)}{l_t-\alpha(t)} \left(q_t^2\right)^{\alpha(t)} e^{-[l_t-\alpha(t)]\ln\left\{z_1(t)-\left[z_1^2(t)-1\right]^{1/2}\right\}} \tag{2.18}$$

where $z_1(t)=1+s/2q_t^2$. It is evident from (2.18) that if $\alpha(t)$, which is constrained by the Froissart[35]

bound to be less than 1 in the s-channel physical region, is greater than a given value of ℓ_t, then we can expect a negative contribution to $B^L_\ell(s)$ - a repulsion - from that partial wave. The lowest allowed value of ℓ_t is zero for an even signature trajectory and one for odd signature, and the contribution of each succeeding (even or odd respectively) partial wave will be much reduced over its predecessor by the exponential factor in (2.18). Thus, an even signature trajectory with $\alpha(t)$ above zero can be expected to give a repulsion, while an odd signature trajectory will give an attraction, if the relevant crossing matrix ($t \rightarrow s$) element is positive.

Where the series (2.17) converges (away from the double spectral function), $\mathrm{Im}R^t_{\ell_t}$ is constrained by unitarity to be positive, so that as this is not the case for P exchange alone, lower lying trajectories could be invoked to provide a cancellation. The normalisation procedure of Chew and Teplitz[82] was based on this idea and consisted of subtracting from the P exchange term $R^t_p(s,t)$ the piece $R^t_p(o,t)$, and adding back the latter partial wave by partial wave. Each partial wave was to be determined in a self-consistent way in each channel by a cycling process. The normalisation procedure is rather arbitrary, since the required cancellation could be provided by neglected pieces of double spectral function. Also, the

inclusion of low-lying trajectories may be in principle open to objection on grounds of double counting.

The Pomeranchuk repulsion has an important physical interpretation, as Chew[83] has discussed, and if a dynamical calculation is to give sensible results, it must be handled properly. To the extent that P exchange controls the diffraction peak, it models the effect of many channels opening at high energy. Thus, in analogy with the situation in nuclear physics, it is expected to narrow resonances and produce Regge trajectories rising to higher values of angular momentum. The important point is that the repulsion is of a longer range than most particle exchange forces, if the range for a given process is measured by the inverse of the logarithmic derivative of R_p^t with respect to t at $t=0$[83]. In a rough way the P repulsion, superposed on a shorter range attraction from the exchange of other quantum numbers, adds a lip to the potential well which traps particles longer and increases the changes of higher partial waves resonating.

A slight paradox arises here, because in potential scattering the presence of inelasticity always results in an effective force which has the properties of an attraction, increasing the binding of a bound state. (It is proportional to the absolute square of the off-diagonal elements of the potential

matrix)[85]. To the extent that potential scattering has been a reliable guide to hadron dynamics, one might expect a closely similar effect from the P, but this is not manifestly so. However, upon closer examination the point is resolved in an illuminating way.

Consider a Regge trajectory function with a dispersion representation of eq.(1.84). Since $\mathrm{Im}\,\alpha(s)$ is positive, $\alpha(s)$ is a Herglotz[86] function and therefore all its derivatives below threshold are positive. Using the identity

$$\left(\frac{\partial x}{\partial y}\right)_z \left(\frac{\partial y}{\partial z}\right)_x \left(\frac{\partial z}{\partial x}\right)_y \equiv -1$$

in the form

$$\left(\frac{\partial \alpha^{(n)}}{\partial \mathrm{Force}}\right)_s = -\left(\frac{\partial s}{\partial \mathrm{Force}}\right)_{\alpha^{(n)}} \left(\frac{\partial \alpha^{(n)}}{\partial s}\right)_{\mathrm{Force}} ,$$

we deduce

$$\delta\alpha^{(n)}(s_B) = -\alpha^{(n+1)}(s_B)\cdot \delta s_B \qquad (2.19)$$

In this expression $\alpha^{(n)}(s)$ is the n^{th} derivative of the trajectory function, $(n=0,1,2,3\ldots)$, and s_B is a position on the trajectory below threshold, say that of a bound state. Eq.(2.19) states that any force (such as inelasticity) which perturbs a bound state so as to increase its binding must not only raise the trajectory, but unless it is linear must also steepen it and make it attain higher values.

The sort of effect we envisage on this basis is for the raising of the trajectory to be accompanied by an increase in $\mathrm{Im}\alpha(s)$ at higher energies, to reflect that region's increased dynamical important. Further, the steepening will persist above threshold in the resonance region, to give more, narrower, recurrences.

We must expect that if the P is to represent the effects of inelasticity it must have not only a long range repulsive component, but a short range attractive one, so that bound states at least do not become less bound. A pure repulsion, which "unbinds" bound states, will not increase trajectory slopes.

From this discussion it is clear that the defects of the Chew-Jones representation are the lack of strength of the forces coming from crossed channel Regge poles (which means that calculated trajectories do not rise high enough), and the simultaneous lack of ability to handle the P repulsion in a satisfactory way. Another defect is the width of diffraction peaks calculated in this approximation is always too big[87] - the amplitude always falls away like t^{-1} (as compared with the observed possibly exponential decrease[88]).

A possible remedy for all these complaints may be achieved by including not only the Chew-Jones strips in the amplitude, but also the corners of the double spectral function between them (compare Fig.1.2

and Fig.2.4), where the latter are calculated using elastic unitarity according to Mandelstam's iteration method.

Before describing this we should point out that the explicit inclusion of several two-body channels in a strip approximation calculation (e.g. $\pi\pi$, $K\bar{K}$, $\pi\omega$, $\eta\rho$, $N\bar{N}$ etc.) has been tried[89] with rather disappointing results, so that before going on to tackle vastly complicated multichannel situations, we should make sure that a single channel calculation has been explored fully.

Equation (1.39) can be re-written in terms of $D_t^{\pm}(s,t)$ defined by (c.f. eqs.(1.44) and (1.45))

$$D_t^{\pm}(s,t) = \frac{1}{\pi}\int \frac{\rho_{st}(s',t) \pm \rho_{us}(s',t)}{s'-s}\,ds' + \frac{1}{\pi}\int \frac{\rho_{tu}(t,u') \pm \rho_{tu}(u',t)}{u'-u}\,du' , \quad (2.20)$$

whereupon it becomes

$$\rho(s,t) = \left(16\pi^2 q_s \sqrt{s}\right)^{-1} \iint \frac{D_t^{\pm}(s,t_1)\, D_t^{\pm}(s,t_2)}{K^{\frac{1}{2}}(s,t,t_1,t_2)}\,\theta(K)\,dt_1\,dt_2 . \quad (2.21)$$

The theta-function defines a region of integration in the t_1-t_2 plane which eq.(1.36) for K gives as

$$t^{\frac{1}{2}} \geqslant t_1^{\frac{1}{2}} + t_2^{\frac{1}{2}} \quad (2.22)$$

at $s=\infty$, and as a smaller region with a curved boundary for finite s[49]. Therefore an iterative procedure

for calculating the elastic double spectral function $\rho(s,t)$ using (2.20) and (2.21) emerges. For (2.22) states that to calculate $\rho(s,t)$ exactly at $t=\bar{t}$, we need to know $D^{\pm}_{t}(s,t)$ only for $t \leqslant \bar{t}$. Thus given a first approximation to $D^{\pm}_{t}(s,t)$ from the Chew-Jones representation, we may "fill in" the corners between the strips with the extra double spectral function implied by the presence of the original strips via elastic unitarity.

If in potential scattering (for a potential satisfying the Mandelstam representation) we were to calculate $\rho(s,t)$ using this procedure, given the first Born approximation to the amplitude as a starting point, at successive steps in the iteration we would in fact be calculating successive terms in the Born series(33). We can regard the Chew-Jones approximation analogously as the first Born terms in an expansion whose higher terms we propose to calculate, and therefore gain more insight as to why its initial applications failed.

We can see in a qualitative way that including the extra terms may go a long way towards remedying the defects we have described. In $\pi\pi$ scattering for example, the inclusion of extra powers of the effectively positive ρ-meson coupling will increase its strength, while the extra powers of the effectively negative P coupling will have alternating signs, so that there is some hope its fierce repulsion would be cancelled, and

its proper effects show as expected in the narrowing of resonances and steepening of trajectories. Also, if with the iterated P contribution included $D^{\pm}_{t}(s,t)$ changes sign for $t_0 \lesssim t \lesssim t_1$, $A(s,t)$ would fall off faster at negative t and a narrower s-channel diffraction peak, closer to experiment, would result[87].

7. Summary.

We have discussed the construction of an amplitude in accordance with the hypotheses of MAFK and MASK as an input to a dynamical calculation using the N/D method. The basic approach is through the interference model, which at present seems to contain no glaring inconsistencies, but which must be used with care. There is some hope of obtaining reasonable quantitative results if a formulation of the model due to Chew and Jones is augmented by adding to the Regge pole terms a "background" piece of double spectral function calculated by the Mandelstam iteration.

The inadequacy of the simple Chew-Jones approximation has caused a renewal of interest in the "old" form of the strip approximation[99, 109], in which elastic unitarity is used to calculate the complete double spectral function by iterating the discontinuity of the crossed-channel poles out to asymptotic values of t and then identifying the s-channel poles from

the asymptotic behaviour of the amplitude,
The numerical accuracy required to calculate trajectories in this way is very great, however, particularly in situations where several trajectories occur one below the other. Our alternative proposal will be advantageous if only a few iterations are needed to get a good approximation to the potential. To test whether our approach is likely to succeed we shall describe in the next Chapter a calculation in potential scattering using similar techniques to attack a soluble problem[90]. This is a preliminary to calculations of pion-pion scattering, which will be described in Chapter Four.

TABLE 2.1. Pion-Nucleon Resonances. Positions and widths are in MeV. Positions with a question mark refer to structures not plainly "resonant".

Partial Wave	This calculation			Phase shift Analysis		
	Position	Width	Elasticity	Position	Width	Elasticity
S_{11}	2100 ?	-	-	1535	120	0.35
				1710	300	0.8
P_{11}	1450	250	0.55	1470	210	0.65
	2000 ?	-	-	1750	330	0.32
P_{13}	1860	300	0.3	1863	300	0.21
D_{13}	1550	300	0.55	1520	115	0.55
				2057	290	0.26
D_{15}	1700	250	0.45	1680	170	0.40
F_{15}	1530	250	0.2	1690	130	0.65
F_{17}	1500	300	0.25	1983	225	0.13
G_{17}	2010	200	0.2	2200	300	0.35
G_{19}	2150	250	0.15	-	-	-
S_{31}	1320	150	0.4	1640	180	0.3
P_{31}	1700	300	0.35	1934	340	0.3
P_{33}	1300	200	0.4	1236	125	1.0
				1688	280	0.1
D_{33}	1700	300	0.15	1691	270	0.14
D_{35}	1700	200	0.1	1954	310	0.15
F_{35}	1550	300	0.1	1913	350	0.16
F_{37}	1550	400	0.1	1950	220	0.4
G_{37}	1350	150	0.01	-	-	-
G_{39}	1500	300	0.01	-	-	-

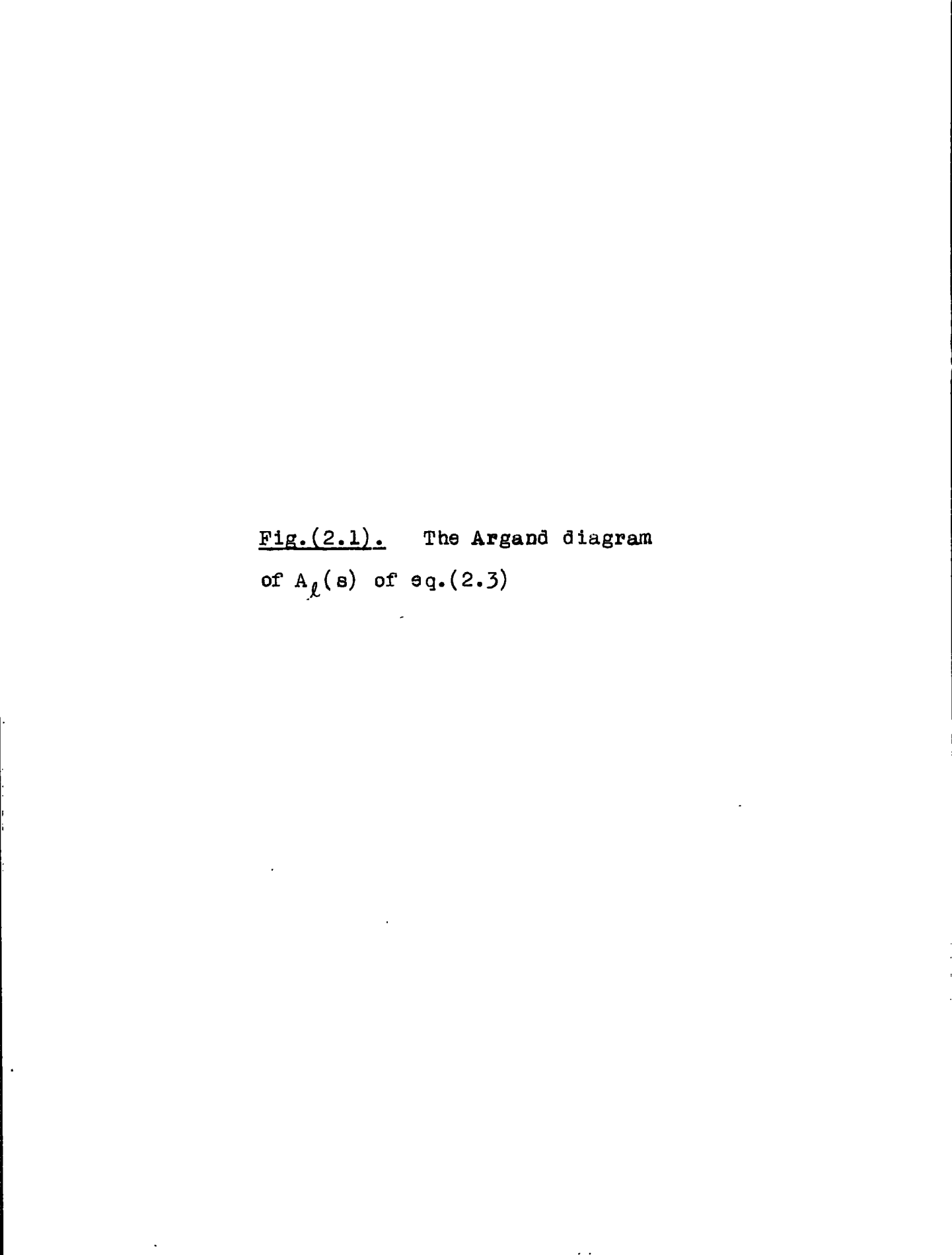

Fig.(2.1). The Argand diagram of $A_\ell(s)$ of eq.(2.3)

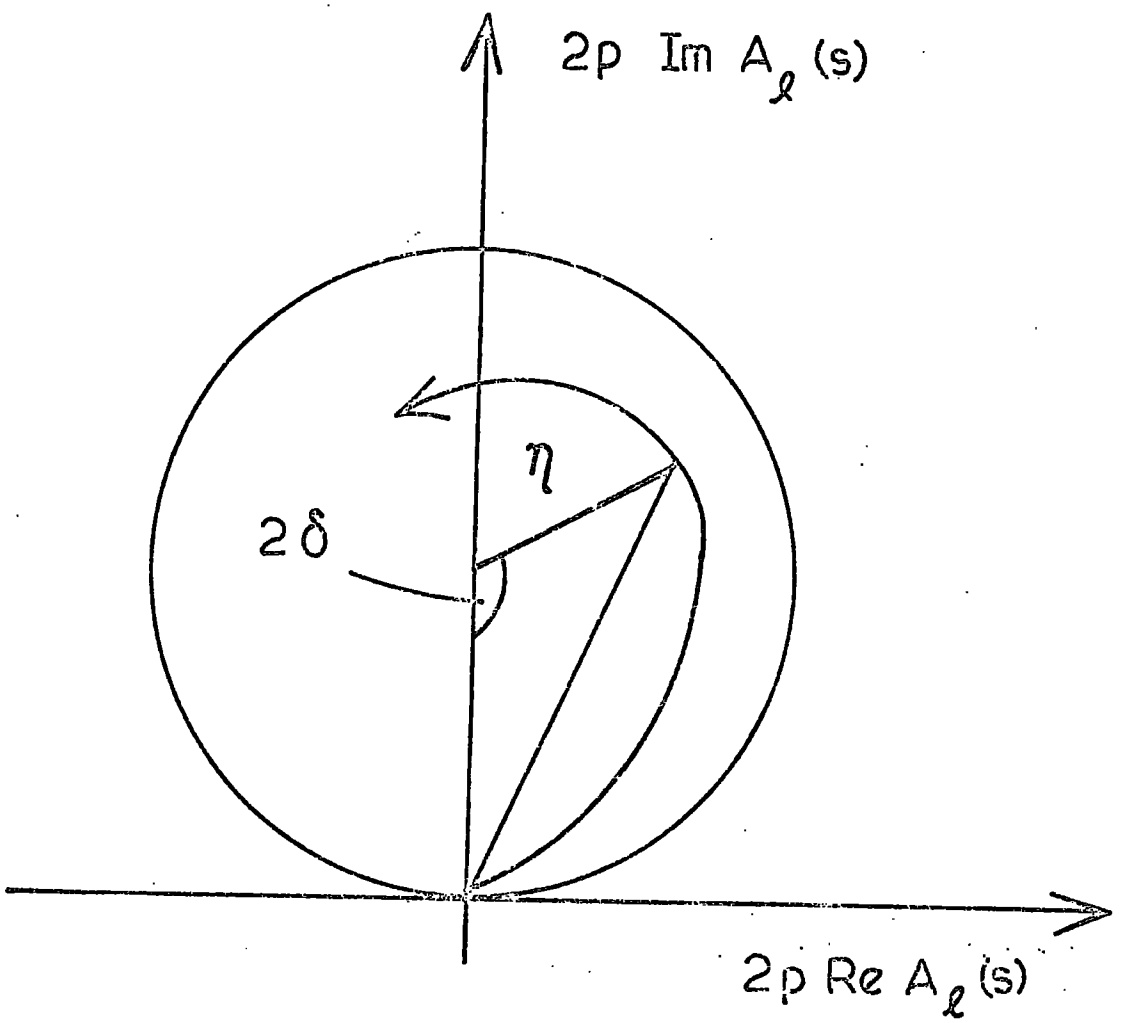

FIG. 2.1

Fig.(2.2). Trajectories for the scalar meson example, with a linear input trajectory of the form a+bt. "Resonance" energy on the output Schmid loops is taken to be where the phase shift moves fastest with s.

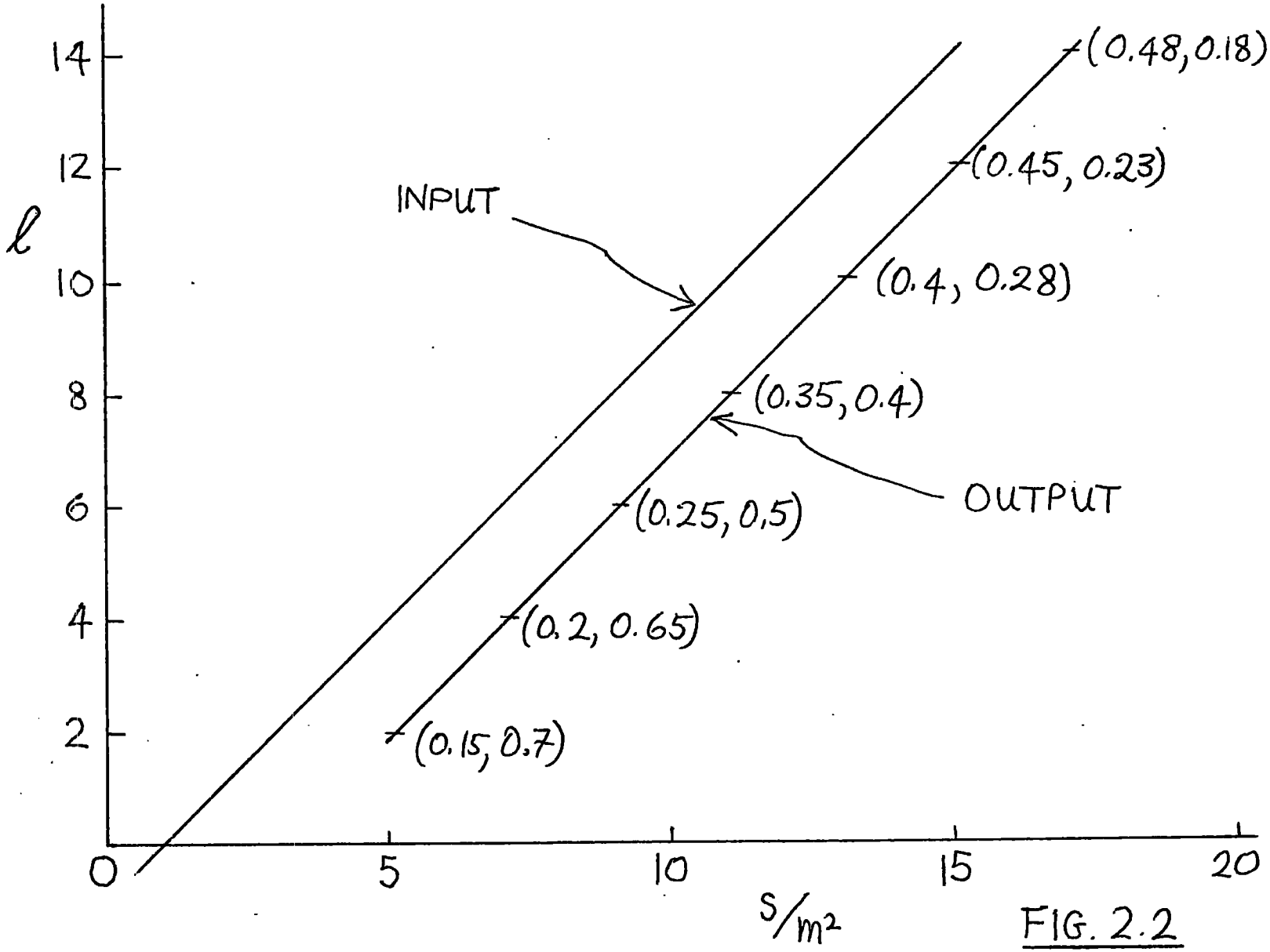
14
12
10
8
6
4
2
ℓ
INPUT
OUTPUT
(0.48, 0.18)
(0.45, 0.23)
(0.4, 0.28)
(0.35, 0.4)
(0.25, 0.5)
(0.2, 0.65)
(0.15, 0.7)
0
5
10
15
20
S/m²

FIG. 2.2

Fig.(2.3). The Schmid loops for the partial waves which correspond most closely to the phase shift results. The full lines are our calculated curves, and the dashed lines are the curves deduced by the CERN analysis, Ref.65. We take the "resonance" point to be where the phase shift moves fastest with s, and we indicate energies in the centre of mass system in MeV.

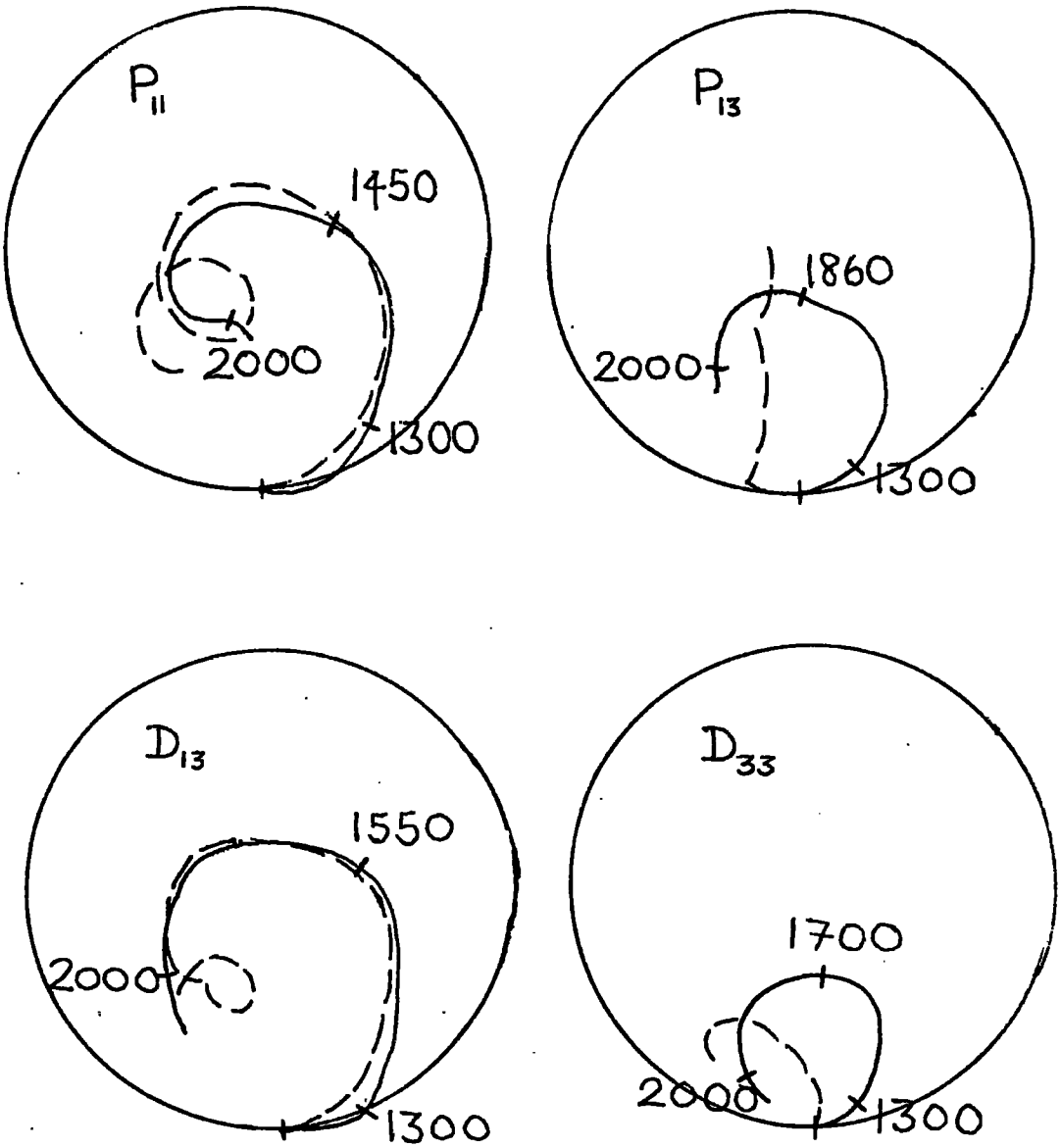
P11
1450
2000
1300
P13
1860
2000
1300
D13
1550
2000
1300
D33
1700
2000
1300

FIG. 2.3

Fig.(2.4). The Mandelstam diagram showing the strips of double spectral function parameterised by Chew and Jones. The notation is explained in the text.

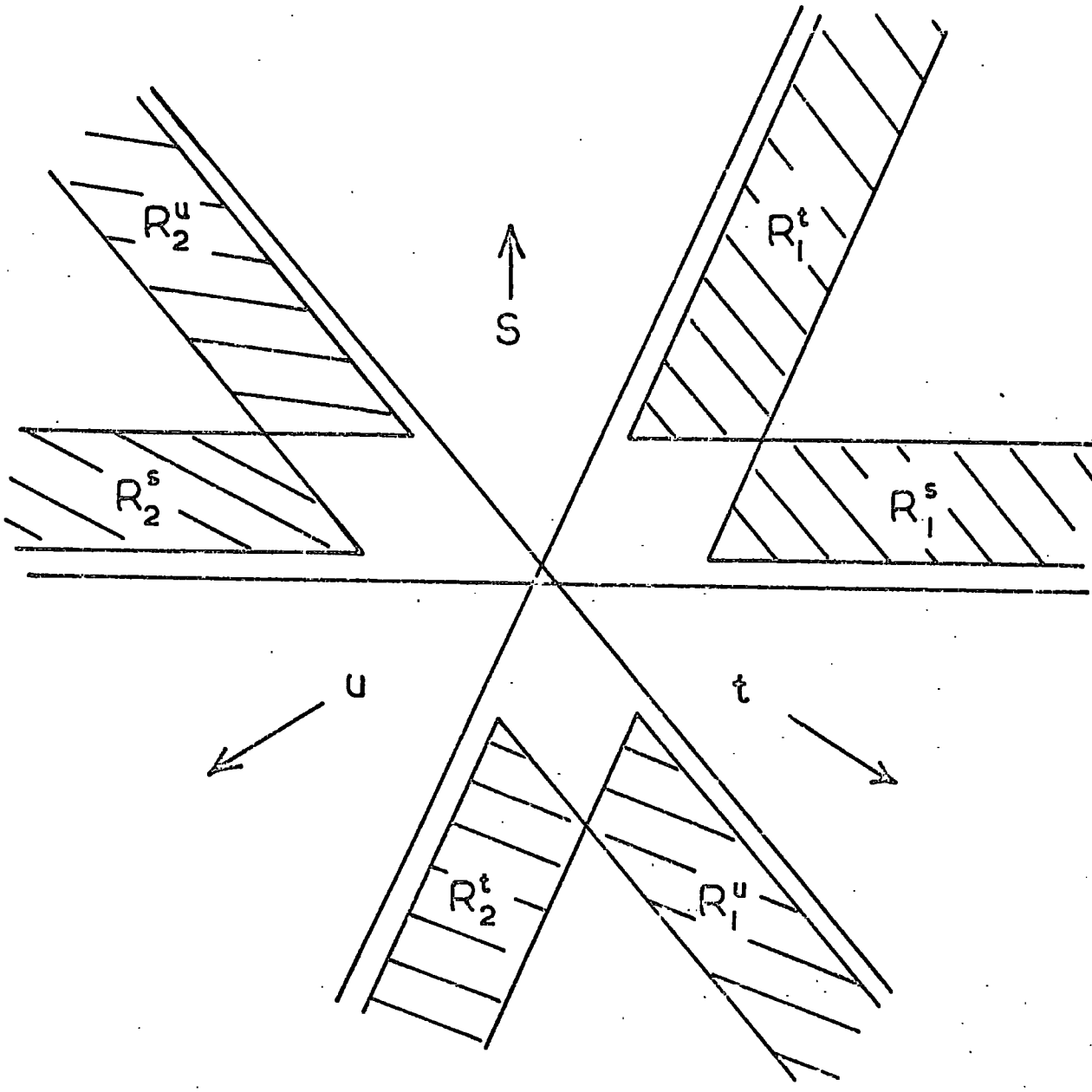

FIG. 2.4

C H A P T E R T H R E E

The Use of Born Approximations in N/D Calculations.

1. Introduction.

We have seen that the forces which generate strongly interacting particles are likely to contain both attractive and repulsive components. This has created difficulties in dynamical calculations where the potention function $B^L_l(s)$ used as input to the N/D equations has been known in only what is essentially the first Born approximation.

It has been found[81] that if a repulsive force is combined with an attractive one in this approximation the effect of the repulsion is often to give stronger binding, i.e., to act as an attraction, in a situation where the opposite should occur.

This fact has been commented on by Kayser[91], and has been noted since by many authors[92-95], particularly in the context of the Dashen-Frautschi type of perturbation calculation.

What is worse, if the repulsion is really strong, it is possible for "ghosts" - in this context resonances with negative residues - to appear[81]. These violate causality, and, like the unexpected attraction, must be due to the inadequacy of the approximation used.

We have described similar defects of the Chew-Jones representation as an approximation to the full potential, and have suggested that a remedy

lies in the inclusion of extra double spectral function, i.e., higher Born terms.

The full Born series for the left-hand cut is of course prohibitively difficult to calculate, and so the question arises as to the order of approximation which is needed to give satisfactory accuracy in an N/D calculation. In other words, we wish to gain some idea of how much double spectral function must be calculated via (elastic) unitarity. The best way of trying to assess this is to examine the situation in single channel potential scattering where we can compare the solution of the N/D equations for various types of potentials treated in various Born approximations with the exact solution of the corresponding Schroedinger equation. We know of course that if we were able to use the exact left-hand cut, the N/D equation would give the exact answer.

Luming [97] has examined the problem for a single attractive potential in the first and second Born approximations, and here we extend his work to include the third Born approximations and also to consider combinations of potentials of different signs and ranges. It is anticipated that this will give us guidance as to the likelihood of obtaining reasonable results with similar approximations to the double spectral functions and left-hand cut in strong interactions.

In the next Section we give some necessary formalism, and in the following one explain how one is able to calculate the lowest orders of approximation to $B_\ell^L(s)$. In Section 4 we give numerical examples which demonstrate how various approximations break down. Section 5 contains an examination of an instructive analytically soluble model, and in the final Section are our conclusions.

2. Formalism of Potential Scattering.

The numerical calculations are made for the nonrelativistic scattering of equal mass scalar particles due to a superposition of N simple Yukawa potentials. Taking $\hbar=c=1$ and choosing the external mas m=1, in the centre of mass system (CMS), the radial Schroedinger equation is

$$\psi''(r) + \left\{ q_s^2 - V(r) - \ell(\ell+1)r^{-2} \right\} \psi(r) = 0, \qquad (3.1)$$

where q_s is the magnitude of the momentum of the particles. The potential is

$$V_i(r) = g_i \frac{e^{-m_i r}}{r}, \qquad (3.2)$$

where

$$V(r) = \sum_{i=1}^{N} V_i(r). \qquad (3.3)$$

Defining the CMS scattering angle to be θ, we introduce variables (corresponding to the invariants of eqs.(1.12) and (1.13)),

$$s=4(1+q_s^2) \tag{3.4}$$

$$t=-(\text{CMS momentum transfer})^2$$

$$=-2q_s^2(1-\cos\theta) \tag{3.5}$$

There is of course no crossing symmetry and we do not consider exchange potentials. The appropriately modified hypotheses of MAFK and MASK hold for the scattering amplitude[42], which therefore has a Mandelstam representation with s and t cuts[33], and displays Regge asymptotic behaviour in t[3]. We can then write a fixed energy dispersion relation of the form (1.44)

$$A(s,t) = \frac{1}{\pi}\int^{\infty} \frac{D_t(s,t')}{t'-t}\,dt' \,, \tag{3.6}$$

and separating out the poles in t[49] we also have

$$D_t(s,t) = \pi\sum_{i=1}^{N} g_i\,\delta(m_i^2-t) + \frac{1}{\pi}\int_{s_0(t)}^{\infty} \frac{\rho(s',t)}{s'-s}\,ds' \,, \tag{3.7}$$

where $s_0(t)$ is the boundary of the double spectral function $\rho(s,t)$ in the s-t plane.

The partial wave series for A(s,t) is of the form (1.41), and "reduced" partial wave amplitudes are defined as in (1.69) and uniquely interpolated in ℓ by the Froissart-Gribov formula (c.f.eq.(1.49))

$$B_\ell(s) = \left(32\pi^2 q_s^{2\ell+2}\right)^{-1} \int^{\infty} Q_\ell(\cos\theta)\, D_t(s,t)\, dt . \tag{3.8}$$

Because there is no u-cut there is no problem of signature.

The N/D equations for B (s) follow exactly as in Section 5 of Chapter One, except that now the phase space factor is

$$\rho_\ell(s) = q_s^{2\ell+1} . \tag{3.9}$$

Using the formula (3.7) the analogue of eq.(1.81) is

$$B_\ell^L(s) = \left(32\pi\, q_s^{2\ell+2}\right)^{-1} \sum_{i=1}^{N} g_i\, Q_\ell\left(1+\frac{m_i^2}{2q_s^2}\right)$$

$$+\left(32\pi^3\right)^{-1} \iint^{\infty} \frac{\rho(s',t)}{s'-s} \left\{ \frac{Q_\ell\left(1+t/2q_{s'}^2\right)}{q_{s'}^{2\ell+2}} - \frac{Q_\ell\left(1+t/2q_s^2\right)}{q_s^{2\ell+2}} \right\} ds'\, dt . \tag{3.10}$$

For our approximations to $\rho(s,t)$ it will be evident that the integrals in (3.10) converge and

$$B_\ell^L(s) \xrightarrow[s\to\infty]{} \text{const.}\ \frac{\ln s}{s^{\ell+1}} . \tag{3.11}$$

From (1.70)(97),

$$N_\ell(s) \xrightarrow[s\to\infty]{} \frac{\text{Const.}}{s} \tag{3.12}$$

neglecting now logarithmic factors (c.f.eq.(1.73a)), so that the N/D equations are well-defined for $-1 < \ell < 3/2$.

In practice, for numerical calculation the infinite upper limits of the N/D equation are replaced by a cutoff s_1, and, as we have already mentioned, this introduced no essential difficulty(76). The equation can be solved by standard matrix inversion techniques(81,98), and the solution is found to be practically independent of s_1, if this is taken sufficiently large.

3. Calculation of Double Spectral Function.

We now turn to the problem of calculating $\rho(s,t)$ using the Mandelstam iteration.

When we refer to the potential function as determined in the n^{th} Born approximation, we mean that it is derived from g_i, m_i and from $\rho(s,t)$ correct to order g_i^n, for all i=1...N. If we were to use this $\rho(s,t)$ in (3.7) to calculate $D_t(s,t)$, and then applied (3.6) to find A(s,t), this would be equivalent to summing the first n terms of the Born series(33). The amplitude would not of course be unitary. What we shall in fact do is to solve the N/D equations, as described above, with $B_\ell^I(s)$ known to the n^{th} Born approximation, and this of course will not give the same results because we shall be enforcing unitarity on our amplitude.

The potential in the first Born approximation is found by setting $\rho(s,t,)=0$ and keeping only the

pole terms in eq.(3.10). Higher Born terms are calculated using eq.(3.7) (c.f.eq.(2.20) and the analogue of eq.(2.21), which in this nonrelativistic situation is (c.f. eqs.(3.9) and (1.71))

$$\rho(s,t) = \left(32\pi^2 q_s\right)^{-1} \iint \frac{D_t(s_+,t_1)\, D_t(s_-,t_2)}{K^{1/2}(s,t,t_1,t_2)}\, \theta(K)\, dt_1\, dt_2 . \qquad (3.13)$$

Eq.(1.36) defines K.

As outlined in the previous Chapter, it is possible to use this equation to calculate the n^{th} Born term from the previous n-1. If we regard Yukawa potential scattering as representing the exchange of a particle, this is analogous to calculating a given ladder graph from a knowledge of the lower order ones, beginning with the single particle exchange diagram - the pole term. For example, when we calculate to order n=3 for N=2 different Yukawa potentials, we sum the graphs depicted in Fig.3.1.

We can find $\rho(s,t)$ explicitly for n=2 and n=3 as follows. Using only the pole term of (3.17) for D_t in (3.13) we derive

$$\rho^{(2)}(s,t) = \sum_{i,j=1}^{N} \rho_{ij}^{(2)}(s,t) , \qquad (3.14)$$

where

$$\rho^{(2)}_{ij}(s,t) = \pi a_{ij}(t) \left\{ s - s_0^{ij}(t) \right\}^{-1/2} , \tag{3.15}$$

and

$$a_{ij}(t) = \frac{g_i g_j}{16\pi} \left\{ t \left[t + \frac{(m_i^2 - m_j^2)^2}{t} - 2(m_i^2 + m_j^2) \right] \right\}^{-1/2} . \tag{3.16}$$

There are $\frac{1}{2}N(N+1)$ distinct terms in the double sum of (3.14) because of the i-j symmetry. (This is evident from the graphs of Fig.3.1).

Each distinct piece of double spectral function $\rho^{(2)}_{ij}(s,t,)$ has a boundary in the s-t plane given by $s=s^{ij}_0(t)=4(1+(m_i m_j)^2 \left[t+\frac{(m_i^2 - m_j^2)^2}{t} -2(m_i^2+m_j^2) \right]^{-1})$. (3.17)
Using (3.7) we then derive

$$D_t^{(2)}(s,t) = \text{pole terms} + \sum_{i,j=1}^{N} D_t^{(2)ij}(s,t) , \tag{3.18}$$

where

$$\begin{aligned} Re\, D_t^{(2)ij}(s,t) &= \pi a_{ij}(t) \left\{ s_0^{ij}(t) - s \right\}^{-1/2} , \\ Im\, D_t^{(2)ij}(s,t) &= 0 , \end{aligned} \tag{3.19}$$

for $s \leq s_0^{ij}(t)$, and

$$\begin{aligned} Re\, D_t^{(2)ij}(s,t) &= 0 , \\ Im\, D_t^{(2)ij}(s,t) &= \rho^{(2)}_{ij}(s,t) , \end{aligned} \tag{3.20}$$

for $s \geq s_0^{ij}(t)$.

Using (3.13) again we find

$$\rho^{(3)}(s,t) = \rho^{(2)}(s,t) + \sum_{i,j,k=1}^{N} \rho^{(3)}_{ijk}(s,t) \quad , \tag{3.21}$$

where terms of order g^3 are given by

$$\rho^{(3)}_{ijk}(s,t) = \frac{g_i}{32\pi q_s} \iint \frac{\delta(m_i^2 - t_1)\ \mathrm{Re}\, D_t^{(2)jk}(s,t_2)\ \theta(K)}{K^{1/2}(s,t,t_1,t_2)}\, dt_1\, dt_2 . \tag{3.22}$$

Using (3.19) this becomes

$$\rho^{(3)}_{ijk}(s,t) = \frac{g_i g_j g_k}{16} \int_{m_j^2+m_k^2}^{L(s,t)} \left\{(-1)(ax^2+2b_1x+c_1)(ax^2+2b_2x+c_2)\right\}^{-1/2} dx \tag{3.23}$$

where we write

$$\begin{aligned} a &= s-4 \\ b_1 &= a(m_1^2+t)+2tm_1^2 \\ c_1 &= a(m_1^2-t)^2 \\ b_2 &= a(m_j^2+m_k^2)+2m_j^2m_k^2 \\ c_2 &= a(m_j^2-m_k^2)^2 \end{aligned} \tag{3.24}$$

We see that symmetry in j and k leaves only N(N+1) distinct terms in the triple sum of (3.21), as might be expected from the graphs of Fig.3.1.

The upper limit of the integral in (3.23) is given by the lowest zero of the denominator

$$L(s,t) = \frac{1}{a(s)} \left\{ \left[b_1^2(t) - a(s)c_1(t) \right]^{1/2} - b_1(t) \right\} \quad , \tag{3.25}$$

and the boundary of $\rho^{(3)}_{ijk}(s,t)$ in the s-t plane is given by

$$L(s,t)=(m_j+m_k)^2, \tag{3.26}$$

which has a solution which we write as

$$s=s_0{}^{ijk}(t). \tag{3.27}$$

In Fig.(3.2) we depict the s-t plane and show the boundaries of $\rho^{(2)}_{ij}(s,t)$ and $\rho^{(3)}_{ijk}(s,t)$ for the case N=2.

The general features of $\rho^{(3)}_{ijk}(s,t)$ are easily found from the expression of (3.24). We find that

$$\rho^{(3)}_{ijk}(s_0{}^{ijk}(t),t)=0, \tag{3.28}$$

and that all the derivatives of $\rho^{(3)}_{ijk}(s,t)$ at $s=s_0{}^{ijk}(t)$ are infinite. Therefore, from its boundary, the function rises sharply to a peak, and then falls away, going eventually proportional to s^{-1} at fixed t and to $t^{-3/2}$ at fixed s. Its main features are sketched in Fig.3.3. This behaviour is to be contrasted with that of $\rho^{(2)}_{ij}(s,t)$, which has an inverse square root singularity at its boundary, and falls monotonically in both s and t, being asymptotically proportional to $s^{-\frac{1}{2}}$ at fixed t and to t^{-1} at fixed s.

The double spectral function cannot readily be calculated to higher order, but the general features are clear. Successively higher terms would have less pronounced peaking close to their boundary, and would fall away faster at high s and t.

The first point agrees with the findings of Bali[99] and of Bransden et al.[100], whose double spectral functions were calculated from the exchange of a Breit-Wigner shape for the ρ-meson in $\pi\pi$ scattering. They found oscillations corresponding to the boundary peaks which died away quickly with increasing t. We obtain more severe oscillations since we are iterating a δ-function, but the singularity at the boundary disappears by the time the third Born term is reached. The oscillations make it extremely difficult to calculate (numerically) higher Born terms for more than one Yukawa potential[101].

The second point follows by inspection of (3.13) and it is clear that successive terms in the iteration have improved asymptotic behaviour by a factor $\sim(st)^{-\frac{1}{2}}$ over their predecessors. We note, however, that the sum of the infinite series - the total double spectral function - must have asymptotic behaviour proportional to $t^{\alpha(s)}$ when it is calculated completely. It is clear that in this case, including terms up to order g^3 only, all our infinite integrals (eqs.(3.10), (1.75) and (1.78)), will converge, and we can solve the N/D equations.

4. Numerical Examples.

In this Section we present, mainly in graphical form, the results of solving the N/D equations with potentials calculated in the manner just described, and compare them with the solution to the corresponding Schroedinger equation[103]. We are mainly interested in potential strengths which are similar to those found in strong interaction physics. The relevant parameter is g/m, where m is the mass of the exchanged particle in units of the reduced mass of the scattering system. According to the calculations of Finkelstein[104], the equivalent, energy-dependent, potential due to the exchange of the ρ-meson in $\pi-\pi$ scattering will correspond to $g/m \approx 3$, over the range of energies between threshold and $100m^2$, and this is a fairly typical order of magnitude for such forces.

Firstly, in Fig.3.4, we plot the position of an S-wave bound state resulting from a single unit range ($m_i=1$) Yukawa potential of the form (3.3) as a function of the strength of the coupling, g_i. Corresponding curves (except for the inclusion of the third Born approximation) are to be found in Refs. 97 and 102. We see that the first Born approximation is not really satisfactory if the potential is strong enough to produce a bound state, but that the third Born approximation is quite good even for large

couplings, and also gives quite a satisfactory account of the secondary bound state which appears for $g > 6.5$.

The corresponding trajectories for two different couplings are given in Fig.3.5, and again for the weaker force, the third Born approximation is very good.

Evidently a very strong force is needed to produce a P-wave resonance. If we arrange combinations of attractive and repulsive potentials to produce the same S- or P-wave states, as in Fig.3.6, we get a somewhat steeper and certainly higher-rising trajectory the larger is the repulsion. It is also found that the width of the P-wave resonance is smaller with a larger repulsion, and this is exactly the effect which we hope for from the P repulsion in dynamical calculations.

Next we want to see how good the various Born approximations are for producing trajectories when both attractive and repulsive forces are present. In Fig.3.7 we show the results for a comparatively weak attractive force and various long-range repulsions. Evidently the lower Born approximations are much less accurate than they are when there is only one attractive force. Indeed we see in Fig.3.8 that the lower Born approximations give trajectories that are in the wrong order - i.e., the trajectory is more

highly bound the stronger is the attraction. This effect is shown with greater clarity in Fig.3.9 where we plot the change in the position of an S-wave bound state due to the presence of a fixed repulsion against the coupling strength of the attractive force. The response of the exact solution to the repulsive perturbation is almost independent of how deeply the state is bound, but this is certainly not true of the lower approximations. Only the third Born approximation is able to give reasonable results for a wide range of couplings.

In Fig.3.10 we plot the same effect the other way round, that is, we fix the strength of the attraction and vary the repulsion. We have chosen a case where none of the Born approximations gives a satisfactory result in that the response in each case is in the wrong direction. The important thing is that as the repulsion is increased, there comes a point at which the position of the bound state has moved off to $s=-\infty$. If the repulsion is increased beyond this the "ghost" phenomenon, mentioned above, appears.

This is readily explained if we examine the behaviour of the corresponding N- and D- functions with, for example, the first Born approximation to $B_{\ell}^{L}(s)$ (see also ref.81). Fig.3.11a shows the form of N- and D- functions when a normal bound state is

produced. In Fig.3.11b more repulsion has been added and the bound state becomes more tightly bound. A further increase in the repulsion results is the development of a pole in the N-function at threshold, as the position of the bound state moves to $-\infty$, and the N- and D-functions flip their signs near threshold. The first zero of the D-function, shown in Fig.11e, corresponds not to a resonance but to a ghost. An examination of (1.78), the equation for N, shows why this happens. The sign change occurs at the point where the integral vanishes at threshold, and we get $N \approx B^L$. Increasing the repulsion further results in the ghost moving first a little closer to threshold, and then further away, finally to vanish as the dip in the D-function fails to reach zero (as in Fig.3.12). Ghosts thus arise only after the bound state has moved off to $-\infty$.

It is evident from Fig.3.9 that the way to check that the order of Born approximation used is adequate is to ensure that when a suitable repulsion is added the bound state is really repelled, and (Fig.3.10) that the amount by which it moves is roughly proportional to the strength of the repulsion. If it is not, a higher approximation is needed. We can anticipate from these examples that whereas the first Born approximation, which is usually used, will nearly

always be unsatisfactory unless the coupling is very weak, the third Born approximation is likely to be good for most of the types of forces encountered in strong interactions, and indeed for rather stronger ones.

5. A Soluble Model.

It is interesting to look at some of the anomalous properties of repulsive forces in a simple soluble model.

Following Kayser[94], we consider S-wave scattering with nonrelativistic kinematics, replacing the left-hand cut by simple poles. With one pole the potential function is

$$B^L(s)=\frac{\lambda}{q_s^2+a^2}\ , \tag{3.29}$$

(a real and positive), which is well-known[105] to be the first Born approximation to the potential

$$V(r) = -4\lambda a\, e^{-2ar}. \tag{3.30}$$

For $\lambda > 2a$, the potential function (3.29) gives rise to a bound state on the physical sheet. If a small long-range perturbation is added, in the form of a second pole at $q_s^2=b^2$, $(b < a)$, the small shift in the bound state position is easily calculated by the Dashen-Frautschi[96] method. Kayser[94] has shown that for weak binding, such that the bound state lies to the right of $q_s^2=-b^2$, a repulsive perturbation

moves the bound state towards threshold, in the correct manner. For a stronger binding force, however, where the bound state lies between the two left-hand poles, a repulsive perturbation appears to act like an extra binding force, moving the bound state to the left.

The reason for this is easily found. The potential function (3.29) is the full left-hand cut for the potential(106).

$$V(r) = \frac{-4\lambda e^{-2ar}}{\left(1+\frac{\lambda}{2a}e^{-2ar}\right)^2} . \tag{3.31}$$

The addition of the second pole at $q_s^2=b^2$, of residue λ' gives the first Born approximation to the potential

$$V(r) = -4\lambda a e^{-2ar} - 4\lambda' b e^{-2br}, \tag{3.32}$$

or the full left-hand cut for the potential(107)

$$V(r) = 2\frac{\left[\frac{d}{dr}F(r)\right]^2 - F(r)\frac{d^2}{dr^2}F(r)}{\left[F(r)\right]^2} \tag{3.33}$$

where

$$F(r) = 1+\frac{\lambda}{2a}e^{-2ar}+\frac{\lambda'}{2b}e^{-2br}-\frac{\lambda\lambda'}{a+b}e^{-(a+b)r} . \tag{3.34}$$

For small λ,λ' the potentials (3.32) and (3.33) are quite similar, and as λ,λ' approach zero (3.33) approaches (3.32).

For large λ i.e., a strong attraction, expressions (3.32) and (3.33) are very different, and it is evident that $\lambda' < 0$ can no longer be interpreted as corresponding to a simple repulsive force.

The conclusion to be drawn from this example is that a given potential function $B_\ell^L(s)$, which corresponds to some Born approximation to a given force, also represents the complete Born series for an often completely different force, which coincides with the first only in the limit of weak coupling. This gives us some insight into the qualitative features of the numerical results presented in Section 4 (although, unlike this example, our results do not depend on the bound state being inside the left-hand cut).

Kayser[94] has shown that these considerations enable us to understand a similar problem, presented by Sawyer[93], in connection with the Dashen-Frautschi method. If the force producing a bound state is approximated by a simple pole, and if the pole is moved slightly to the left, leading, according to (3.29) and (3.30), to a weakening of the binding force because of the decrease of its range, a Dashen-Frautschi calculation predicts that the bound state becomes more tightly bound. By inspection of (3.31), however, it is clear that an increase of a does not correspond simply to a decrease in the range of V(r);

the change is more complicated, and as Kayser has shown, leads not to a weakening but to a strengthening of the binding force. Therefore the result of the perturbation calculation of Sawyer is in no way anomalous (c.f. ref.95).

Unfortunately this simple model is unable to encompass the ghosts which our numerical calculations have produced. The left-hand poles correspond to a potential V(r) that satisfies the conditions for the amplitude to have a Mandelstam representation(33). Therefore causality will not be violated and ghosts cannot be produced. The potentials V(r) corresponding to the functions $B_\ell^L(s)$ used in our numerical calculations must violate the Mandelstam representation. Our approximations have mutilated the analytic properties of the potentials to such an extent that they cease to bear any relation to the forces they are supposed to approximate, and therefore nonsensical results occur.

6. Summary.

We have solved the N/D equation for potential scattering with various Born approximations to the left-hand cut, and compared the results with the corresponding exact solutions. It turns out that the first Born approximation, which is most commonly used,

is often quite inadequate, especially when we have to deal with combinations of attractive and repulsive forces. In this situation repulsions may have anomalous effects, leading to spurious attractions, and possibly to ghosts. Both of these unpleasant features are removed for a wide variety of potential strengths, including those likely to be encountered in particle physics, if the third Born approximation is used.

We therefore have good reason to hope for considerable improvement over previous work in a calculation of strong interaction dynamics based on the Chew-Jones representation augmented by higher Born terms in the form of extra "corner" pieces of double spectral function. We have a little reservation, however, because these examples have not thrown very much light on the way to handle the peculiar features of the P repulsion, because this force is hardly likely to bear much resemblance to a simple energy-independant Yukawa potential.

In the next Chapter we describe some calculations of pion-pion elastic scattering, using the augmented Chew-Jones representation for the scattering amplitude.

Fig.(3.1). The unitarity diagrams for two different Yukawa potentials up to the third Born approximation.

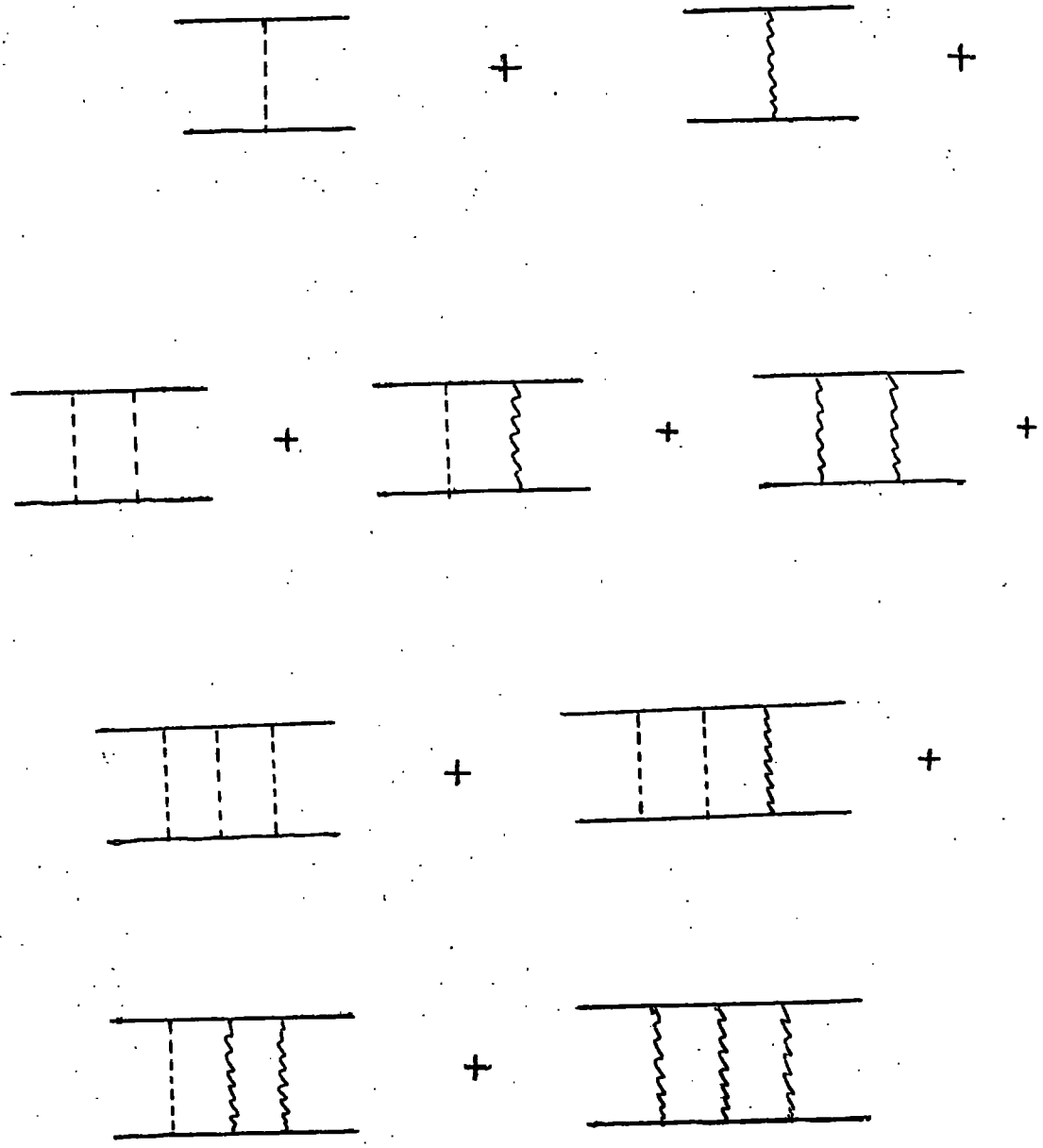

FIG. 3.1

Fig.(3.2). A sketch of the s-t plane singularities for two Yukawa potentials, showing the positions of the poles at $t=m_1^2$, and $t=m_2^2$, and the curved boundaries of the double spectral function for the second and third Born approximations.

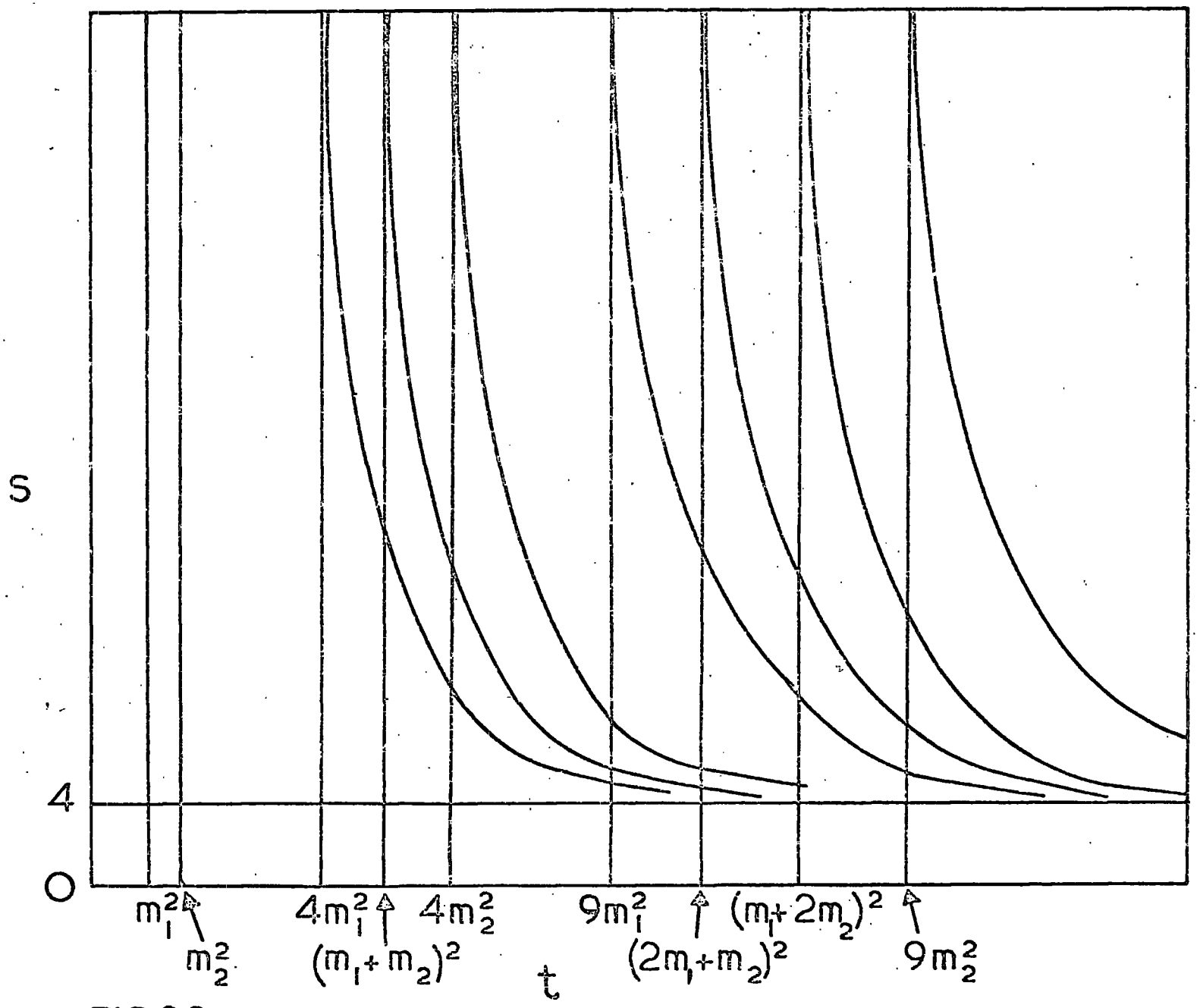

FIG.3.2

Fig.(3.3). A piece of double spectral function $\rho^{(3)}_{ijk}(s,t)$ plotted against t for three values of s.

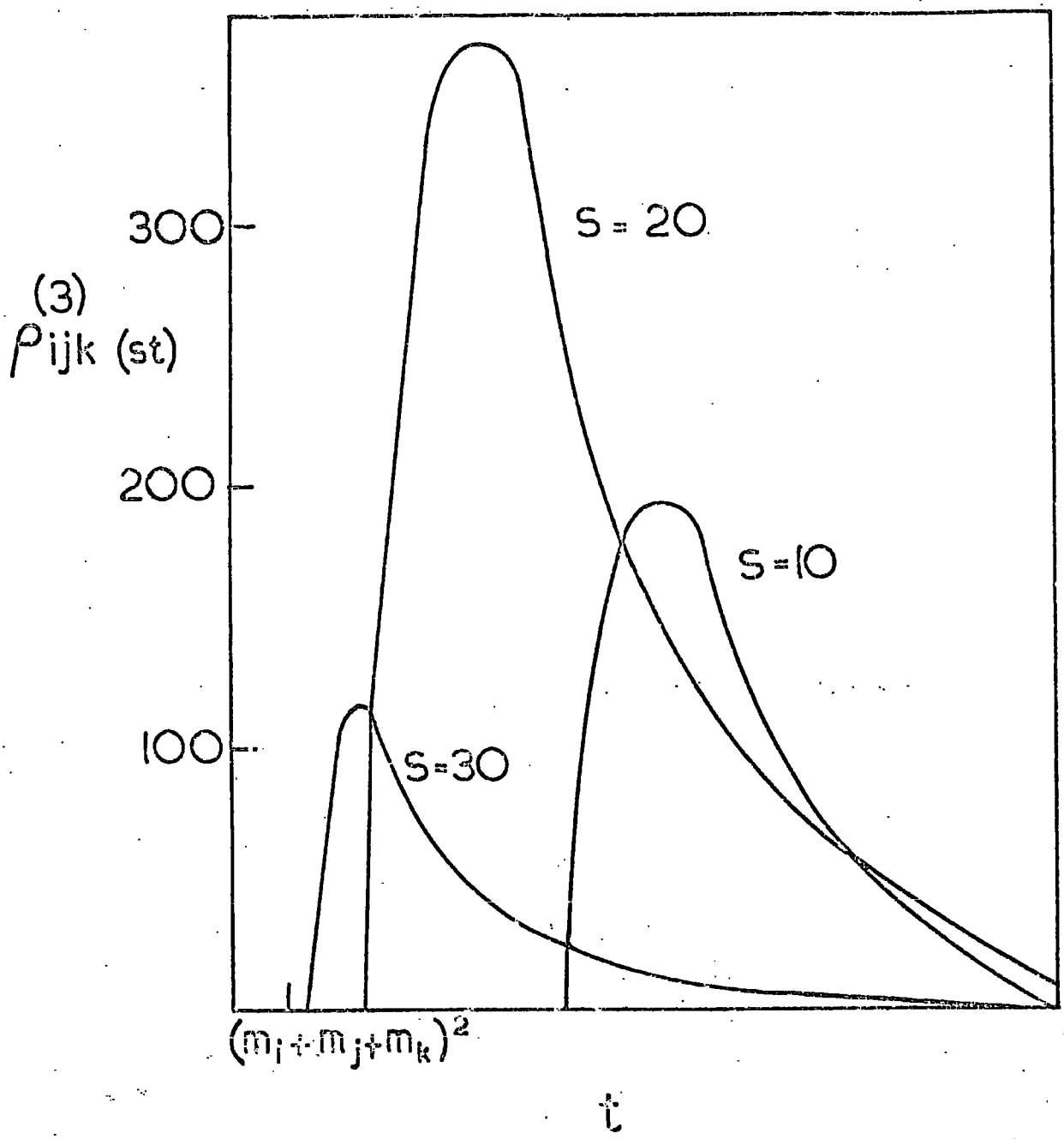

FIG.3.3

Fig.(3.4). S-wave bound state positions plotted against coupling constant for a single unit range attractive Yukawa potential. Here and throughout the symbols E, B3, B2, B1 denote the exact, third Born, second Born, and first Born approximations respectively, and the primary and secondary bound states are indicated in each case.

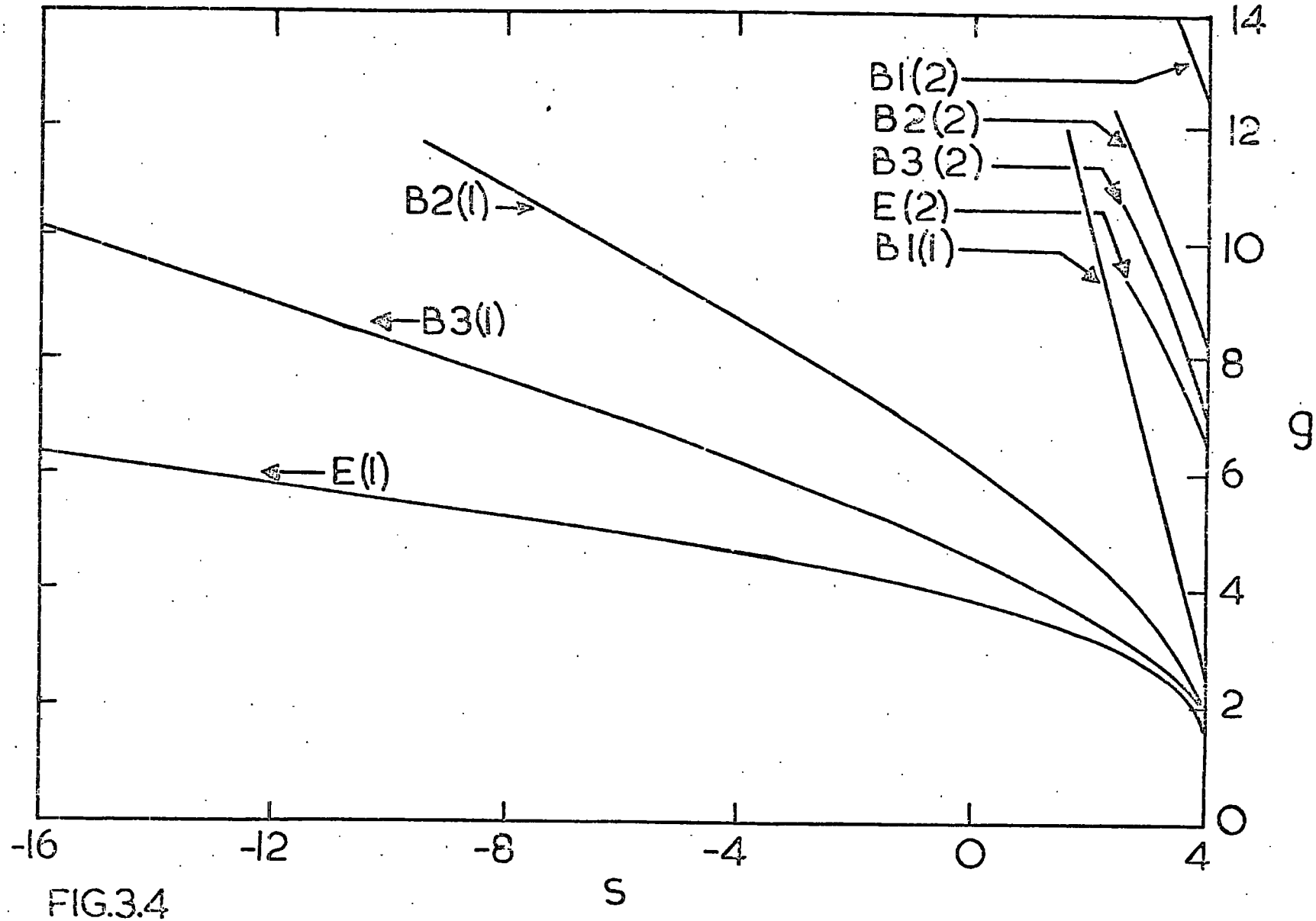

FIG.3.4

Fig.(3.5). Regge trajectories for a single attractive Yukawa potential; (a) $V=-3e^{-r}/r$; (b) $V=-8e^{-r}/r$. The notation is as for Fig.(3.4).

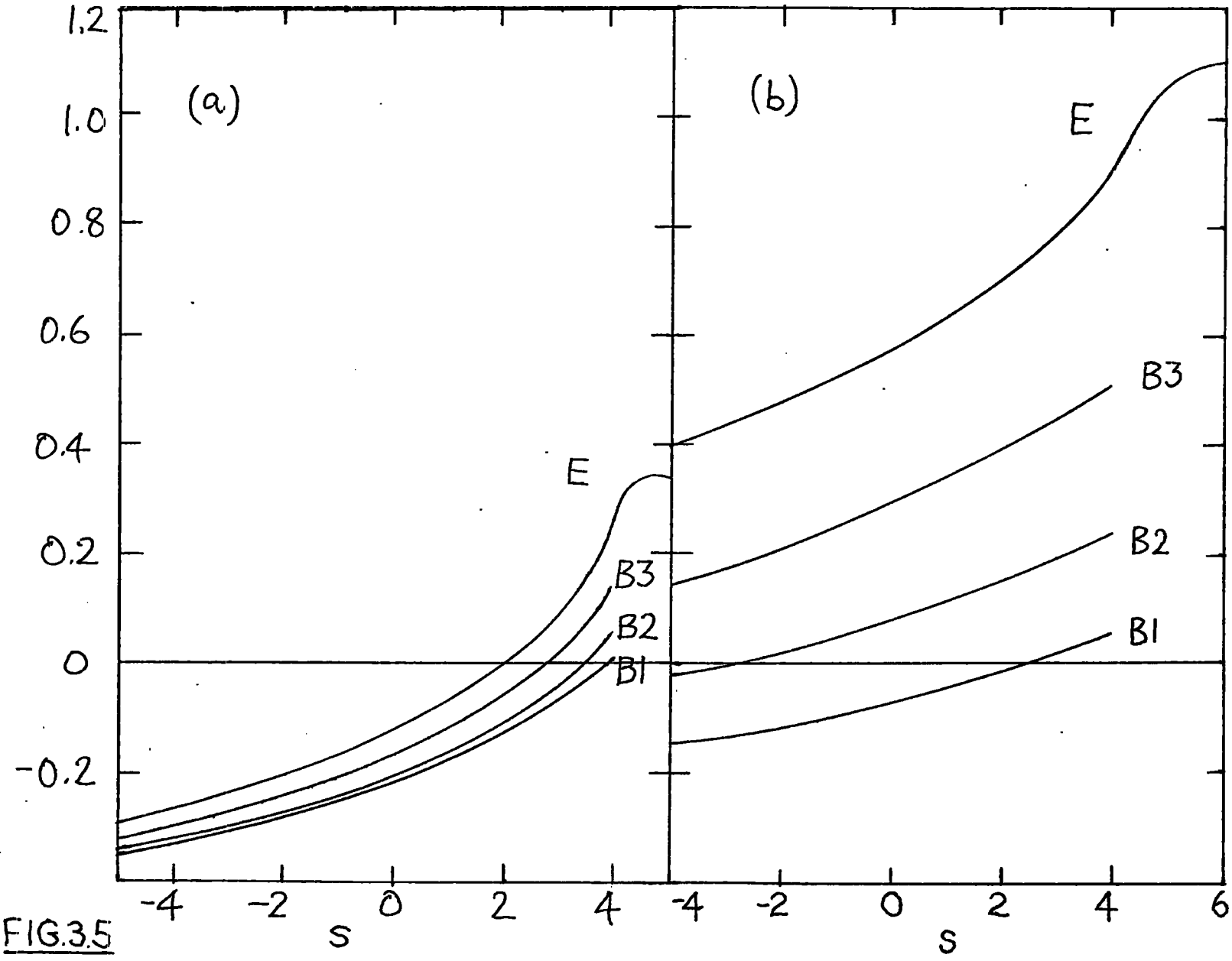

FIG.3.5

Fig.(3.6). An S-wave bound state and a P-wave resonance produced by various forces.

The potentials for the P-wave resonance are:-

(a) $V=-24.3e^{-r}/r + 7.5e^{-0.3r}/r$,

(b) $V=-18e^{-r}/r + 5e^{-0.3r}/r$,

(c) $V=-8e^{-r}/r$;

and for the S-wave bound state:-

(d) $V=-14e^{-r}/r + 3.8e^{-0.3}/r$,

(e) $V=-7e^{-r}/r + 2e^{-0.3r}/r$,

(f) $V=-3e^{-r}/r$.

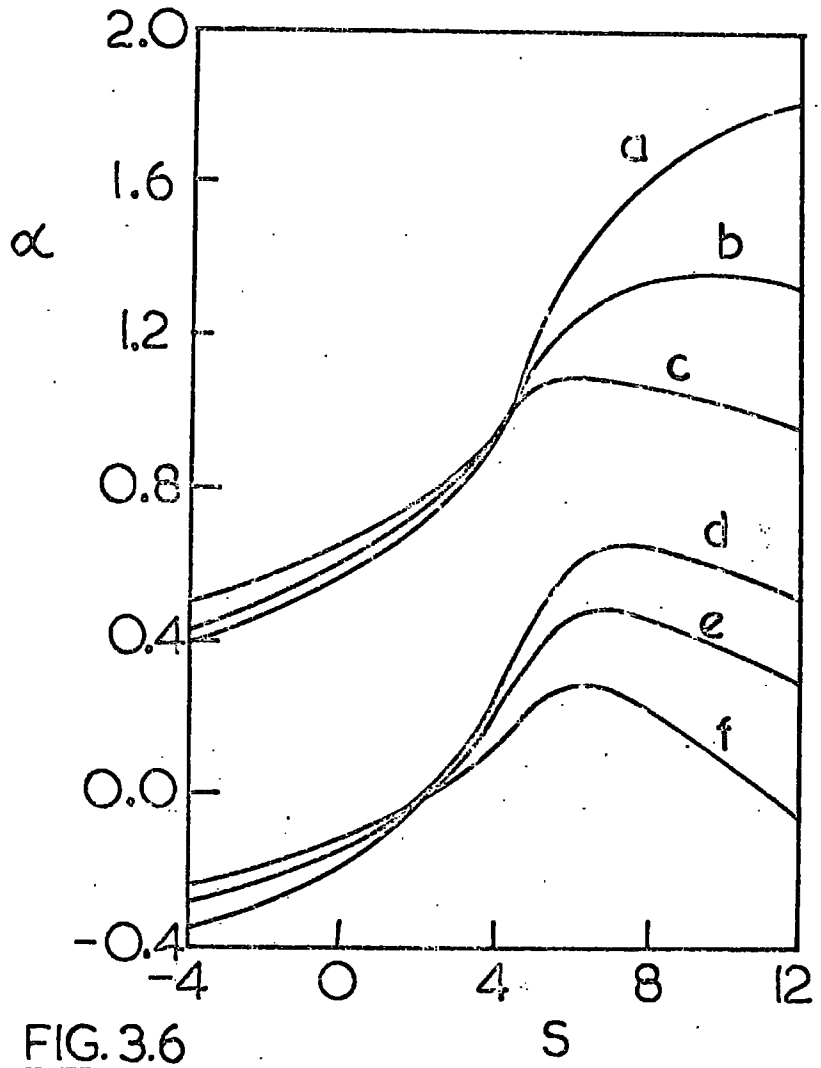

FIG. 3.6

Fig.(3.7). Regge trajectories for attractive forces combined with various longer range repulsions. The potentials are:-

(a) $V=-3e^{-r}/r$,

(b) $V=-3e^{-r}/r + 0.5e^{-0.3r}/r$,

(c) $V=-3e^{-r}/r + 1.0e^{-0.3r}/r$.

The notation is as for Fig.(3.4).

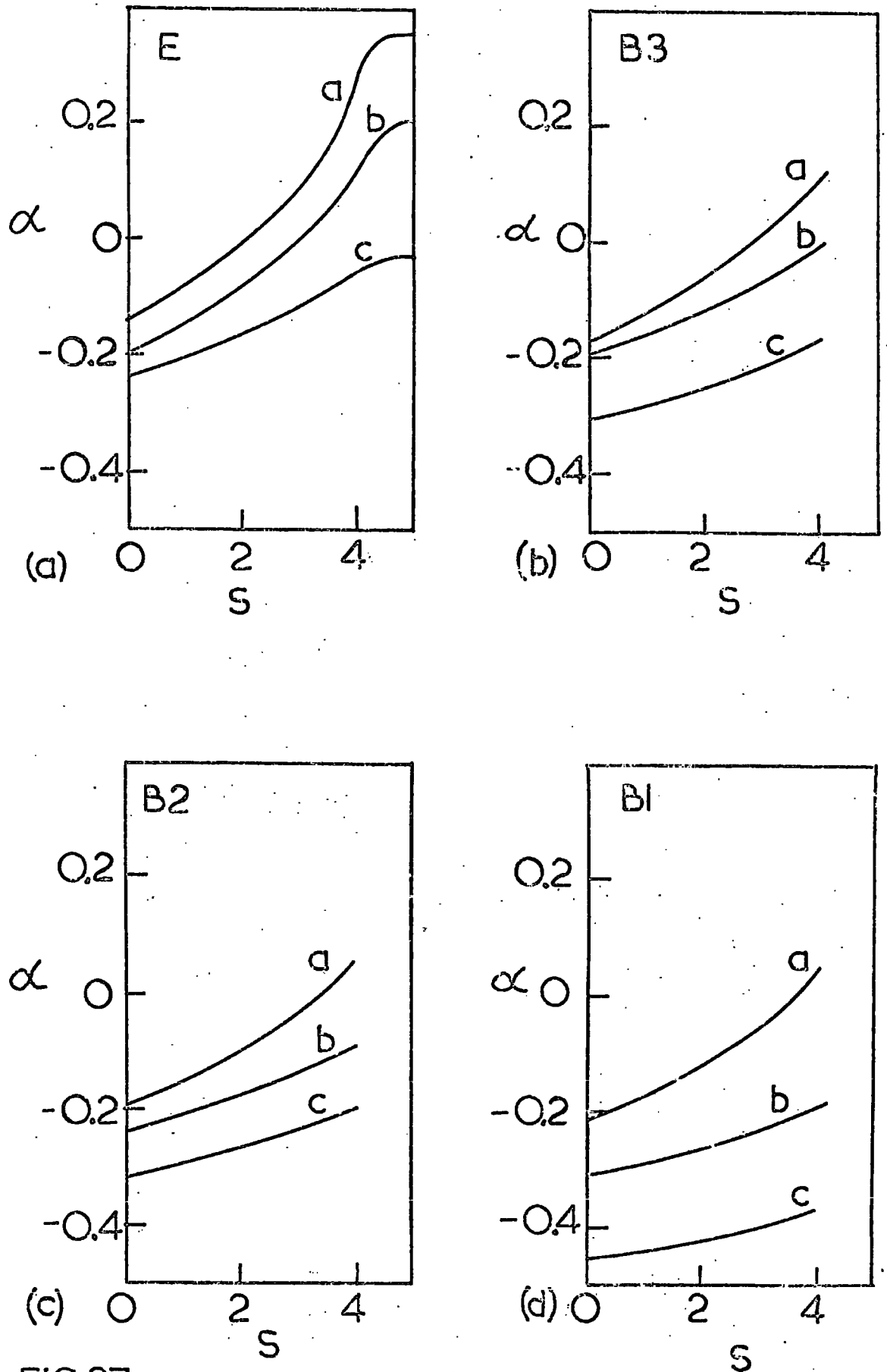
E
a
b
c
0.2
0
-0.2
-0.4
α
(a)
0
2
4
S
B3
a
b
c
0.2
0
-0.2
-0.4
α
(b)
0
2
4
S
B2
a
b
c
0.2
0
-0.2
-0.4
α
(c)
0
2
4
S
B1
a
b
c
0.2
0
-0.2
-0.4
α
(d)
0
2
4
S

FIG. 3.7

Fig.(3.8). Regge trajectories as for Fig.(3.7) but with a stronger attraction. The three cases are:-

(a) $V=-8e^{-r}/r$,

(b) $V=-8e^{-r}/r + 1.5e^{-0.3r}/r$,

(c) $V=-8e^{-r}/r + 3.0e^{-0.3r}/r$.

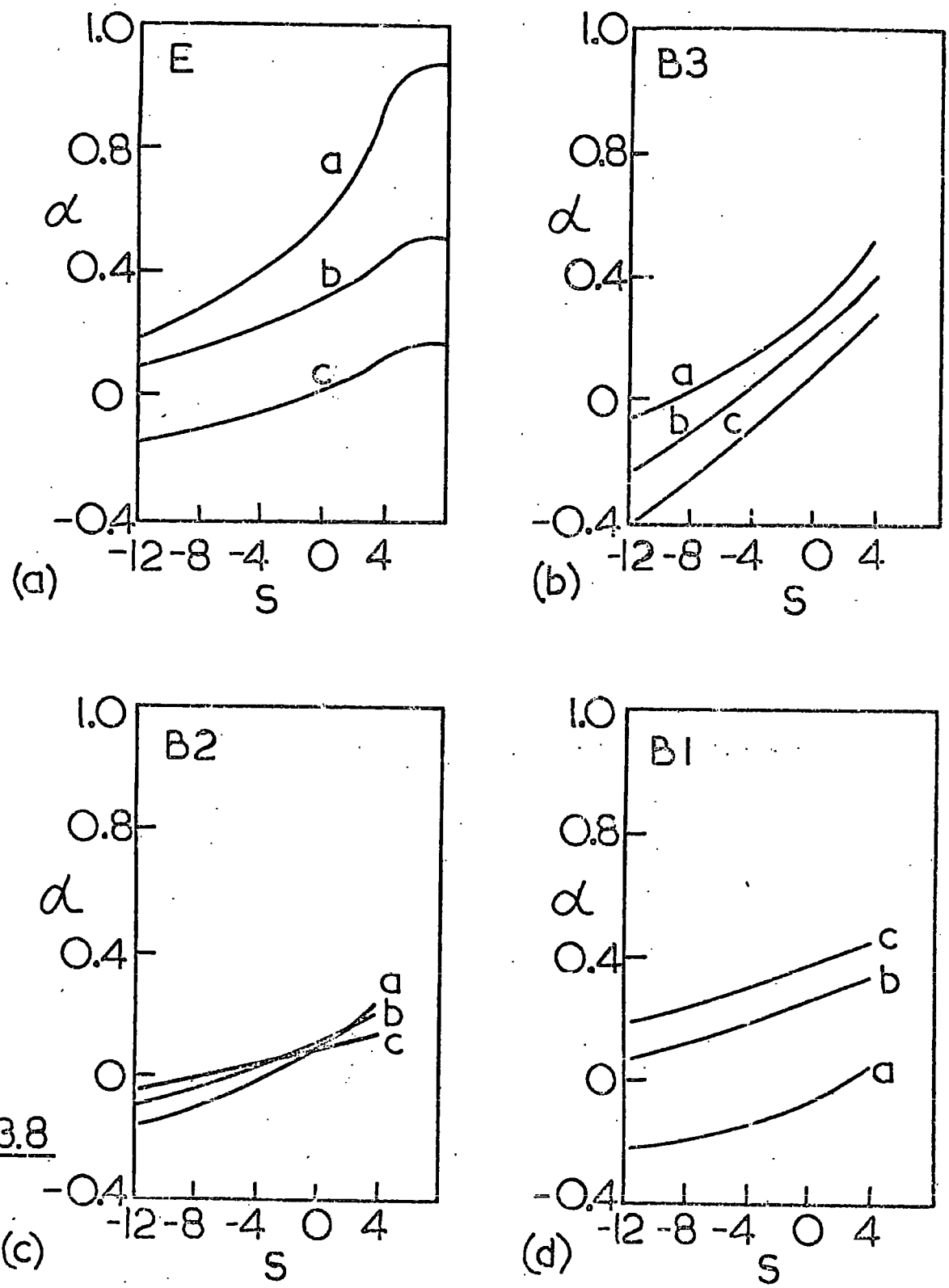

FIG. 3.8

Fig.(3.9). The shift δs_b of the bound state position when the potential $V=-g_A e^{-r}/r$ is changed to $V=-g_A e^{-r}/r + 0.1e^{-0.3r}/r$. The notation is as for Fig.(3.4).

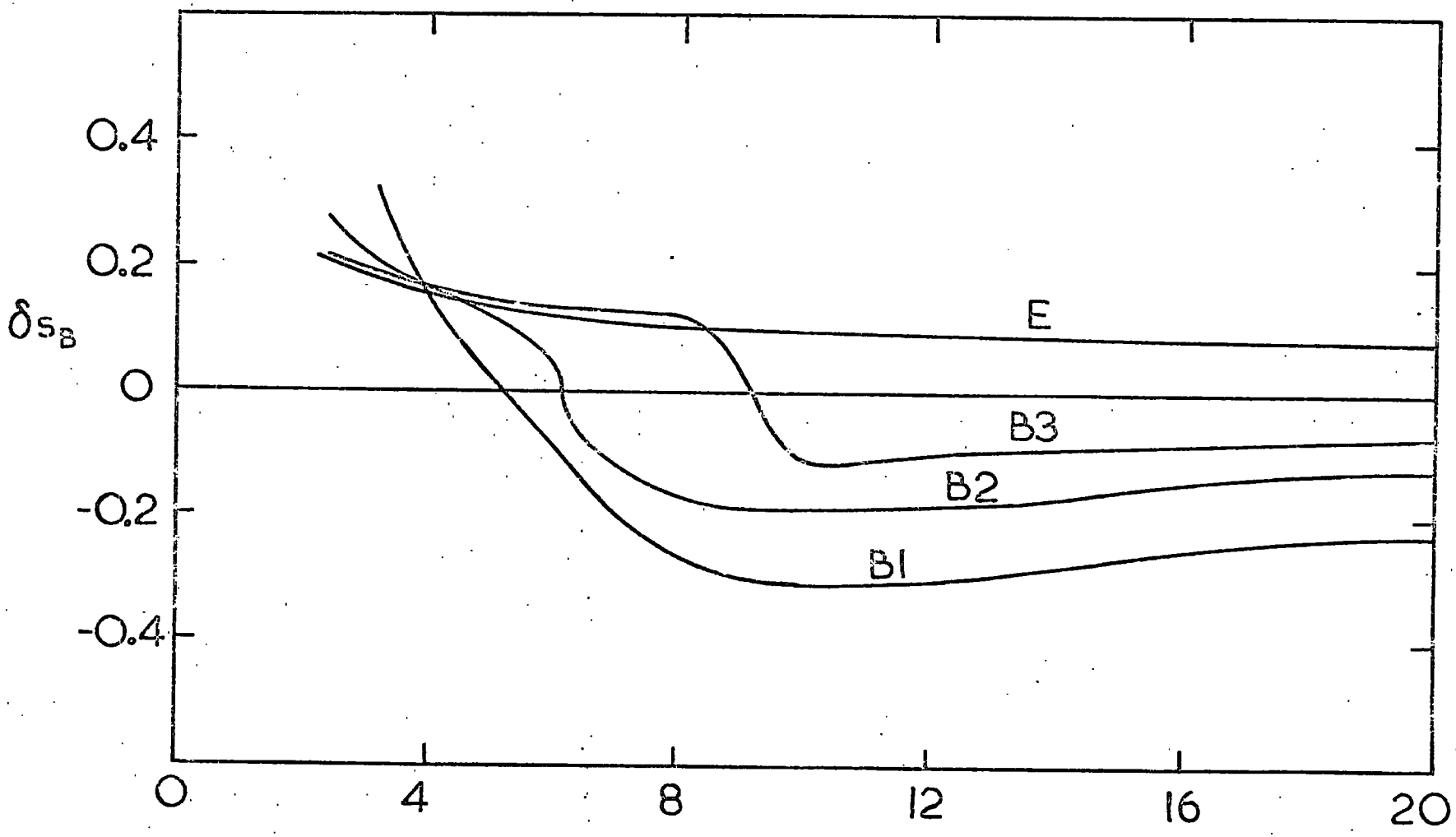

FIG. 3.9

Fig.(3.10). The shift $\delta\varsigma_B$ of bound state position when the potential $V=-11e^{-r}/r$ is changed to $V=-11e^{-r}/r + g_R e^{-0.3r}/r$. The notation is as for Fig.(3.4).

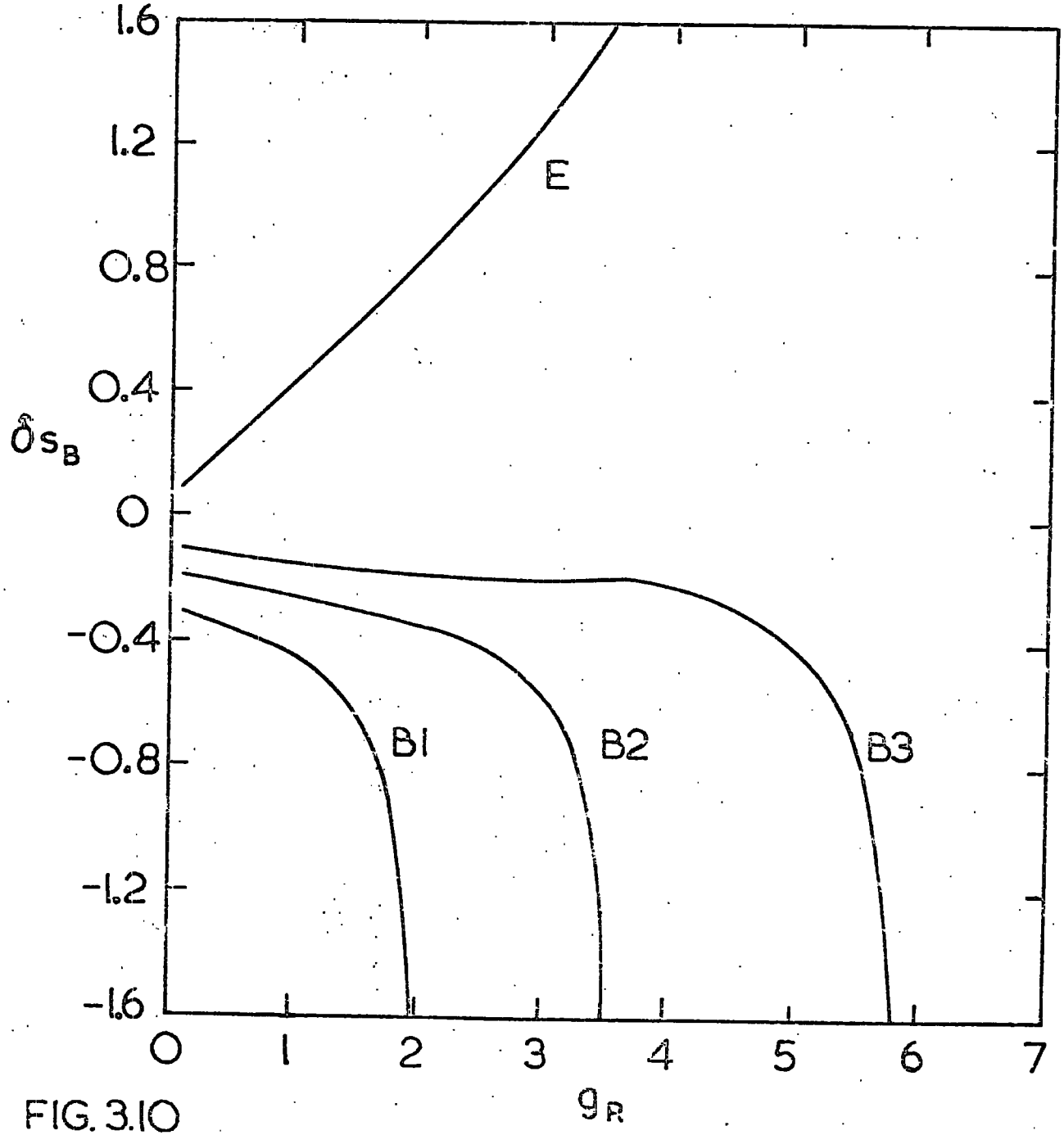

FIG. 3.10

Fig.(3.11). A sketch of the potential function $B_0^L(s)$, and the N- and D-functions, for the potential $V=-11e^{-r}/r + g_R e^{-0.3r}/r$ in first Born approximation. The three cases are:

(a) $g_R = 2.7$,

(b) $g_R = 3.0$,

(c) $g_R = 3.3$.

Over this range, $B_0^L(s)$ changes only slightly.

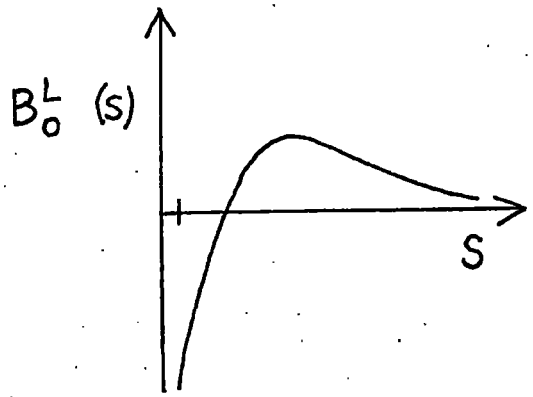

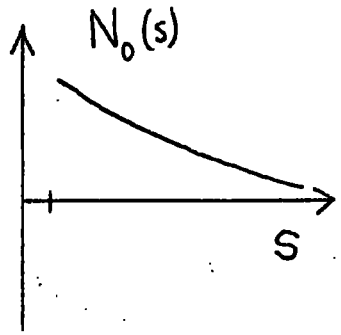

(a)

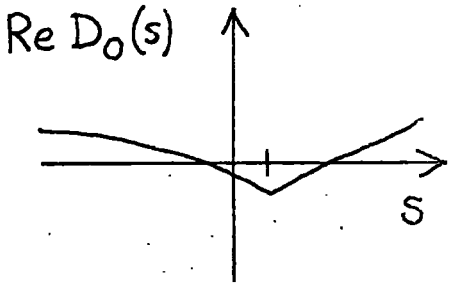

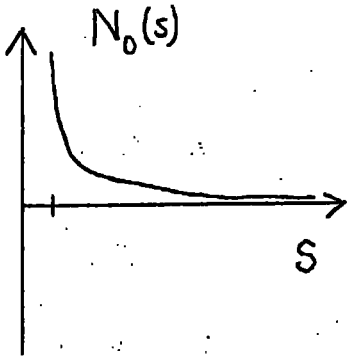

(b)

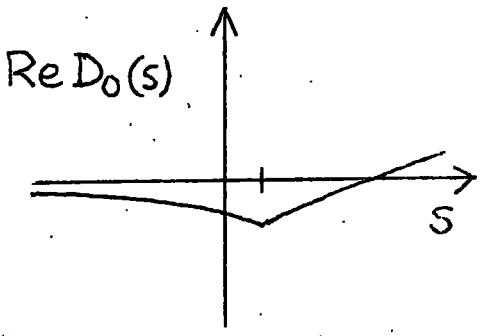

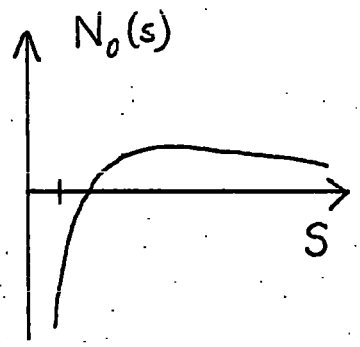

(c)

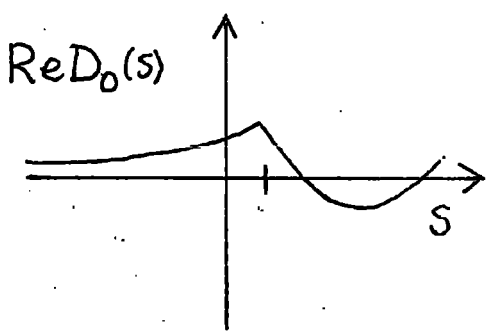

FIG. 3.11

Fig.(3.12). A sketch of the S-wave D-functions for the potential $V=-11e^{-r}/r + g_R e^{-0.3r}/r$ in first Born approximation. The two cases have:-

(a) $g_R = 3.3$,

(b) $g_R = 8.0$.

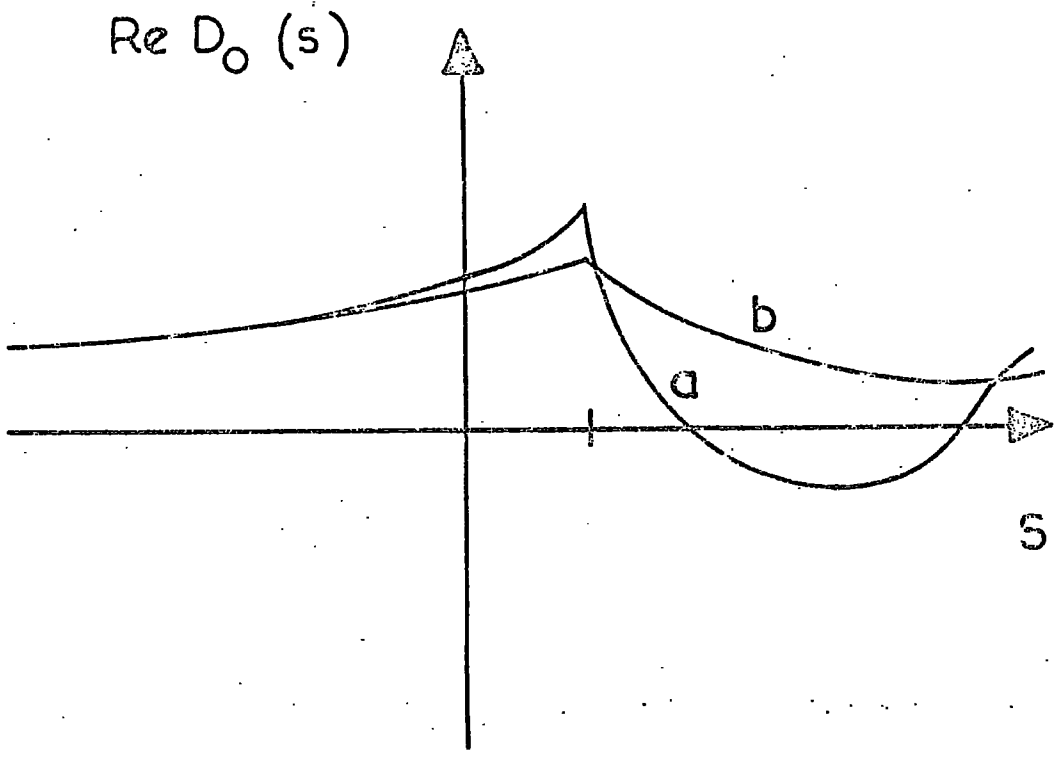

FIG. 3.12.

C H A P T E R F O U R

Calculations of pion-pion scattering

1. Introduction.

In this Chapter we describe some calculations of pion-pion elastic scattering according to the maximal analyticity postulates set out in Chapter One. We use a generalised interference model for the scattering amplitude, namely the Chew-Jones approximation, described in Chapter Two, augmented by extra pieces of double spectral function calculated from the elastic unitarity equations. We enforce unitarity on partial wave amplitudes using the N/D method. From the results of Chapter Three we suspect that inclusion of the third Born term will be sufficient to guarantee more reliable (if not more realistic) results than hitherto achieved.

In the next Section we give the necessary formalism (relegating some detailed algebra to the Appendix), and in Section Three present results of a rho-meson bootstrap. We obtain an s-channel vacuum trajectory not included in the input, which we identify with the P. In Section Four we begin to investigate the $\pi\pi$ system with both P and ρ trajectories in the crossed channel, and find some indications that a reasonable account of the vacuum repulsion may be possible. It does not seem likely, however, that the present calculational scheme will give results that agree very closely with experiment.

2. Formalism of pion-pion scattering.

The pion has zero strangeness, $I^G=0^-$, $J^P=1^-$, positive change conjugation parity, and a mass of about 140 MeV(66). Its simple quantum numbers and low mass mean that it is copiously produced in strong interaction, and plays a large part in carrying the long range component of the nuclear force. If we approach the problem of strong interactions with at first necessarily limited objectives, and try to isolate one system for study, the pion-pion interaction is a natural choice because of its simplicity and importance. The overall structure of the low energy dynamics appears to be dominated by the ρ-meson at about 750 MeV, and since this has predominantly elastic decay(66) it would not be a totally hopeless first approximation to treat the problem as completely elastic using the N/D techniques so far employed. We shall see, however, that some inelasticity is implied in our dynamical scheme, and we shall modify our approach accordingly.

We neglect electromagnetic effects and deal throughout with amplitudes of definite isospin, $A^I(s,t,u)$, $I=0,1,2$. The process of crossing is thus complicated by the necessity to use a crossing matrix to relate t and u channel amplitudes to those in the s-channel. We have, as is well known,(6)

$$A^I(s,t,u) = \beta^{II'}A^{I'}(t,s,u) \qquad (4.1a)$$

$$= (-1)^I \beta^{II'}(-1)^{I'}A^{I'}(u,t,s), \qquad (4.1b)$$

where

$$\beta^{II'} = \begin{Bmatrix} 1/3 & 1 & 5/3 \\ 1/3 & 1/2 & -5/6 \\ 1/3 & -1/2 & 1/6 \end{Bmatrix} \qquad (4.2)$$

and the index I' is summed from 0 to 2.

Each amplitude A^I obeys the Mandelstam representation, and because the pion is pseudoscalar (a three-pion vertex is thus forbidden), has double spectral regions as shown in Fig.4.1 (where the Chew-Jones strips are also depicted). Each of the six curved boundaries has an asymptote at $4m_\pi^2$ in one direction and $16m_\pi^2$ in the other, corresponding to the lack of a three pion intermediate state in the unitarity sum, e.g. (1.20), and the impossibility of the simple box diagram:

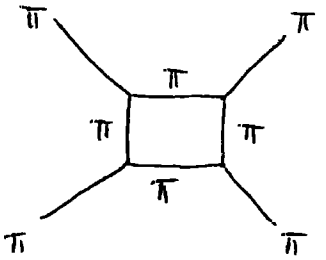

We begin by constructing s-channel amplitudes of definite signature, and in this connection we note that the interchange $t \leftrightarrow u$,

($z_s \leftrightarrow -z_s$), corresponds to an interchange of (identical) pions. Therefore to preserve Bose statistics the signature factor $\pm$ is equal to $(-1)^I$, and so only even angular momentum states contribute to I=0, 2 amplitudes and only odd angular momentum states to the I=1 amplitude.

We split each of the three double spectral regions into two contributions, each elastic in a different channel. What in the scalar meson case of Chapter One was labelled ρ_{st} now consists of ρ_{st} and ρ_{ts}, the former elastic in s, the latter in t. Similar decompositions are made for what were ρ_{su} and ρ_{tu}, see Fig.4.1. This re-labelling facilitates the introduction of the Chew-Jones representation, where $R_1{}^t$ contributes to ρ_{ts}, $R_2{}^u$ to ρ_{us} etc.

Using eq.(1.45) for $A^{\pm}(s,t)$, and remembering (4.1) etc., we have in this convention (see Appendix),

$$A^I(s,t) = \frac{1}{\pi}\int \frac{dt'}{t'-t} D_t^I(s,t'), \tag{4.3}$$

where

$$D_t^I(s,t) = v^I(s,t) + d^I(s,t), \tag{4.4}$$

$$d^I(s,t) = \frac{1}{\pi}\int \frac{ds'}{s'-s} \rho_{st}^I(s',t), \tag{4.5}$$

and

$$v^I(s,t) = \frac{\beta^{II'}}{\pi}\left\{ \int \frac{ds'}{s'-s} \rho_{ts}^{I'}(s',t) + (-1)^{I'} \int \frac{du'}{u'-u}\left[\rho_{tu}^{I'}(s,u') + (-1)^I \rho_{ut}^{I'}(s,u')\right] \right\}. \tag{4.6}$$

Re-labelling again, we reserve the symbol ρ_{st} for only that portion of the s-elastic double spectral function in the corner between the strips R_I^s and R_I^t, and similarly use the other five symbols ρ. Then our interference model approximation to $A^I(s,t)$ consists of replacing in eqs.(4.5) and (4.6) the double spectral function by the appropriate strips plus the corresponding corner pieces.

To calculate the corner pieces, we concentrate on ρ_{st}, which we obtain from s-channel elastic unitarity in the form of eq. (2.21),

$$\rho_{st}^I(s,t) = (16\pi^2 q_s \sqrt{s})^{-1} \iint \frac{D_t^I(s_+,t_1)\, D_t^I(s_-,t_2)}{K''^2(s,t,t_1,t_2)}\, \theta(K)\, dt_1\, dt_2. \qquad (4.7)$$

Other pieces are obtained by a simple permutation of variables s,t and u. That is, because each channel contains an identical process, for a given isospin ρ_{ts} is the same function of t as ρ_{st} is of s, and so on. We note that when ρ_{st} is known out to a given t, ρ_{tu}, (which is the same function of u as ρ_{st} is of t), is known only to the same limited value of u, so that the integral over it in (4.6) has to be cut off. The error thus introduced was found numerically to be negligible, since the whole contribution of any reasonable ρ_{tu} is itself very small, and was in fact neglected.

If the double spectral function ρ_{st} calculated from (4.7) is important to the dynamics, the implication is that ρ_{ts} is equally so, and of course the integral over it in eq.(4.6) is uncertain for an exactly similar reason. The only way to estimate it would be to carry out a "macro-iteration", using the results of one iteration to begin another, and, with the not unreasonable expectation of convergency, carry on until ρ_{ts} was unchanged. The consistency of this procedure as stated is questionable, however, as the presence of ρ_{st} implies t-channel inelasticity (e.g., multiple ρ-meson exchange), and therefore the presence of ρ_{ts} implies an equal degree of s-channel inelasticity which renders invalid the elastic unitarity assumption underlying eq.(4.7). A solution would be to modify (4.7) in some way to take account of inelasticity at the second and subsequent steps in the "macro-iteration". However, such a procedure involves immense numerical effort, and it is not clear that it would yield any useful improvement over the simpler approximation that was in fact used.

Our approach was to neglect altogether the contribution of ρ_{ts} to (4.6) in the iteration, but estimate for the effects of its implied presence by using N/D equations modified according to the method of Frye and Warnock[46], with the inelasticity parameter

η calculated from ρ_{ts} (obtained by permutation of s and t from ρ_{st}) as we shall describe.

To determine ρ_{st} we need $D_t^I(s,t)$ evaluated in the corner where $4m_\pi^2 \leq s,t \leq s_1$, and clearly $R_1^s(s,t)$, which is contained in $d^I(s,t)$, eq.(4.5), does not contribute here. To begin the iteration we thus set $D_t^I = v^I$, where the latter contains only the contribution of the strips R_1^t and R_2^t, since R_1^u has no t-discontinuity in the relevant region. Therefore our starting t-discontinuity is given by, (see Appendix)

$$D_t^I(s,t) = \beta^{II'}\Delta_t \left\{ \Gamma^{I'}(t) \left[\frac{P_{\alpha(t)}(-z_t) + (-1)^{I'} P_{\alpha(t)}(z_t)}{\sin \pi\alpha(t)} \right.\right. \tag{4.8}$$

$$\left.\left. + \frac{1}{\pi} \int_{-4q_t^2}^{s_1} P_{\alpha(t)}(z_t') \left[\frac{1}{s'-s} + \frac{(-1)^{I'}}{s'-u} \right] ds' \right] \right\},$$

where

$$\Gamma(t) = -16\pi^2 (2\alpha(t)+1)\, \gamma(t) \left(q_t^2/s_0\right)^{\alpha(t)},$$

and a summation over isospin I', and t-channel trajectories is implied. We have altered (2.14) into a form suitable for $q_t^2 > 0$, and neglected Q-functions. We shall describe our parameterisations of $\alpha(t)$ and $\gamma(t)$ - both needed above threshold where they are complex - in the next Section.

The numerical computations were carried out by calculating $D_t^I(s,t)$, as given by eqs.(4.4)-(4.6) for s-values between $4m_\pi^2$ and s_1 at successively greater

t-values, with the corner piece of double spectral function ρ_{st} given by (4.7) in terms of $D_t^I(s,t)$ at lesser t-values. The contributions from ρ_{tu} and ρ_{ut} were small, and were thus ignored because their inclusion increased tenfold the computer time required. The contribution of ρ_{ts} was neglected to the extent described above. Thus the entire contribution of v^I is given by the starting discontinuity, eq.(4.8).

In general the starting discontinuity D_t of eq.(4.8), which has a large-s behaviour proportional to $s^{\alpha(t)}$, may increase with s, and so it is evident from eqs.(4.4) - (4.7) that, unless very delicate cancellations occur in the iteration procedure, as s_1 is increased the contribution to the amplitude of ρ_{st} calculated in this way could be made arbitrarily large[108], in contradiction to the spirit of the interference model[109]. To overcome this difficulty we followed the prescription of Bali et al.[109], and multiplied the double integral of (4.7) by a factor $\left(1+\exp\left((s-s_1)/\Delta\right)\right)^{-1}$, $(\Delta>0)$, to damp down ρ_{st} at large s.

The calculation of the contribution to the potential function $B_I^I(s)$ of the Chew-Jones asymptotic strips is straightforward (see Appendix), and has been given in detail by Collins and Teplitz[80]. Like these authors we found numerically that the

contribution of the direct channel strip R_I^S to B_ℓ^L was entirely negligible, as were the terms involving integrations over $\Gamma(t)$ for $t > s_1$. Ignoring these terms, we find

$$B_\ell^L(s)_{strips} = \beta^{II'}\left(32\pi^2 q_s^{2l+2}\right)^{-1}\int_{-\infty}^{0} dt\,\left[\mathrm{Im}\,Q_\ell(z_s)\right]\Gamma^{I'}(t)$$

$$\times\left\{\frac{1}{\pi}\int_{-4q_t^2}^{s_1} P_{\alpha(t)}(z_t')\left[\frac{1}{s'-s}+\frac{(-1)^{I'}}{s'-u}\right]ds'\right.$$

either

$$+\left[\frac{P_{\alpha(t)}(z_t)+(-1)^{I'}P_{\alpha(t)}(-z_t)}{\sin\pi\alpha(t)}\right] \qquad \text{if } z_t > -1$$

or

$$\left.+\left[\xi(\alpha(t))\,P_{\alpha(t)}(-z_t)-\frac{2}{\pi}Q_{\alpha(t)}(-z_t)\right]\right\} \qquad \text{if } z_t < -1 \qquad (4.9)$$

where $\xi(\alpha(t)) = \cot\frac{\pi\alpha(t)}{2}$ for $I' = 0, 2$, and $-\tan\frac{\pi\alpha(t)}{2}$ for $I'=1$. As in (4.8), a summation over isospin I' and trajectories is understood.

The contribution of the corner pieces of double spectral functions to $B^L(s)$ follows immediately from (1.81), and is

$$B_\ell^L(s)_{\text{ITERATED}} = (32\pi^3)^{-1}\int_{4m_\pi^2}^{S_1}\left[\int_{S_0(t)}^{S_1}(-1)^I\frac{\rho_{st}^I(s',t)}{s'-s}\left\{\frac{Q_\ell(z_{s'})}{q_{s'}^{2\ell+2}}-\frac{Q_\ell(z_s)}{q_s^{2\ell+2}}\right\}ds'\right.$$

$$+\beta^{II'}\int_{u_0(t)}^{S_1}\frac{\rho_{ts}^{I'}(s',t)}{s'-s}\left\{\frac{Q_\ell(z_s)}{q_s^{2\ell+2}}-\frac{Q_\ell(z_{s'})}{q_{s'}^{2\ell+2}}\right\}ds'$$

$$+(-1)^I\beta^{II'}(-1)^{I'}\frac{Q_\ell(z_s)}{q_s^{2\ell+2}}\int_{S_0(t)}^{S_1}\frac{\rho_{ut}^{I'}(u',t)}{u'-u(t)}du'$$

$$\left.+\beta^{II'}(-1)^{I'}\frac{Q_\ell(z_s)}{q_s^{2\ell+2}}\int_{u_0(t)}^{S_1}\frac{\rho_{tu}^{I'}(u',t)}{u'-u(t)}du'\right]dt. \qquad (4.10)$$

Here the boundaries of the pieces of double spectral functions are $s_0(t)=4(1+16/(t-16))$ and $u_0(t)=16(1+4/(t-4))$, in units where $m_\pi^2=1$. All the pieces of double spectral function are included in this expression, where their contribution is not small(110).

Equations (4.9) and (4.10) give the input for the Frye-Warnock[46] N/D equations. To derive these equations, we write (c.f. eq.(2.3)),

$$B_\ell(s) = \left[\eta_\ell(s)\, e^{2i\delta_\ell(s)} - 1\right] \Big/ 2i\rho_\ell(s) \,, \tag{4.11}$$

where $\rho_\ell(s) = 2q_s^{2\ell+1}/\sqrt{s}$. In the decomposition B=N/D, D now carried an elastic unitarity cut from threshold to s_1, and N has a left-hand cut, a right-hand cut above s_1, and the inelastic part of the unitarity cut from s_{IN} ($=16m_\pi^2$) to s_1. The derivation of ref.[5] for $s_1 = \infty$ carries over to give

$$\tilde{N}_\ell(s) = \tilde{B}_\ell^L(s) + \frac{1}{\pi}\int_{4m_\pi^2}^{s_1} \frac{\tilde{B}_\ell^L(s') - \tilde{B}_\ell^L(s)}{s'-s}\, \tilde{\rho}_\ell(s')\, \tilde{N}_\ell(s')\, ds' \tag{4.12}$$

where

$$\tilde{B}_\ell^L(s) = B_\ell^L(s) + \frac{1}{\pi} P\int_{s_{IN}}^{s_1} \frac{1-\eta_\ell(s')}{2\rho_\ell(s')} \frac{ds'}{s'-s} \,, \tag{4.13}$$

(P denoting Cauchy principal value),

$$\tilde{N}_\ell(s) = \frac{2\eta_\ell(s')}{1+\eta_\ell(s)}\, Re\, N_\ell(s) \,, \tag{4.14}$$

and

$$\tilde{\rho}_\ell(s) = \rho_\ell(s) \Big/ \eta_\ell(s) \,.$$

Also

$$D_\ell(s) = 1 - \frac{1}{\pi}\int_{4m_\pi^2}^{s_1} \frac{\tilde{\rho}_\ell(s')\,\tilde{N}_\ell(s')}{s'-s}\,ds' . \qquad (4.15)$$

Given $B_\ell^L(s)$ and $\eta_\ell(s)$ these equations can be solved for $\tilde{N}_\ell(s)$ and $D_\ell(s)$. Because

$$\mathrm{Im}\, N_\ell(s) = \frac{1-\eta_\ell(s)}{2\rho_\ell(s)}\,\mathrm{Re}\, D_\ell(s) \quad , \qquad s > s_{IN} \quad , \qquad (4.16)$$

we can form a dispersion relation for $N_\ell(s)$ (~~neglecting Im$N_\ell(s)$ for $s \gg s_1$~~), and so calculate residues $\gamma(s)$ and trajectories $\alpha(s)$ in the way outlined in previous Chapters.

To calculate $\eta_\ell(s)$, we write for the (reduced) partial wave amplitude (4.11) the unitarity equation (c.f.(1.70)),

$$\mathrm{Im}\, B_\ell(s) = \rho_\ell(s)\,|B_\ell(s)|^2 + \mathrm{Im}\, B_\ell^{IN}(s) \quad , \qquad (4.17)$$

where

$$\mathrm{Im}\, B_\ell^{IN}(s) = \frac{1-\eta_\ell^2(s)}{4\rho_\ell(s)} . \qquad (4.18)$$

The inelastic cut (i.e. Im$B_\ell^{IN}(s)$) comes from the term $\rho_{ts}(s,t)$ in the equation that corresponds to (4.10) for $B_\ell(s)$. Therefore

$$\eta_\ell(s) = \left\{1 - 4\rho_\ell(s)\,\mathrm{Im}\, B_\ell^{IN}(s)\right\}^{+1/2} \quad , \qquad (4.19)$$

where

$$\mathrm{Im}\, B_\ell^{IN}(s) = \left(32\pi^3 q_s^{2\ell+2}\right)^{-1} \int_{4m_\pi^2}^{S_1} \beta^{II'} \rho_{ts}^{I'}(s,t)\, Q_\ell(z_s)\, dt . \qquad (4.20)$$

In the next Section we apply this method to a bootstrap of the ρ-meson trajectory(111).

3. A rho-meson bootstrap.

It has been shown in previous pion-pion calculations(80,81) that the force from rho exchange generates not only an I=1 s-channel trajectory but also a higher-lying I=0 trajectory. The reason is essentially that the crossing matrix element from I=1 to I=0 is twice that to I=1, see eq.(4.2). The second trajectory we identify with the Pomeranchon, P, and in this Section we ignore its presence and concentrate on finding a self-consistent rho. Inclusion of only one trajectory enables us to make a comprehensive search for self-consistency and to examine thoroughly the effect of the cut-off parameters (Δ and s_1) on our solution.

To calculate the starting discontinuity for the Mandelstam iteration we need a parameterisation of $\alpha(t)$ and $\gamma(t)$ above threshold, $t > 4m^2$. Within the context of this calculation both are real analytic in t cut from $4m^2$ to ∞ along the positive

real axis. We write dispersion relations (eq.(1.84)),

$$\alpha(t) = \alpha(\infty) + \frac{1}{\pi}\int_{4m_\pi^2}^{\infty} \frac{Im\,\alpha(t')dt'}{t'-t}\,, \tag{4.21}$$

and

$$\gamma(t) = \frac{1}{\pi}\int_{4m_\pi^2}^{\infty} \frac{Im\,\gamma(t')\,dt'}{t'-t}\,, \tag{4.22}$$

and use parameterisations of the type introduced by Ahmadzadeh Sakmar[112] for the imaginary parts:

$$Im\,\alpha(t) = \frac{C_1 x^\lambda}{(x-a_1)^2 + b_1^2} \tag{4.23}$$

and

$$Im\,\gamma(t) = \frac{c_2 x^\lambda (x-d)}{(x-a_2)^2 + b_2^2} \tag{4.24}$$

where $x=t-4m^2$. Inserting these forms into eqs.(4.21) and (4.22), the integrals may be evaluated by choosing a suitable contour to give

$$\alpha(t) = \alpha(\infty) + \frac{C_1\,\mathrm{cosec}\,(-\pi\lambda)}{(x-a_1)^2 + b_1^2}\left\{ (e^{-i\pi}x)^\lambda + \right. \tag{4.25}$$

$$\left. + \frac{(a_1^2+b_1^2)^{\lambda/2}}{b_1}\left[(x-a_1)\sin\lambda\theta_1 + b_1\cos\lambda\theta_1\right]\right\}$$

for $-1 < \lambda < 2$, and

$$\gamma(t) = \frac{c_2\,\mathrm{cosec}\,(-\pi\lambda)}{(x-a_2)^2 + b_2^2}\left\{ (e^{-i\pi}x)^\lambda (x-d) + \frac{(a_2^2+b_2^2)^{\lambda/2}}{b_2} \times \right. \tag{4.26}$$

$$\left. \times\left[\left((d-a_2)(x-a_2)+b_2^2\right)\sin\lambda\theta_2 - b_2(x-a_2)\cos\lambda\theta_2\right]\right\}$$

for $-1 < \lambda < 1$, where $\theta_i = \tan^{-1}(b_i/a_i)$. The form of these functions is shown in Fig.4.2 (see also Fig.5.2). Note that $\mathrm{Im}\,\alpha$ must be positive by unitarity, but there is no such restriction on $\mathrm{Im}\,\gamma$. Both imaginary parts must vanish at threshold for $\alpha(4m_\pi^2) > -\frac{1}{2}$. We are also assuming that $\alpha(s)$ approaches a constant at large s, as it does in potential scattering. If $\alpha(s) \longrightarrow \infty$ we cannot expect our single-channel bootstrap to work, although it may still give a reasonable approximation to the trajectory over a limited region of s near s=0. (See the next Chapter for a discussion of this, also ref.130). The input width of the rho meson corresponding to these functions is given by

$$\Gamma_{in} = \frac{\mathrm{Im}\,\alpha(m_\rho^2)}{m_\rho\ \mathrm{Re}\,\alpha'(m_\rho^2)} \approx \frac{\mathrm{Re}\,\gamma(m_\rho^2)}{m_\rho\ \mathrm{Re}\alpha'(m_\rho^2)} \cdot \rho_l(m_\rho^2). \qquad (4.27)$$

These parameterisations were used in the iteration to find the elastic double spectral function for a given value of s_1 and Δ. It is evident that the number of iterations needed to find ρ^{st} depends on how large is s_1. The main weight of the starting t-discontinuity is at the point where $\mathrm{Im}\,\alpha(t)$ is a maximum, and since this must be above the ρ mass (through which the trajectory rises) the number of iterations needed for, say, $s_1 = 2000 m_\pi^2$ is only 6 or 7. (The results of Chapter Three indicate that three

iterations should be sufficient for a reliable approximation to the potential). The calculated double spectral function is then used to calculate the potential and inelasticity functions for the N/D equations.

There are thus eleven input parameters for the calculation, a, b, c_1, $\alpha(\infty)$, d, a_2, b_2, c_2, s_0, s_1 and Δ. The first eight of these are to be adjusted to make the input and output trajectories and residues self-consistent for given values of Δ, s_0 and s_1. Our bootstrap is only really self-consistent if the dependence on the choice of Δ and s_1 is small. Since Δ only determines the width of the cutoff function of the iteration the results are in fact only trivially dependent on it, as Fig.4.3 shows. In the rest of the results we quote, Δ is fixed at $50m_\pi^2$. Also the scale factor in the residue function which is supposed for consistency to be about $\frac{1}{4}s_1$ to $\frac{3}{4}s_1$[113] we fixed at $s_0=200m_\pi^2$.

A self-consistent rho trajectory is shown in Fig.4.2. It has been chosen so that its parameters correspond to the physical rho-meson by having $\alpha(30)=1$, and the experimental input width $\Gamma_{in}=147$MeV.[114] The trajectory is not qualitatively different from those obtained in previous work[80, 81], where the second and higher Born terms were not included, but

a good deal of extra force has been obtained.

Part of this extra force is due to the inclusion of inelasticity, as shown by Fig.4.4, which includes the trajectory with $\eta_\ell(s)=1$, as well as with the calculated values. The variation of $\eta_\ell(s)$ with s for various ℓ-values is shown in Fig.4.5. The corresponding values above s_1 (calculated by using $\mathrm{Im}B^I_\ell(s)$ as given by the asymptotic strip) are also indicated in the figure. They do not match completely, of course, since nothing has been done to make them consistent, but the discrepancy is not too bad, except that for $\ell \lesssim 0.2$ unitarity is violated above s_1. This problem has been noted previously[81], and is due to the fact that the self-consistent residues tend to have too large a value of $\gamma(t)$ for $t<0$. This is compensated by having a large $\alpha'(t)$ in the region of the ρ-meson by putting the peak of $\mathrm{Im}\alpha(t)$ not too far above the particle (see Fig.4.2). The problem[81] of a large input width to generate enough force to produce a reasonable output trajectory is thus circumvented.

The dependence of the results on the choice of s_1 is shown in Fig.4.6. We see that the position of $\alpha(o)$ is little affected by the value of this parameter provided we take $s_1 \gtrsim 800m_\pi^2$, and is much reduced by the inclusion of higher Born approximations.

The slope $\alpha'(0)$ tends to decrease with increasing s_1, but again the higher Born approximations make the results almost independent of this arbitary parameter if it sufficiently large. The dependence is certainly not so great as to make one feel that it is playing a dominant role.

In Fig.4.7 we show the variation of ρ_{st} with t for some values of s. The first peak corresponds to the first iteration of those in $D_t(s,t)$ due to the particle at $t=m_\rho^2$ and the maximum of $\mathrm{Im}\alpha(t)$ above it, and the subsequent maxima are due to the further iterations. The double spectral function has settled down to its asymptotic behaviour at $t \approx 1000\, m_\pi^2$, and so we take this as our preferred value of s_1. The double spectral function calculated in this way matches smoothly on to the asymptotic strip region above s_1.

The chief problem in this type of calculation is the range of parameters over which "reasonable" self-consistency can be obtained. We have found that at the unitarity limit $\alpha(0)=1.0$, it is possible to obtain such a solution, and for lower values down to $\alpha(0)=0.17$. Some examples are shown in Fig.4.8.

It will be noted that the basic shape of the residue function is always the same, agreeing with the Chew-Teplitz form[113].

$$\gamma(t) = \text{const.}\ \alpha'(t)\left(\bar{t}-t\right) Q_{\alpha(t)}\left(1+\frac{2m_\rho^2}{\bar{t}-4}\right),\quad \bar{t}\sim\frac{s_1}{2}\ ) \tag{4.28}$$

which can be seen to be an inevitable consequence of the N/D equations for slowly-varying (with s) potential functions $B_\ell^L(s)$.

We have $\mathrm{ReD}_{\alpha(s)}(m^2)=0$, and eq.(2.15),

$$\frac{\gamma(m^2)}{\alpha'(m^2)} = \frac{N_\alpha(m^2)}{\mathrm{ReD}'_\alpha(m^2)}$$

If $B_\ell^L(s)$ is slowly varying, the integrals for N and ReD' both can be approximately evaluated at $t=\bar{t}$. Using a delta-function approximation for the crossed channel resonance (at m_ρ^2), its partial wave projection is a Q-function, giving eq.(4.28). There is striking agreement between this prediction and explicit numerical calculations[80, 81].

The only way for the Chew-Teplitz form to be avoided is for $B_\ell^L(s)$ to vary rapidly, perhaps changing sign, between threshold and s_1. The need for such oscillations if we are to find residues with a rapid decrease for negative t, like those found in many fits to the experimental data[56], has been discussed by Collins[87]. With only the attractive rho-exchange potential we cannot expect sign-changes, although we can hope that they will result in a satisfactory treatment of the

vacuum repulsion. The form of $\mathrm{Im}\gamma(t)$ in (4.24) has been chosen to reproduce (4.28) for negative t, and the change of sign at $t=4m_\pi^2+d$ seems the easiest way to do this.

Since the output shape of $\gamma(s)$ is always much the same, the values of d, a_2 and b_2 are more or less fixed. The values of λ should correspond to the known threshold behaviour of $\mathrm{Im}\gamma(t)$ which is (see eq.(1.86))

$$\mathrm{Im}\,\gamma(t) \underset{t\to t_0}{\sim} (t-t_0)^{\alpha(t_0)+\frac{1}{2}}.$$

In practice we have fixed $\lambda=0.5$ for all $\alpha(0)$. This has been found to make rather little difference so long as λ does not approach one too closely, when the dispersion integral for γ diverges. The only really free parameter, which is not determined by the shape of the output residue, is the overall magnitude, c_2. It is this which is determined by demanding self-consistency of input and output, and ranges from $c_2=0.093$ for $\alpha(0)=1$ to $c_2=0.028$ for $\alpha(0)=-.17$.

Similarly the range of shapes of the output trajectories exhibited in the solution of Fig.4.8 is very limited, and the only really significant free parameter in (4.25) is the absolute height of the trajectory determined by $\alpha(\infty)$. Again λ was fixed at 0.5, although in this case the integral (4.21)

converges for $\lambda < 2$. The values of a_1, b_1 and c_1 are essentially fixed by the form of the output. As far as we have been able to discover, the trajectories shown in Fig.4.8 span the full range of parameters for which reasonable self-consistency can be achieved. It has not proved possible to get a self-consistent solution with $\alpha(\infty) < 0$ for any choice of input parameters, since such trajectories produce much too little force. To get a trajectory like the experimental rho[64] we would like a much smaller curvature, but Fig.4.8 shows that the amount of curvature is always about the same.

It is seen from Fig.4.2 that, as in earlier calculations[80, 81], although the input and output trajectories agree very closely for $t < 0$ it is not possible to make them agree for $t \gg 0$, and in fact $\mathrm{Re}D_\ell(s)$ for $\ell \gtrsim 0.9$ does not have a zero in the solution shown in Fig.4.8. The output widths quoted in Figs.4.4 and 4.8 were obtained by plotting the partial wave cross-section. They show something of an improvement over previous calculations[80, 81, 89, 115], but the problem of achieving a satisfactorily narrow rho width has certainly not been solved.

There is a related difficulty in that, because of the bunching of $\mathrm{Im}\alpha(t)$ in a peak just above the $_{\Lambda}^{\mathrm{rho}}$ mass, D_t calculated from (4.8) also has a peak there, and has the sort of shape plotted in Fig.4.9. Normally one

would expect the maximum of D_t to be at $t=m_\rho^2$, (there is a secondary peak there), corresponding to the vanishing of $\sin \pi\alpha(t)$. A large $\mathrm{Im}\alpha(t)$ of this sort is essential to our parameterisation if we are to obtain a trajectory with a curvature like that of the output. This peak implies that there is a peak of the t-channel cross-section, but no such peak is found in the s-channel. Full crossing symmetry has thus not been achieved. In Bali's calculations[99], (see Fig.8 of his paper), $\mathrm{Im}\alpha(t)$ was a continuously increasing function right up to $t=s_1$, and the iteration of such an input would not settle down to its asymptotic form until $t \gg s_1$. We can hope to improve the satisfaction of crossing symmetry by choosing our parameters to ensure that the t- and s-channel partial wave cross-sections are consistent, but it is probably not worth worrying about this until the Pomeranchon has been included as well.

4. Pomeranchuk Exchange.

Within the confines of the present calculation, the leading vacuum singularity is a simple pole. On the basis of phenomenological fits to data[71, 56], which seem to require an unusually flat effective Pomeranchon trajectory, and in the expectation that branch points are present in the

ℓ-plane[110], other, sometimes more complicated, structures coupling to the vacuum quantum numbers have been suggested[117] to explain the apparent tendency of total cross-sections either to approach a constant[30] or to decrease very slowly[118] at large energies. In addition there is firm evidence[119] of a second pole, the P', and recently the presence of a third pole has been suggested[120]. There has been no sign in this or previous work[81] of lower-lying poles in the direct channel, and to begin with we shall insert only a single I=0 pole in the crossed channel.

The first results of putting in the P are given in Fig.4.10. We began with the self-consistent solution of Fig.4.2, and fitted, to the output I=0 trajectory and residues, formulae of the form (4.25) and (4.26). Using the resulting expressions for $\alpha(t)$ and $\gamma(t)$ for the crossed P pole, and the self-consistent parameters for the rho, we obtained solutions for the direct channel P and ρ as indicated.

The first satisfactory feature of the results is that solutions have appeared at all. In previous work[81] using the simple Chew-Jones approximation - the first Born term - the effect of the P was to give a repulsion large enough to completely swamp the rho attraction, and, as we have

explained, led to the use of the Chew-Teplitz normalisation procedure.

Two further points are immediately apparent; firstly the output trajectories are steepened, and secondly the residues are decreased. Evidently inclusion of the extra Born terms has been sufficient to compensate for the unrealistic repulsion of the first, and it is clear that the hoped-for narrow rho resonance may well appear in a fully self-consistent solution. However, with the parameterisations used for input Regge poles there is no large change in the shapes of the solution for $\alpha(s)$ and $\gamma(s)$, and so the overall agreement with experiment may be only marginally improved. Further calculations are in progress.

5. Summary.

The preliminary applications of our dynamical scheme to elastic pion-pion scattering show that it gives some (not unexpected) improvement over previous work. Inclusion of the P contribution seems to have been achieved in a more meaningful way than before, and some of its expected important effects promise to appear.

Use of the N/D method has not allowed trajectories to be followed properly above threshold,

but the indications are that the trajectory turns over rather quickly, possibly without reaching $\ell=1$, and certainly nowhere near $\ell=2$. Similarly, since there are no superconvergence conditions built into our potential[121], the trajectory endpoint, $\alpha(\infty)$, must be above $\ell=-1$, and in fact ends up above $\ell=0$. There is little tendency towards anything approaching exponential form for $\gamma(t)$ at $t \ll 0$, but addition of the P gives a sharper fall-off because it makes $B_\ell^L(s)$ vary more within the strip.

A good deal of further work remains to be done, but, as we explain in the next and last Chapter, it may well be fruitless.

Fig.(4.1). The Mandelstam diagram for pion-pion scattering, showing the Chew-Jones strips, and the corner pieces of double spectral function calculated from unitarity. The notation is explained in the text.

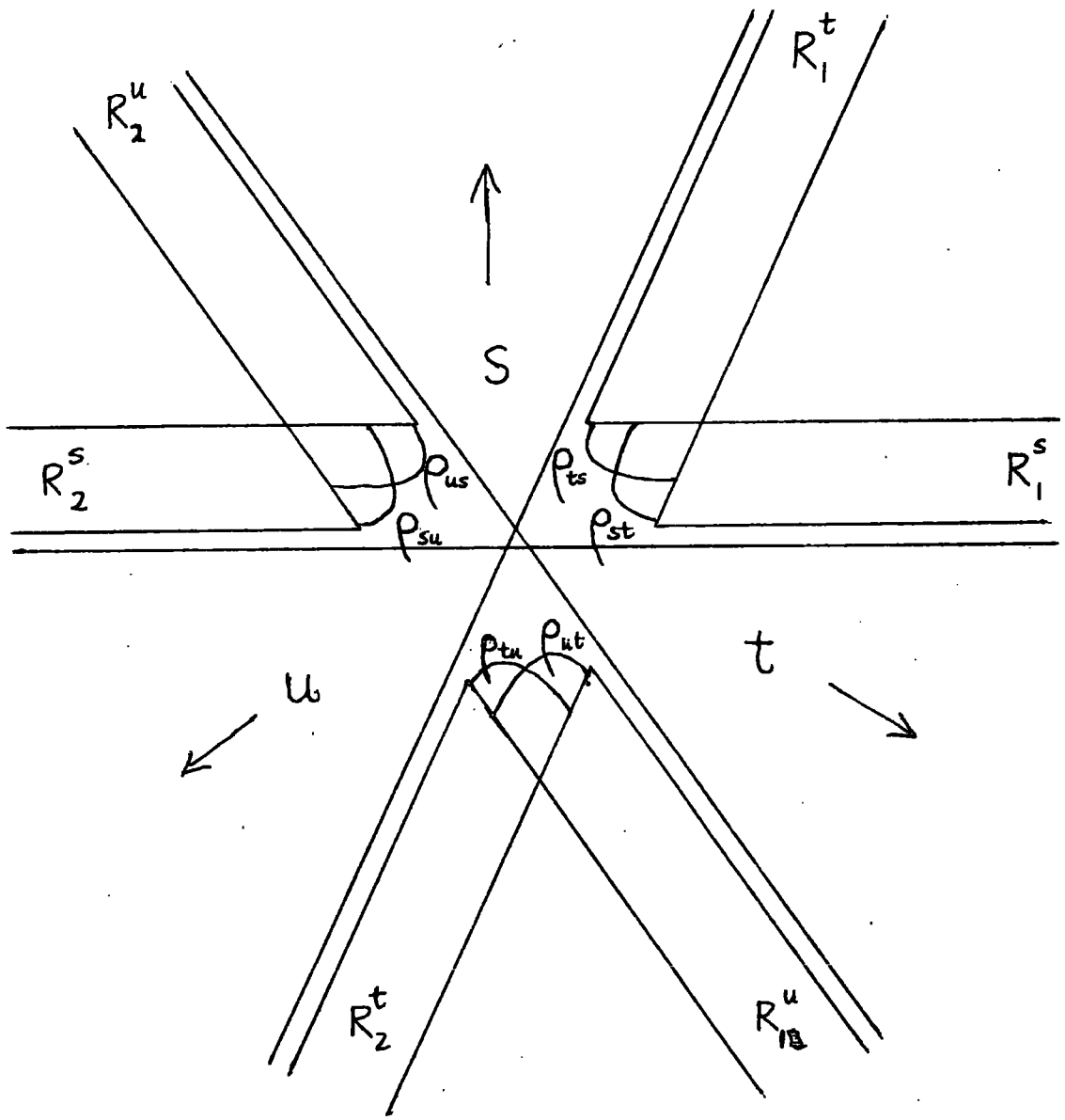
R_1^t
R_2^u
S
R_2^s
R_1^s
ρ_{us}
ρ_{ts}
ρ_{su}
ρ_{st}
ρ_{tu}
ρ_{ut}
u
t
R_2^t
R_1^u

FIG. 4.1

Fig.(4.2). Self consistent rho trajectory, and residue, functions (input Re α = ——, input Im α = — —, output Re α_ρ and Re α_ρ = - - - - -). The parameters (see text) are s_1=1000, Δ =50, s_0=200, a_1=47.0, b_1=3.94, c_1=1.05, a_2=540.0, b_2=392.5, c_2=0.068, d=420, all in m_π^2 units. This corresponds to an input rho width Γ_{in} =147 MeV, but the output width Γ_{out} =340 MeV.

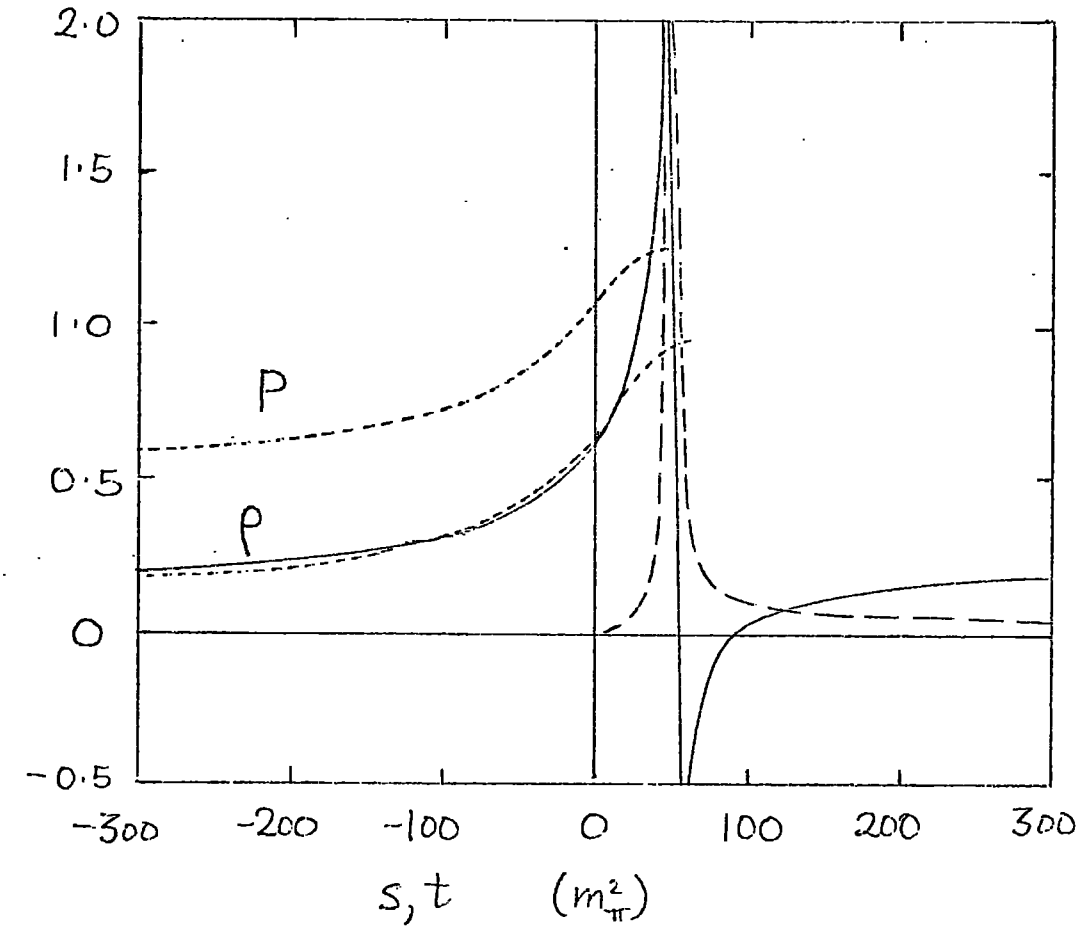
2·0
1·5
1·0
0·5
0
−0·5
P
ρ
−300
−200
−100
0
100
200
300
s, t (m²π)

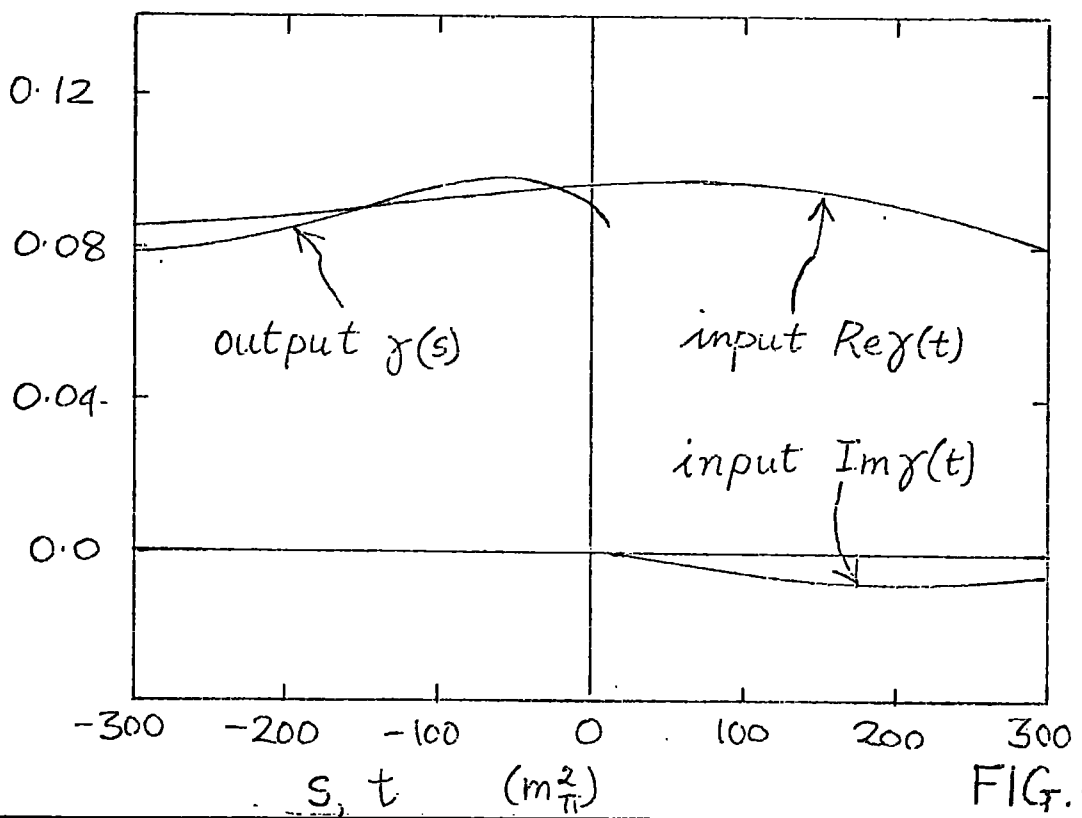
0·12
0·08
0·04
0·0
output γ(s)
input Reγ(t)
input Imγ(t)
−300
−200
−100
0
100
200
300
s, t (m²π)

FIG. 4.2

Fig.(4.3). The output rho trajectories which result with the indicated values of Δ . All the other parameters are as in Fig.(4.2).

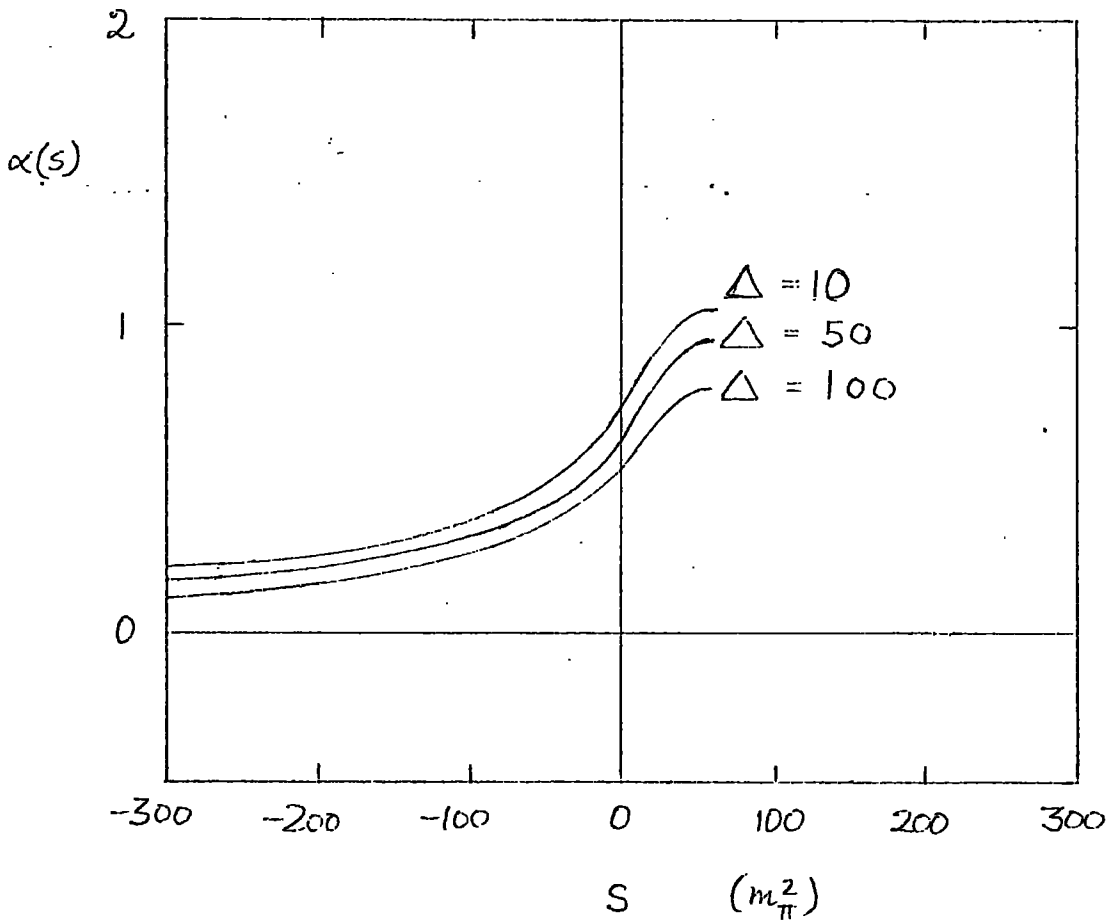

FIG. 4.3

Fig.(4.4). (a)The self consistent rho trajectory of Fig.(4.2), (b) is the output trajectory obtained when η is set equal to 1, and (c) that obtained when only the strip contributions are included in the left-hand cut, i.e. the first Born approximation.

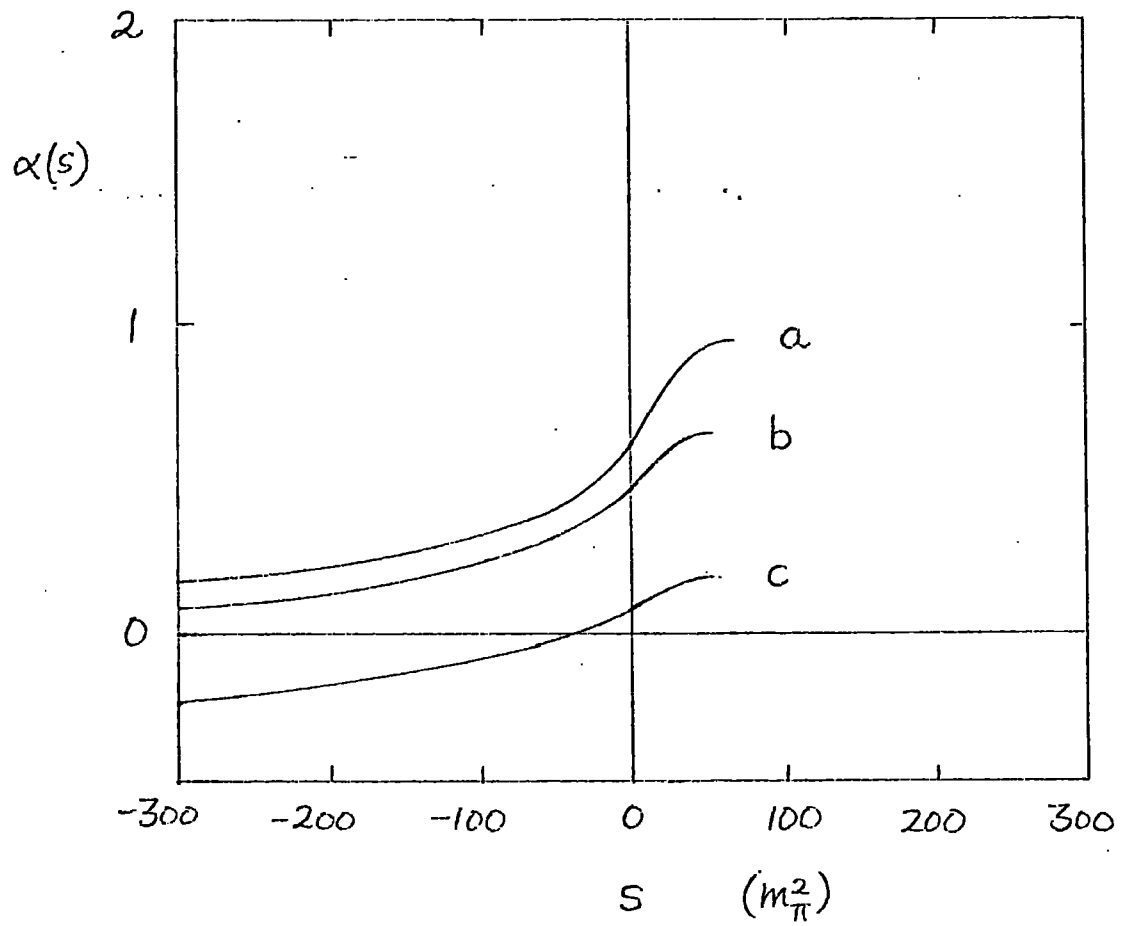

FIG. 4.4

Fig.(4.5). A plot of the inelasticity $\eta_\ell(s)$ against s with the parameters of Fig.(4.2), for (a) ℓ =1.0, (b) ℓ =0.2, and (c) ℓ =0.0. The values calculated from the strips above s_1(=1000) are also shown and we wee that for $\ell < .2$ unitarity is violated at s_1.

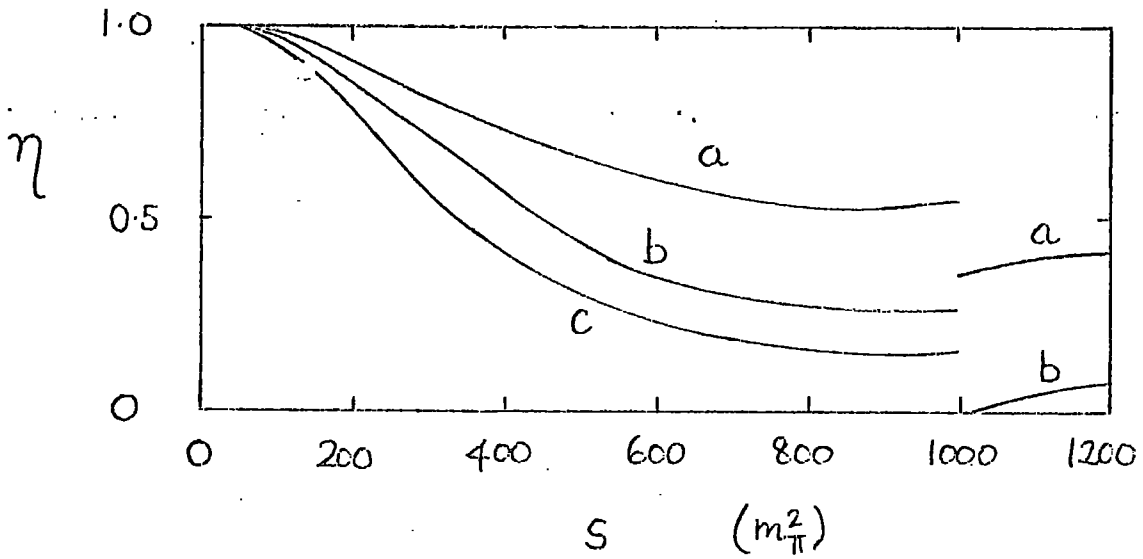

FIG. 4.5

Fig.(4.6). Plots of $\alpha(o)$ and $\alpha'(o)$ against s_1 with all the other parameters fixed. The three cases are (a) the complete calculation, (b) η set equal to 1, and (c) only the strip contributions included in left-hand cut. The dependence on the choice of s_1 is much reduced by including the elastic double spectral function.

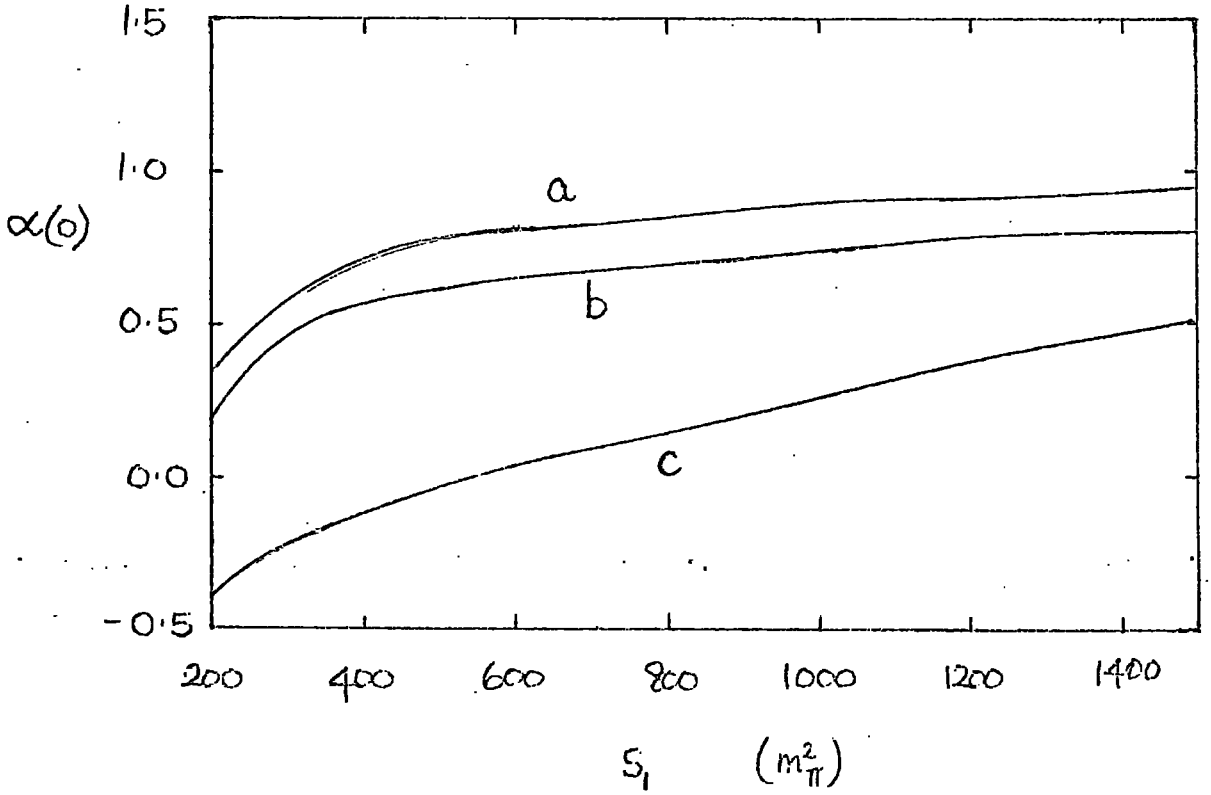
1·5
1·0
0·5
0·0
-0·5
α(0)
a
b
c
200
400
600
800
1000
1200
1400
S_1 (m_π^2)

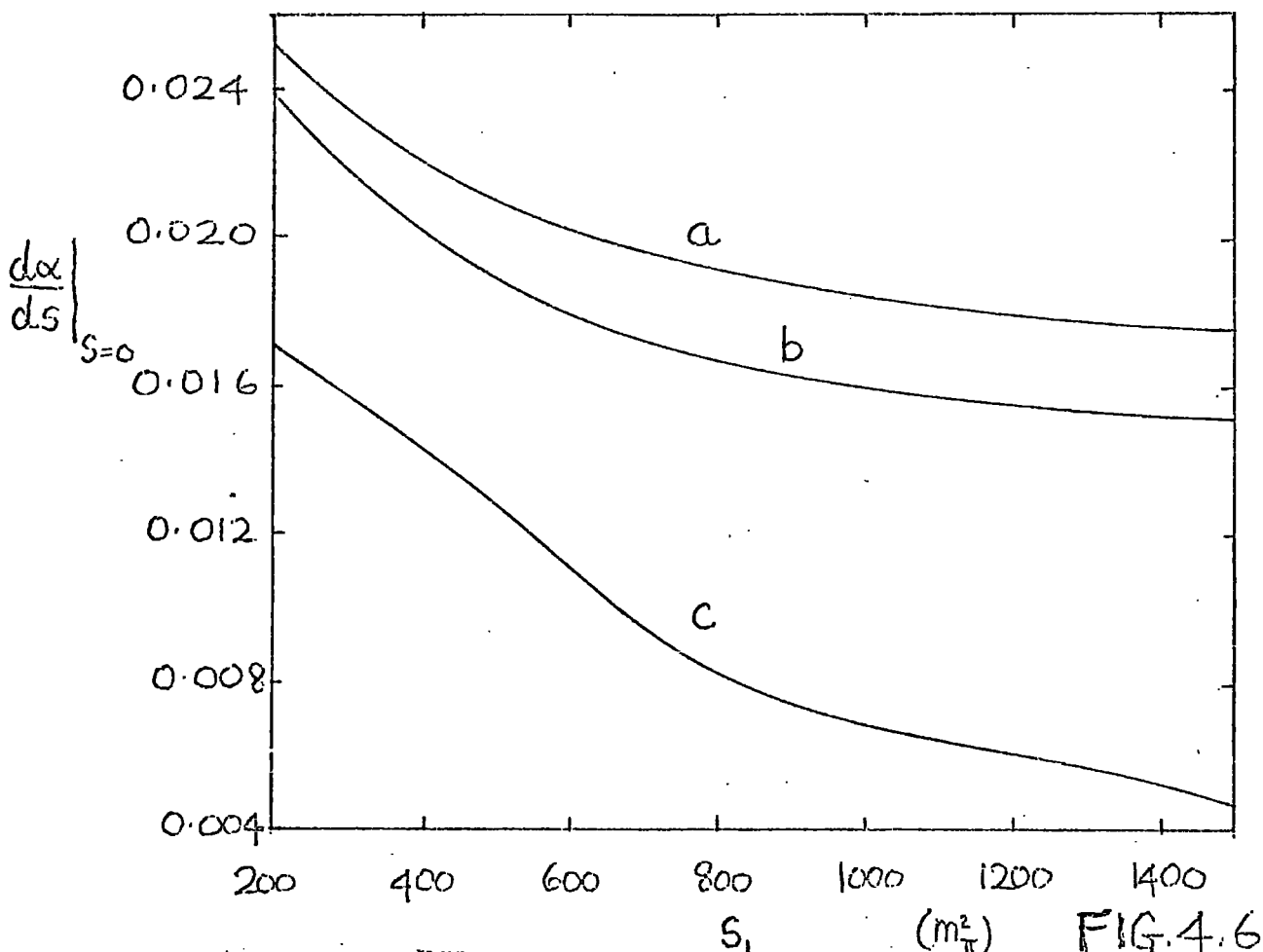
0·024
0·020
0·016
0·012
0·008
0·004
$\left.\frac{d\alpha}{ds}\right|_{S=0}$
a
b
c
200
400
600
800
1000
1200
1400
S_1 (m_π^2)

FIG. 4.6

Fig.(4.7). A plot of $\rho_{st}^{I=1}(s,t)$ against t for two values of s. The dashed line is the asymptotic strip for $t < s_1$, and matches on rather well showing that we have indeed reached the asymptotic region for $t \gtrsim 1000\, m_\pi^2$.

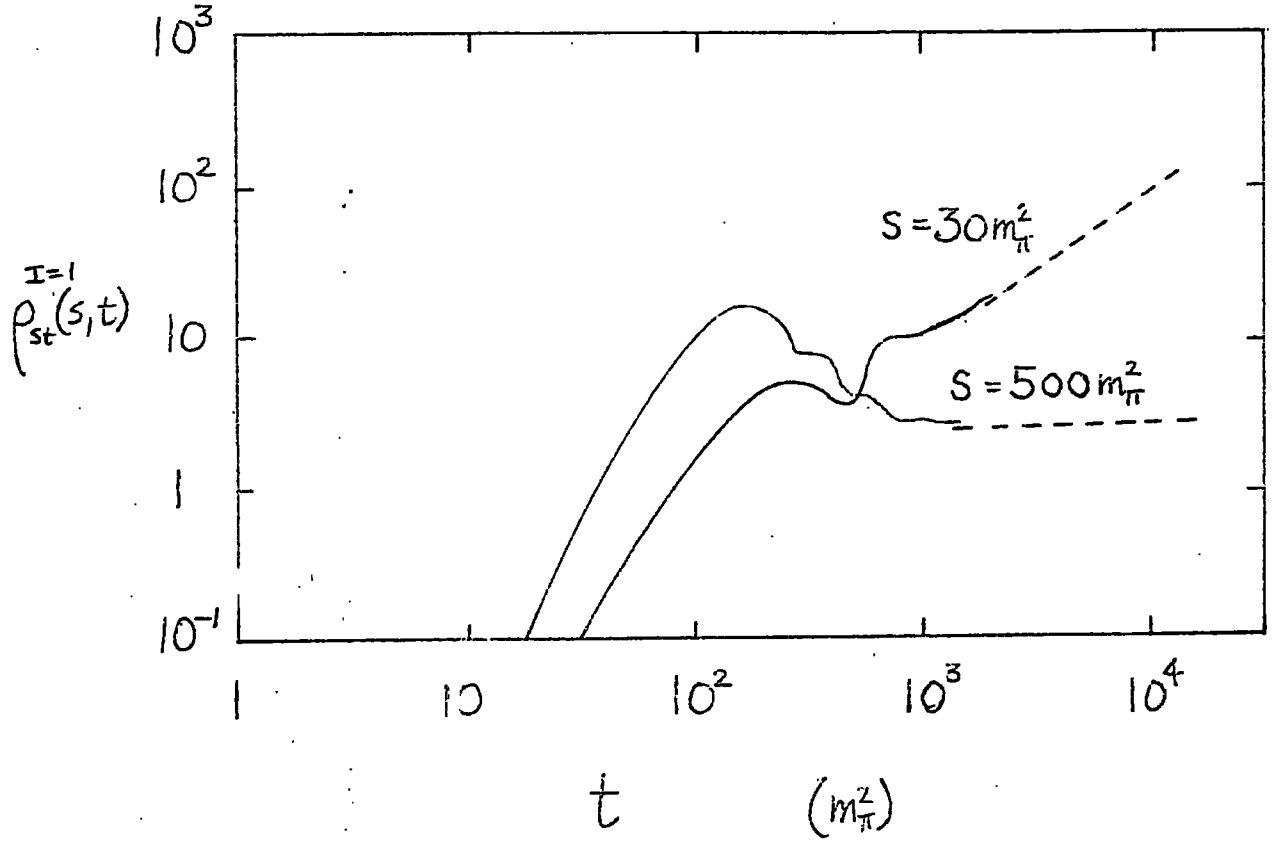
10^3
10^2
10
1
10^{-1}
$\rho^{I=1}_{st}(s,t)$
$s = 30 m_\pi^2$
$s = 500 m_\pi^2$
1
10
10^2
10^3
10^4
t (m_π^2)

FIG. 4.7.

Fig.(4.8). Self consistent rho (i) trajectories, and (ii) residues, with (a) $\alpha(0)=1.0$. $\alpha(\infty)=0.49$, (b) $\alpha(o)=0.57$, $\alpha(\infty)=0.17$, and (c) $\alpha(o)=0.17$, $\alpha(\infty)=0.03$. The dashed lines are the output, and the full lines the input Regge functions. Once $\alpha(\infty)$ has been decided upon the demand for self consistency fixes the shape of the trajectory. The width of the $\ell=1$ resonances in the three cases are (a) bound state, (b) 350 MeV, (c) 630 MeV. Note that case (b) is similar to, but slightly different from, Fig.(4.2). The parameters which have been changed are $b_2=400$ and $C_2=0.76$. This indicates the amount of variation which can be tolerated in these parameters.

(i)

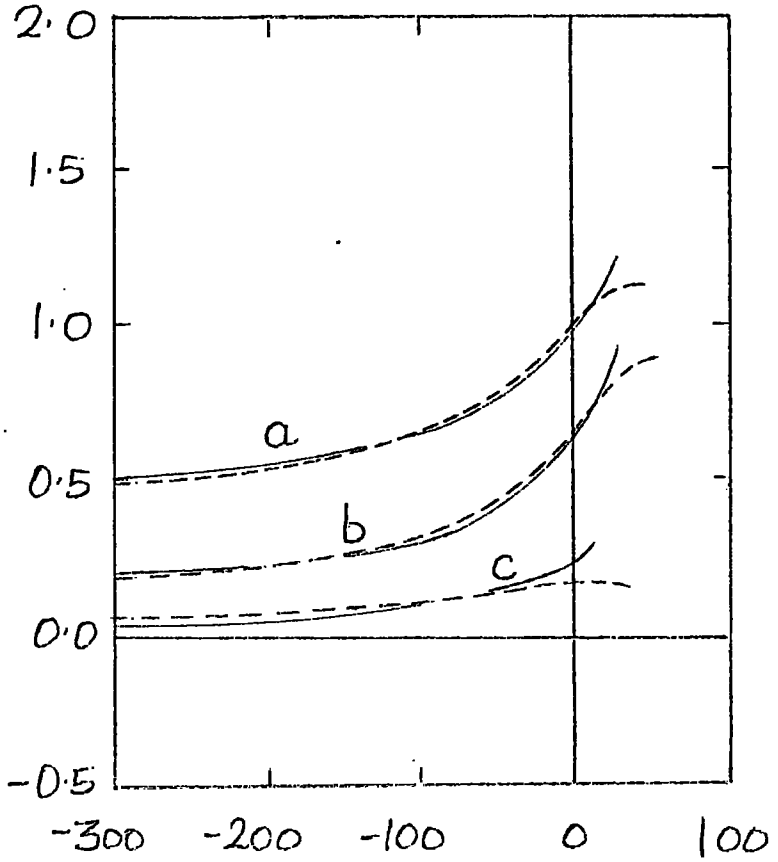
2·0
1·5
1·0
0·5
0·0
-0·5
a
b
c
-300
-200
-100
0
100

(ii)

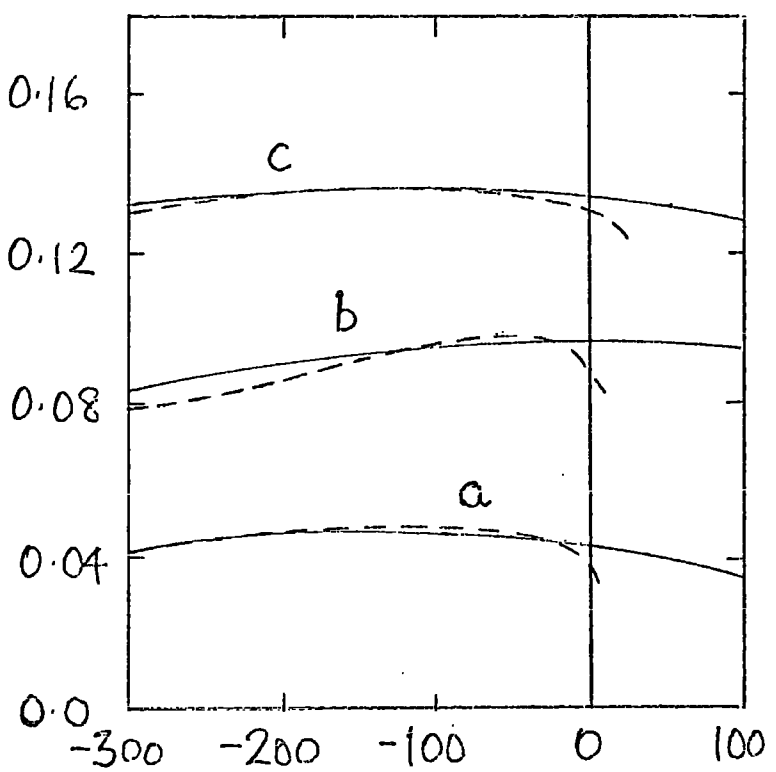
0·16
0·12
0·08
0·04
0·0
c
b
a
-300
-200
-100
0
100

FIG. 4.8

Fig.(4.9). A plot of $\log_{10} D_t^{I=1}(s,t)$ against t for $s = 15m_\pi^2$. It shows the first peak of D_t due to the particle at $t=30m_\pi^2$ and the second and larger peak due to that of $\mathrm{Im}\,\alpha$ at $t=47m_\pi^2$.

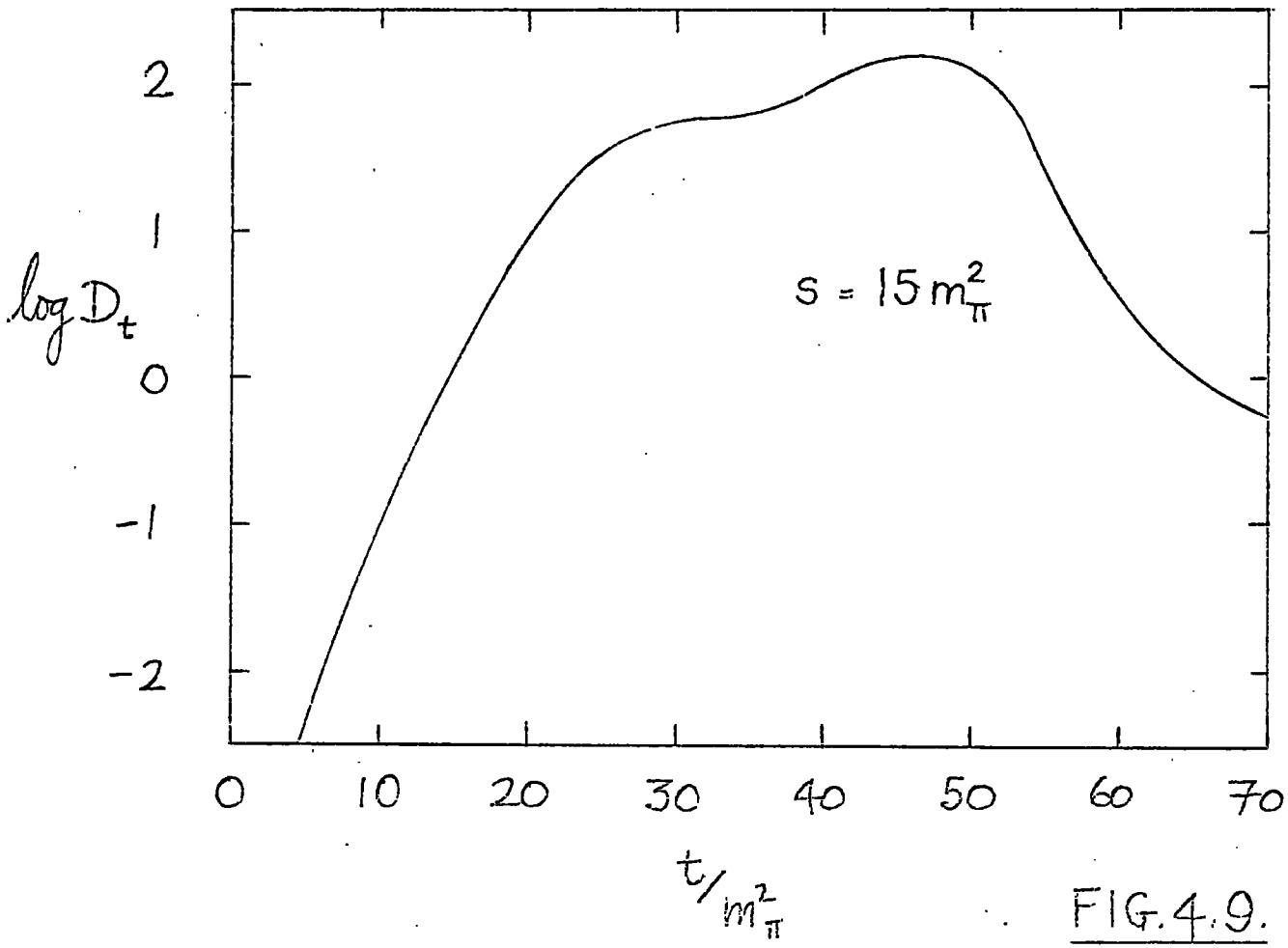

FIG. 4.9.

Fig.(4.10). Trajectory and residue functions for the case when P exchange is included. The full lines are the input (t-channel) functions, and the dashed lines the output (s-channel) ones. Shown also as a dotted line are the output trajectory and residue functions for the self consistent solution of Fig.(4.2).

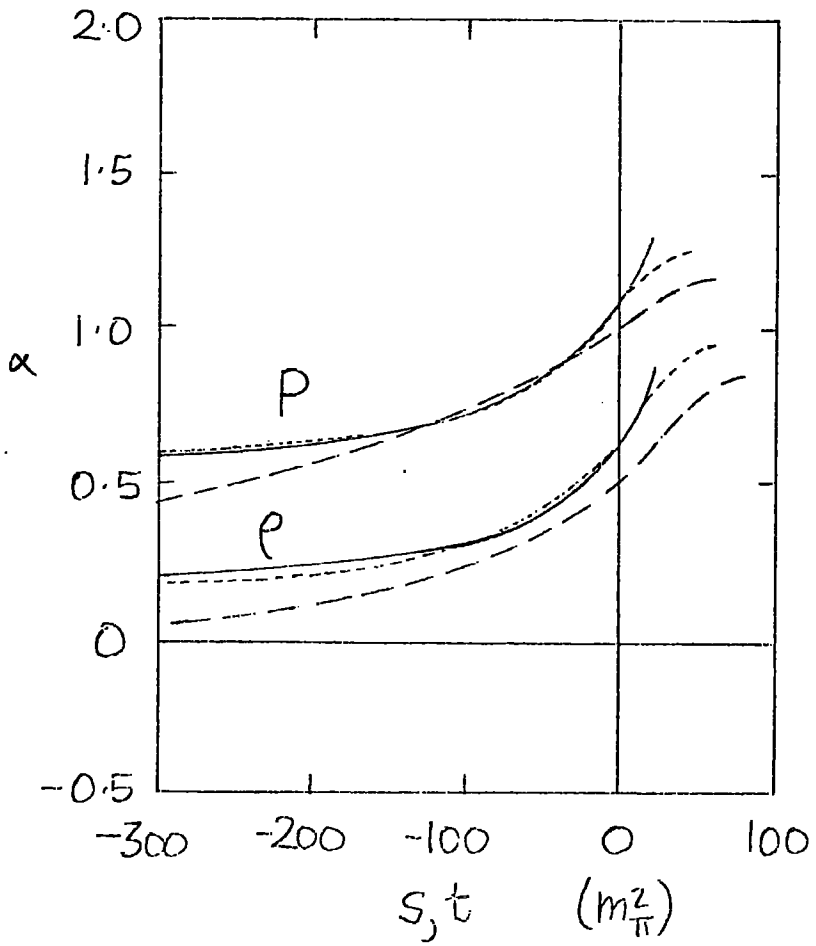
2·0
1·5
1·0
0·5
0
-0·5
α
P
ρ
-300
-200
-100
0
100
s, t (m²π)

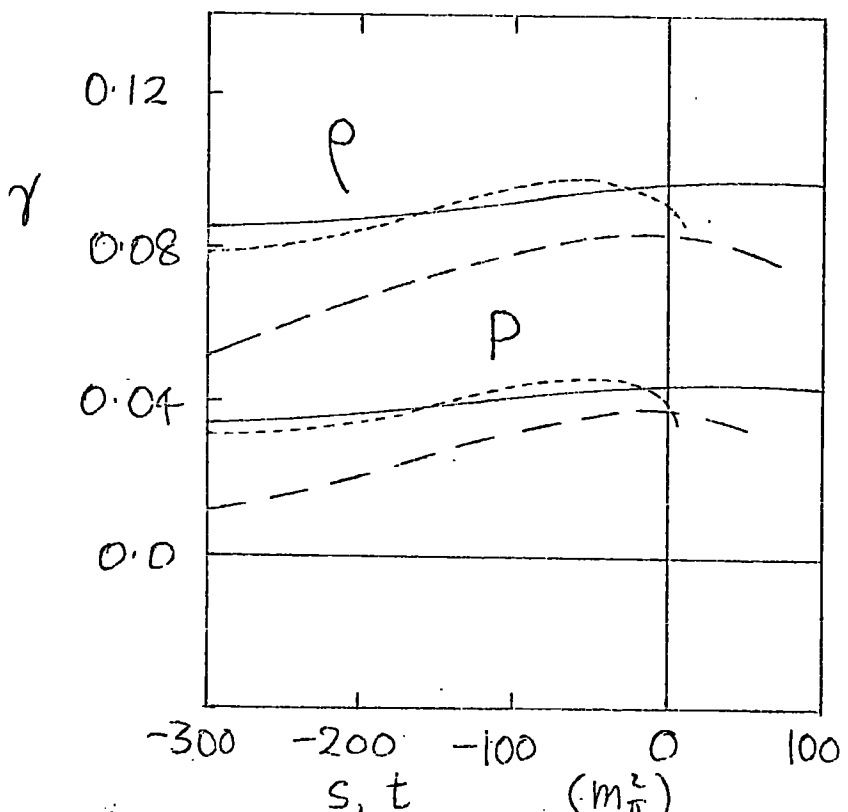
0·12
0·08
0·04
0·0
γ
ρ
P
-300
-200
-100
0
100
s, t (m²π)

FIG. 4.10.

C H A P T E R F I V E

Linear Regge Trajectories

1. Introduction.

The nature of a particular Regge trajectory for negative values of s (=(energy)^2) can be determined by fitting the near-forward angular dependence of the high energy power behaviour of the amplitude for the crossed channel process with (a sum of) formulae like (2.9). A particularly clear-cut case is the rho meson trajectory in $\pi^- p$ charge exchange[64], where it is the only prominent t-channel contribution. The trajectory so deduced[64] is approximately of the form $\alpha(s)=0.57+s$ between $s=-0.9$ GeV^2 and $s=0$. Linear trajectories (with s) for both baryons and mesons fit a wide range of processes[5], and, if they are extrapolated to positive s, there appear in many cases[5] resonances suitably placed to be their recurrences. Particular examples are the nucleon isobars[73], and the R, S, T, U mesons[122] seen in missing mass experiments[123]. It seems that the linearity may persist up to at least 6GeV^2.

The rho meson trajectories calculated in the previous Chapter had completely different behaviour, being much shallower below threshold and turning over quickly above it. The more or less correct behaviour close to zero was achieved at the cost of bunching $\mathrm{Im}\,\alpha(t)$ into a large spike at about $s=45m_\pi^2$ (energy $\sim$ 950 MeV), so that the recurrence at $\mathrm{Re}\,\alpha=3$ was very

light. We are now faced with the question of what modification our model needs to reproduce experiment more closely.

The defect of all models based on elastic unitarity is that Levinson's Theorem[124] constrains the calculated trajectories to turn over. However it is easy to imagine that as we increase the energy the trajectory could become strongly coupled to the new channels that open up, and so continue to rise.[125] Models have been proposed on this basis[126], and we note the similarity to the P-repulsion model. If linear behaviour were to persist indefinitely so that $\alpha(s) \sim s$ as $s \to \infty$, then the amplitude $A \propto t^{\alpha(s)}$ would not be uniformly power bounded and the Mandelstam representation for A would not hold, unless the residues $\gamma(s)$ were exponentially damped[127]. (A behaviour $\gamma(s) \to \text{const.}\alpha(s)^{-\alpha(s)}$ has been suggested;[128] preliminary comparisons with experiment[129] are favourable). Neither indefinitely rising trajectories nor exponentially damped residues are likely to be produced in our model with a finite number of channels, but one might hope that by including several low-mass ones reasonable agreement might result in a corresponding energy region close to s=0, where interest lies.

In the next Section we shall show[130] that such a hope is untenable if the currently accepted linear extension of the rho and A_2 trajectories are correct.

2. Dynamical consequences of a linear trajectory.

From eq.(1.64) a Regge pole $\alpha(s)$ gives to the ℓ^{th} s-channel partial wave a contribution of the form $R(s)(\ell - \alpha(s))^{-1}$, and if $\mathrm{Im}\alpha'(s) \ll \mathrm{Re}\,\alpha'(s)$ we derive eq.(1.65), which, by comparison with the Breit-Wigner form $(m^2-s-im\Gamma)^{-1}$, gives for the full width at half-height of the resonance at $s=m^2$ the expression

$$\Gamma \simeq \mathrm{Im}\,\alpha(m^2) \Big/ m.\ \mathrm{Re}\,\alpha'(m^2). \tag{5.1}$$

We consider the ρ and A_2 trajectories, upon which are supposed to be the ρ, R, and T, and the A_2, S, and U mesons respectively: see Fig.5.1. From eq.(5.1), using the widths given by Rosenfeld et al.,[66] we derive the values of $\mathrm{Im}\,\alpha$ given in Fig.5.2. The important point to note is that the high mass states are very narrow, so that $\mathrm{Im}\,\alpha(s)$ must be small at high energy. This would not be so if the trajectories were strongly coupled to higher threshold channels.

We assume that $\alpha(s)$ obeys a dispersion relation of the form (1.84),

$$\mathrm{Re}\,\alpha(s) = a + \frac{1}{\pi} P\int_{s_0}^{\infty} \frac{\mathrm{Im}\,\alpha(s')\,ds'}{s'-s}, \tag{5.2}$$

where s_0=threshold $(=(2m_\pi)^2$ for α_ρ, and $=(3m_\pi)^2$ for $\alpha_{A_2})$. A reasonable fit to $\mathrm{Im}\,\alpha(s)$ is obtained using the parameterisation of Ahmadzadeh and Sakmar[112] (c.f.eq.(4.25),

$$\mathrm{Im}\ \alpha(s) = \frac{C x^{\lambda}}{(x-d)^2 + e^2}\ , \qquad (5.3)$$

where $x = s - s_0$, and $\lambda = 0.0001$, $d = 2.0\ (\mathrm{GeV})^2$, $e = 1.0\ (\mathrm{GeV})^2$, and $C = 0.31$ for the rho trajectory and 0.145 for the A_2. The slope of Re $\alpha(s)$ is not very sensitive to the choice of λ. The trajectories found from eq.(5.2) using (5.3) are shown in Fig.5.2, and we see that the contribution of the integral is negligible. So although with a suitable choice of a we can make either trajectory pass through any given point, there is no hope of obtaining the correct slope if eq.(5.1) holds good.

If we do not neglect Im $\alpha'(s)$ in comparison with Re $\alpha'(s)$, the Regge pole gives a partial wave amplitude proportional to[142]

$$\left\{ m^2 - s + \frac{\alpha_I(m^2)\,\alpha_I'(m^2)}{|\alpha'(m^2)|^2} - \frac{i\,\alpha_I(m^2)\,\alpha_R'(m^2)}{|\alpha'(m^2)|^2} \right\}^{-1}, \qquad (5.4)$$

where $\alpha_I = \mathrm{Im}\,\alpha$, $\alpha_R = \mathrm{Re}\,\alpha$. If Im $\alpha' \approx$ Re α', it is clear from (5.4) that a larger Im α would be possible for a fixed width Γ. The third term, proportional to Im $\alpha'(m^2)$, is part of the so-called "resonance shift"[131]. For the $N^*(1238)$, for example, it is well-understood[131], and is equal to about 13 MeV, (x 1238 MeV). The width of this resonance is about ten times as big[66]

indicating $\alpha'_I / \alpha'_R \leq 0.1$ at $s = M_{N^*}^2$. The resonance shift for mesons is less well-understood, but one might expect a similar order of magnitude(131). In any case, it is difficult to ~~conceive of both Im α and Im α' being large together but not separately if eq.(5.2) is to be satisfied.~~ make Im α large at low s unless Im α' is also large. (To check this point we attempted to fit - by a least squares method - the linear rho trajectory of Fig.5.1, and the widths of the recurrences (Fig.5.2), using (5.2) and (5.4) to calculate Re $\alpha(s)$ and Γ for various parameterisations of Im $\alpha(s)$. We were not able to find any satisfactory solutions; always Im $\alpha'(s) \ll$ Re $\alpha'(s)$, and to achieve Re $\alpha(s) \sim s$ it was necessary to have Im $\alpha(s) \sim s$ over the same region).

Another possible flaw in our argument lies in the assumption that (5.2) holds. It is possible for trajectory functions to develop left-hand cuts if two of them cross(5), but it is doubtful if these can play an important role in the dynamics since the sum of the two discontinuities have to vanish. There is no evidence for crossing trajectories, except that the very poor polarisation data in the process $\bar{\pi} p \to \bar{\pi}^0 n$ is consistent with no decrease with energy, and the trajectory-crossing model is the only simple one that does not predict a power decrease(5). However the data has very big errors.

We now consider the implications of our result and the possibilities of solving the difficulties

it raises. First of all we note that it does not help to change the form of Im $\alpha(s)$ so that it tails off slowly, i.e., like $s^{-\varepsilon}$ where ε is small and positive. This would allow us to make the contribution of the integral of (5.2) as large as we like, but the contribution to $d\alpha/ds$ for small s would still be negligible.

We appear to be faced with three alternatives:

(a) Eq.(5.2) for $\alpha(s)$ requires an additional subtraction,

$$\mathrm{Re}\,\alpha(s) = a + bs + \frac{1}{\pi} P \int_{s_0}^{\infty} \frac{\mathrm{Im}\,\alpha(s')ds'}{s' - s} \quad , \tag{5.5}$$

where the arbitrary constant b is responsible for the slope of the trajectories in the low energy region. This is a very unpalatable suggestion in the present context, for it means that, unlike potential scattering, the "forces", (double spectral functions) do not determine the important parameters of the trajectories and hence are not responsible for the existence of particles. In fact this would kill the whole bootstrap philosophy, ~~for it essentially implies that MASK does not hold as we have stated it - it would be necessary to introduce elementary particles to continue correctly in angular momentum.~~

(b) The curve for Im $\alpha(s)$ rises again at higher energies. This would seem to imply that there was

some other mass "scale" in the problem. This would be the case if, for example, the mesons were made up of very heavy particles, e.g., "quarks"[132] - although SU(3) properties are irrelevant. It is then found that if we assume that the trajectories are (at least to a good approximation) bound states of these quarks (i.e., of a $q\bar{q}$ pair), <u>then the straightness of the trajectories is inevitable, and independent of any further assumptions about the $q\bar{q}$ potential</u>.

To see this we re-write eq.(5.2)

$$Re\ \alpha(s) = \alpha(\infty) + \frac{1}{\pi} P \int_{s_T}^{\infty} \frac{Im\,\alpha(s')\,ds'}{s' - s} \tag{5.6}$$

where now the integral begins at s_T, the $q\bar{q}$ threshold, and we assume that it converges. Since s_T is very large[133], and Im $\alpha(s)$ has to be positive, we can approximate it by a delta function at $s=s_p > s_T$ if we are concerned only with $s \ll s_T$.

Thus

$$\alpha(s) = \alpha(\infty) + \frac{g}{s_p - s} \quad , \tag{5.7}$$

($s \ll s_p$, $s_p > s_T$), which can be written

$$\alpha(s) = \alpha(\infty) + \frac{g}{s_p} + \frac{gs}{s_p^2} + \frac{gs^2}{s_p^3} + \cdots \quad . \tag{5.8}$$

Since the trajectory passes through (say) the rho, we must have

$$1 = \alpha(\infty) + \frac{g}{s_p - m_\rho^2} , \tag{5.9}$$

so that

$$\alpha(\infty) \approx 1 - \frac{g}{s_\rho} . \tag{5.10}$$

The slope of the trajectory at s=0 is g/s_p^2, which according to Fig.5.1 is about 1 GeV^{-2}, so that (5.10) gives

$$\alpha(\infty) \approx 1 - s_\rho / (1\,GeV)^2 . \tag{5.11}$$

Hence the trajectory must pass through many ($\sim s_p/(1GeV)^2$) negative integers, which requires that the $q\bar{q}$ potential be such that a large number of superconvergence relations[134] (SCR) are satisfied. There is no obvious objection to this, as similar SCR must also obtain when the external particles involved have spin[135] but it means that the $q\bar{q}$ potential must be quite unlike the simple forms which have sometimes been used in the literature[136], and which force $\alpha(\infty)=-1$. We note that the quadratic and higher term in eq.(5.8) are negligible in the physically interesting region.

(c) The interpretation of the heavy mesons as recurrences of the ρ and A_2 is wrong. In this

connection it is worth noting that the missing mass experiment[123] was biassed against the detection of broad states, which may have been present as recurrences of those trajectories, but which escaped undetected. There is however, some recent evidence[137] that the R (sometimes called the g meson) does in fact have $J^P=3^-$ and isospin I=1, as required if it is to be on the rho trajectory.

3. Conclusion.

Unfortunately there are at present no other meson trajectories where recurrences can be identified or reasonably speculated[66]. For baryons there is the complication that the trajectory function has a left-hand cut, and the possible N^* recurrences[33] show widths if anything increasing with energy[65,66]. However it is interesting to note that two heavy and very narrow (masses 3690 and 3245 MeV, widths 50 and 35 MeV) N^* bumps have been reported[138,139]. These are well above the limits of presently feasible phase shift analyses, and so there is no evidence of their spins, but they are possibly high, and thus could mean that Imα for their trajectories is small at high energy. It would be very interesting to know if small widths are a general feature of heavy, high-spin

resonances lying on steep linear Regge trajectories. If they are, it is difficult to see how the bootstrap model could succeed.

Fig.(5.1). The boson resonances interpreted as lying on linear Regge trajectories. The straight lines are

$$\alpha_\rho(s) = 0.43 + 0.948s$$

$$\alpha_{A_2}(s) = 0.26 + 1.011s$$

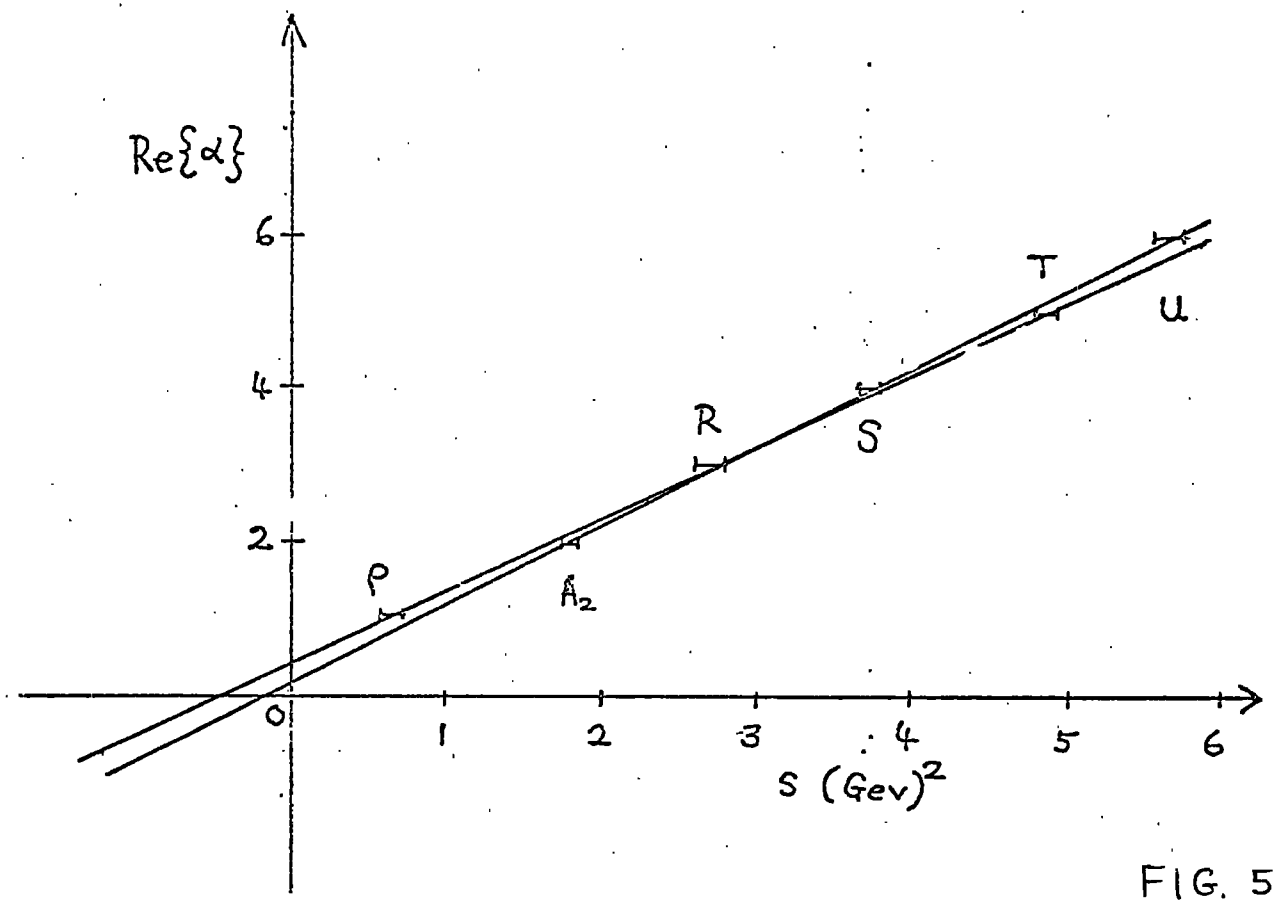

FIG. 5.1

Fig.(5.2). The value of Im $\alpha(s)$ obtained from eq.(5.1), and fitted by eq.(5.3) for the ρ and A_2 trajectories. The real parts of $\alpha(s)$ are obtained from eq.(5.2) with a taken arbitrarily to be zero.

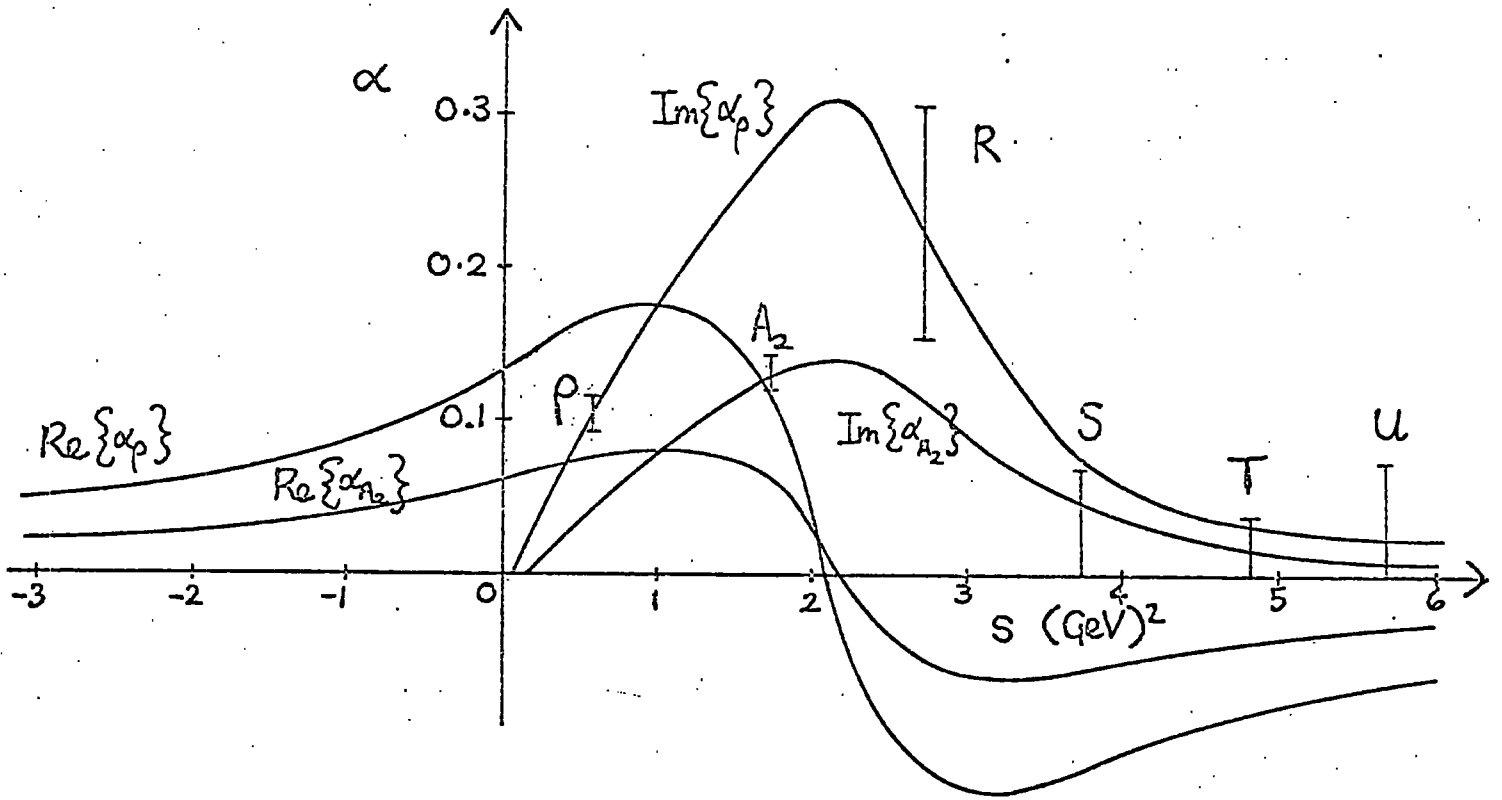

FIG. 5.2

A P P E N D I X

Amplitudes of Definite Signature

a. General.

We wish to construct pion-pion amplitudes of definite s-channel signature. We have eq.(1.42),

$$A(s,t,u) = A_R(s,t,u) + A_L(s,t,u), \tag{A.1}$$

and eq.(1.43),

$$A^{\pm}(s,t) = A_R(s,t,u) \pm A_L(s,u,t). \tag{A.2}$$

We have used the fact that for elastic scattering the interchange $z_s \leftrightarrow -z_s$ is equivalent to the interchange $t \leftrightarrow u$. Writing a fixed -s dispersion relation for $A(s,t,u)$ (neglecting poles) we have eq.(1.17),

$$A(s,t,u) = \frac{1}{\pi}\int \frac{dt'}{t'-t} D_t(s,t',u) + \frac{1}{\pi}\int \frac{du'}{u'-u} D_u(s,t,u'). \tag{A.3}$$

Note that we are giving the following significance to the order of arguments. The symbols (x,y,s) denote ((c.m.energy)^2,-(c.m.momentum transfer)^2,-(c.m.crossed momentum transfer)^2). The two term on the R.H.S. of (A.3) are A_R and A_L of (A.1) respectively. Using (A.2),

$$\begin{aligned} A^{\pm}(s,t) &= \frac{1}{\pi}\int \frac{dt'}{t'-t} D_t(s,t',u) \pm \frac{1}{\pi}\int \frac{du'}{u'-t} D_u(s,u,u') \\ &= \frac{1}{\pi}\int \frac{dt'}{t'-t}\left[D_t(s,t',u) \pm D_u(s,u,t')\right], \end{aligned} \tag{A.4}$$

the second equality following from a simple re-labelling of dummy variables. Note that for clarity we are giving some independent significance to the third argument of the discontinuity functions, although, of course, there is always the constraint $s+t+u = \sum m^2$.

From eqs.(1.26) and (1.27) we have, referring to Fig.1.2,

$$D_t(s,t,u) = \frac{1}{\pi}\int \frac{ds''}{s''-s}\,\rho_{st}(s'',t,u) + \frac{1}{\pi}\int \frac{du''}{u''-u}\,\rho_{tu}(s,t,u''), \qquad (A.5)$$

and

$$D_u(s,t,u) = \frac{1}{\pi}\int \frac{ds''}{s''-s}\,\rho_{su}(s'',t,u) + \frac{1}{\pi}\int \frac{dt''}{t''-t}\,\rho_{tu}(s,t'',u). \qquad (A.6)$$

Therefore

$$D_u(s,u,t) = \frac{1}{\pi}\int \frac{ds''}{s''-s}\,\rho_{su}(s'',u,t) + \frac{1}{\pi}\int \frac{dt''}{t''-u}\,\rho_{tu}(s,t'',t)$$

$$= \frac{1}{\pi}\int \frac{ds''}{s''-s}\,\rho_{su}(s'',u,t) + \frac{1}{\pi}\int \frac{du''}{u''-u}\,\rho_{tu}(s,u'',t), \qquad (A.7)$$

upon re-labelling the dummy variable. Substituting (A.5) and (A.7) into (A.4) we have

$$A^{\pm}(s,t) = \frac{1}{\pi^2}\int \frac{dt'}{t'-t}\left\{\int \frac{ds''}{s''-s}\left[\rho_{st}(s'',t',u) \pm \rho_{su}(s'',u,t')\right]\right.$$

$$\left. + \int \frac{du''}{u''-u'}\left[\rho_{tu}(s,t',u'') \pm \rho_{tu}(s,u'',t')\right]\right\}, \qquad (A.8)$$

which is just eq.(1.45).

b. Pion-pion scattering.

For pion-pion amplitudes we refer to Fig.4.1, and write

$$A(s,t,u) = R_1^s(s,t,u) + (-1)^I R_2^s(s,u,t)$$
$$+ \beta^{II'}\left[R_1^t(t,s,u) + (-1)^{I'} R_2^t(t,u,s)\right]$$
$$+ (-1)^I \beta^{II'}(-1)^{I'}\left[R_1^u(u,t,s) + (-1)^{I'} R_2^u(u,s,t)\right], \qquad (A.9)$$

where I', the crossed channel isospin is summed from 0 to 2. Here each term R is to be understood to contain not just the appropriate Chew-Jones strip, but also the associated corner piece of double spectral function. For example, R_1^s has ρ_{st}, R_2^s has ρ_{su}, R_2^t has ρ_{tu} etc., where now these symbols have a different meaning from that in eq. (A.8), as is evident from Figs.4.1 and 1.2.

Eq. (A.9) makes transparent the correct way to replace the double spectral functions of eq.(A.8) with the pion-pion double spectral functions. We have

$$\rho_{st}(s,t,u) \longrightarrow \rho_{st}^I(s,t,u) + \beta^{II'}\rho_{ts}^{I'}(t,s,u),$$
$$\rho_{su}(s,t,u) \longrightarrow (-1)^I \rho_{su}^I(s,u,t) + (-1)^I \beta^{II'}\rho_{us}^{I'}(u,s,t),$$
$$\rho_{tu}(s,t,u) \longrightarrow \beta^{II'}(-1)^{I'}\rho_{tu}^{I'}(t,u,s) + (-1)^I \beta^{II'}(-1)^{I'}\rho_{ut}^{I'}(u,t,s). \qquad (A.10)$$

Substituting (A.10) into (A.8), and putting $(-1)^I$ for the $(\pm)$ signs in that equation, gives

$$A^{\pm}(s,t) = \frac{1}{\pi^2}\int \frac{dt'}{t'-t}\left\{\int \frac{ds''}{s''-s}\left[\rho^{I}_{st}(s'',t',\not{u}) + \beta^{II'}\rho^{I'}_{ts}(t',s'',\not{u})\right.\right.$$

$$\left. + \rho^{I}_{su}(s'',t',\not{u}) + \beta^{II'}\rho^{I'}_{us}(t',s'',\not{u})\right] + \int \frac{du''}{u''-u'}\left[\beta^{II'}(-1)^{I'}\rho^{I'}_{tu}(t',u'',\not{s})\right.$$

$$+ (-1)^{I}\beta^{II'}(-1)^{I'}\rho^{I'}_{ut}(u'',t',\not{s}) + (-1)^{I}\beta^{II'}(-1)^{I'}\rho^{I'}_{tu}(u'',t',\not{s})$$

$$\left.\left. + \beta^{II'}(-1)^{I'}\rho^{I'}_{ut}(t',u'',\not{s})\right]\right\}, \qquad \text{(A.11)}$$

from which the final result is

$$A^{I}(s,t) \equiv \frac{1}{2}A^{\pm}(s,t) = \frac{1}{\pi}\int \frac{D^{I}_{t}(s,t',\not{u})}{t'-t}\,dt', \qquad \text{(A.12)}$$

where

$$D^{I}_{t}(s,t,\not{u}) = \frac{1}{\pi}\int \frac{ds'}{s'-s}\left[\rho^{I}_{st}(s',t,\not{u}) + \beta^{II'}\rho^{I'}_{ts}(t,s',\not{u})\right]$$

$$+ \frac{\beta^{II'}}{\pi}(-1)^{I'}\int \frac{du'}{u'-u}\left[\rho^{I'}_{tu}(t,u',\not{s}) + (-1)^{I}\rho^{I'}_{ut}(u',t,\not{s})\right]. \qquad \text{(A.13)}$$

These two equations are just eqs.(4.3) -(4.6)

c. The Chew-Jones Approximation.

In the Chew-Jones approximation, we have from eq.(A.9),

$$A^I(s,t,u) = R^I(s,t,u) + \beta^{II'} R^{I'}(t,s,u)$$

$$+\beta^{II'}(-1)^{I'}\left[R^{I'}(t,u,s) + (-1)^I R^{I'}(u,t,s)\right], \qquad (A.14)$$

where R^I now stands for any strip on Fig.4.1; the order of arguments differentiates them. Eq.(2.13) gives

$$R^I(x,y,z) = \frac{\Gamma^I(x)}{2}\left\{\frac{P_{\alpha(x)}\left(1+\frac{2y}{x-4m_\pi^2}\right)}{\sin\pi\alpha(x)} + \frac{1}{\pi}\int_{4m_\pi^2-x}^{s_1}\frac{dy'}{y'-y}\,P_{\alpha(x)}\left(-1-\frac{2y'}{x-4m_\pi^2}\right)dy'\right\}, \qquad (A.15)$$

$$x+y+z = 4m_\pi^2.$$

The starting discontinuity for the Mandelstam iteration is that piece of $D_t^I(s,t,u)$ which is non-zero for $4m^2 \leq s,t \leq s_1$. By inspection of (A.14) and (A.15) this is $\beta^{II'}\left[R^{I'}(t,s,u)+(-1)^{I'}R^{I'}(t,u,s)\right]$, or eq.(2.13).

d. The potential function.

In eq.(A.14), only $R^I(s,t,u)$ is cut in s between $s_0=4m_\pi^2$ and s_1. Therefore the rest of the amplitude contributes unsubtracted to $B_\ell^I(s)$, giving a contribution, (using eq.(1.79)),

$$B_\ell^L(s)_{\text{CROSSED}} = (32\pi^2 q_s^{2l+2})^{-1} \int_{-\infty}^{0} \text{Im}\left\{ Q_\ell(z_s(s,t)) \right\} \times$$

$$\times \beta^{II'} \left\{ R^{I'}(t,s,u) + (-1)^{I'} R^{I'}(t,u,s) \right.$$

$$\left. + (-1)^{I+I'} R^{I'}(u,t,s) \right\} dt. \qquad \text{(A.16)}$$

The contribution of $R^I(s,t,u)$ is calculated by projecting out its contribution to $B_\ell(s)$, identifying the left-hand cut discontinuity of this function, and dispersing over it, neglecting the right-hand cut altogether. The Froissart-Gribov projection, eq.(1.49), gives

$$B_\ell(s)_{\text{DIRECT}} = (32\pi^2 q_s^{2l+2})^{-1} \int_{4m_\pi^2}^{\infty} Q_\ell(z_s(s,t))\, \Delta_t \left\{ R^I(s,t,u) \right\} dt \,, \qquad \text{(A.17)}$$

whose left-hand cut runs from $s=-\infty$ to $s=4m^2-s_1$, and is due to the cut in $Q_\ell(z_s)$.

Here

$$\text{Im}\, Q_\ell(z) = \frac{\pi}{2} P_\ell(z) \,, \qquad \text{(A.18)}$$

(c.f. (1.48)), so that

$$B_\ell^L(s)_{DIRECT} = (64\pi^2 q_s^{2\ell+2})^{-1} \int_{-\infty}^{4m_\pi^2 - s_1} \frac{ds'}{s'-s} \quad \times$$

$$\times \int_{s_1}^{\max t(s')} P_\ell(z_{s'}) \; \Delta_t \left\{ R^I(s',t,u) \right\} \, dt \, , \qquad \text{(A.19)}$$

where the t-integral starts at s_1 where the t-cut of R^I begins, and finishes at the highest value allowed by the value of s' in the outer integral. Using (A.15) for the various terms R in (A.17) and (A.19), with some effort one derives the explicit expression for $B_\ell^L(s)$ that is eq.(10) of ref.80, which reduces, as explained, to eq.(4.9), when numerically small terms are neglected.

REFERENCES and NOTES

References and Notes

(1) G. F. Chew, "The Analytic S-Matrix", W. A. Benjamin Inc., N.Y. (1966).

(2) G. F. Chew and S. C. Frautschi, Phys. Rev. Letters 7, 394 (1961).

(3) T. Regge, Nuovo Cimento 14, 951 (1959); ibid. 18 947 (1960).

(4) R. J. Eden, P. V. Landshoff, D. I. Olive and J. C. Polkinghorne, "The Analytic S-Matrix", C.U.P.(1966)

(5) P. D. B. Collins and E. J. Squires, Springer Tracts in Modern Physics, Vol.45, Springer-Verlag, Heidelberg (1968).

(6) G. F. Chew and S. Mandelstam, Phys. Rev. 119, 467 (1960).

(7) H. Yukawa, Proc. Math. Soc. Japan, 17, 48 (1935).

(8) See, e.g., G. Kallen, "Elementary Particle Physics", Addison-Wesley, London (1964).

(9) P. A. M. Dirac, "Principles of Quantum Mechanics", 4th Edition, O.U.P. (1958).

(10) The (inessential) complications arising from superselection rules are discussed by H. P. Stapp, U.C.R.L. 10843, (1963).

(11) W. Heisenberg, Z.Phys., 120, 513, 673 (1943).

(12) A. O. Barut, "The Theory of the Scattering Matrix", MacMillan, N.Y., (1967); J. R. Taylor, J.Math.Phys., 7, 181, (1966).

(13) E. Leader, Phys. Rev. 166, 1599 (1968).

(14) The usual units, defined by $\hbar=c=1$, are used unless otherwise specified. A four-vector we write as $(p_0, \underline{p})$, with a metric of signature $(1,-\underline{1})$, so that the mass-shell constraint is $m^2 = p_0^2 - |\underline{p}|^2$.

(15) Eden et al., ref. 4, p.187.

(16) Dirac, ref. 9, p.15.

(17) H. P. Stapp, Phys. Rev. 139, B257 (1965).

(18) J. Gunson, J. Math. Phys., 6, 827, 845, 852 (1965); D. I. Olive, Phys. Rev. 135, B745 (1964).

(19) D. I. Olive, Nuovo Cimento 37, 1422 (1965).

(20) J. Bros, H. Epstein and V. Glaser, Comm.Math.Phys.1, 240 (1965).

(21) Eden et al., ref. 4, p.243.

(22) S. Mandelstam, Phys.Rev. 112, 1344 (1958).

(23) L. D. Landau, Nucl.Phys. 13, 181 (1959).

(24) R. E. Cutkosky, J.Math.Phys. 1, 429 (1960), Rev.Mod.Phys. 33, 446 (1961).

(25) Given in detail by Collins and Squires, ref.5, Section I.9.

(26) R. Oehme, Phys.Rev. 121, 1840 (1961); R. Blankenbeckler, M. L. Goldberger, S. W. MacDowell and S. B. Trieman, Phys.Rev.123, 692 (1961).

(27) M. Gell-Mann, M. L. Goldberger and W. Thirring, Phys.Rev. 95, 1612 (1954).

(28) A more detailed derivation of equations (1.20) and (1.21) is given by Eden et al., ref.4, Sections 1.3 and 4.6.

(29) S. J. Lindenbaum, Brookhaven preprint of Irvine Conference Report (1967).

(30) S. J. Lindenbaum, Oxford Conference Report (1965).

(31) J. Hamilton, Edinburgh Summer School (1963).

(32) S. Mandelstam, Phys.Rev. 115, 1741, 1752 (1959).

(33) R. Blankenbeckler, M. L. Goldberger, N. N. Khuri and S. B. Trieman, Ann.Phys.(N.Y.) 10, 62 (1960).

(34) This has not stopped its being extended to general processes, see H. P. Stapp and J. L. Wright, UCRL - 17861 (1967).

(35) M. Froissart, Phys.Rev. 123, 1053 (1961).

(36) A. Martin, Phys.Rev. Letters 9, 410 (1962).

(37) Unless otherwise specified, all our statements about special functions are taken from A. Erdelyi (ed.): "The Bateman Manuscript Project, higher transcendental functions", McGraw-Hill,(N.Y.), 1953.

(38) M. Froissart, Talk at La Jolla Conference, 1961 (unpublished); V. N. Gribov, JETP 41, 677 (1961).

(39) E. C. Titchmarsh, "The Theory of Functions", 2nd ed., O.U.P. (1939), p.186.

(40) A. Sommerfeld, "Partial Differential Equations in Physics", Academic Press (N.Y.) (1949); G. N. Watson, Proc.Roy.Soc.,95 83 (1918).

(41) E. J. Squires, "Complex Angular Momentum and Particle Physics", Benjamin (N.Y.) (1963)

(42) R. G. Newton, "The Complex J-plane", Benjamin (N.Y.), (1964).

(43) G. F. Chew, S. C. Frautschi and S. Mandelstam, Phys.Rev. 126, 1202 (1962).

(44) A. O. Barut and D. Zwanziger, Phys.Rev. 127, 974 (1962); J. R. Taylor, Phys.Rev. 127, 2257 (1962).

(45) J. L. Uretsky, Phys.Rev. 123, 1459 (1961).

(46) G. Frye and R. L. Warnock, Phys.Rev.130, 478 (1963).

(47) S. Mandelstam, Ann.Phys.(N.Y.) 21, 302 (1963).

(48) L. Castillejo, R. H. Dalitz and F. J. Dyson, Phys.Rev. 101, 453 (1956).

(49) S. C. Frautschi, "Regge poles and S-Matrix Theory", Benjamin (N.Y.) (1963).

(50) D. Atkinson, K. Dietz and D. Morgan, Ann.Phys. (N.Y.) 37, 77 (1966)
E. J. Squires, Nuovo Cim. 34, 1751 (1964).

(51) J. B. Hartle and C. E. Jones, Phys.Rev.Letters 14, 801 (1965); Phys.Rev.140, B90 (1965).

(52) L. Van Hove, Edinburgh Summer School (1966).

(53) Of course, this simple argument must be modified to account for the very fast fall of differential cross-sections at wide angles.

(54) V. Barger and D. Cline, Phys.Rev. 155, 1792 (1967); V. Barger and M. Olsson, Phys.Rev.151, 1123 (1966).

(55) S. D. Drell and A. Hearn, preprint SLAC-PUB-176.

(56) Reviewed by Collins and Squires, ref.5.

(57) V. Barger and L. Durand, Phys.Letters 26B, 588 (1968). L. Durand, Phys.Rev. 166, 1680 (1968).

(58) R. Dolen, D. Horn and C. Schmid, Phys.Rev.166, 1768 (1968).

(59) A. Logunov, L. D. Soloviev and A. N. Tavkhelidze, Phys.Letters 18, 652 (1967).

(60) This is taken verbatim from ref.(58), with appropriate changes in notation.

(61) C. Schmid, Phys.Rev.Letters 20, 689 (1968).

(62) P. D. B. Collins, R. C. Johnson and E. J. Squires, Phys.Letters 27B, 23 (1968)

(63) see A. Donnachie, Edinburgh Summer School (1966) for greater detail.

(64) F.Arbab and C. B. Chiu, Phys.Rev.147, 1645 (1966); G. Höhler, J. Baacke and G. Eisenbeiss, Phys.Letters 22, 203 (1966).

(65) C. Lovelace, Heidelburg Conference Report (1967).

(66) A. H. Rosenfeld et al., Rev.Mod.Phys.40, 77 (1968).

(67) L. Bertocchi, Heidelburg Conference Report (1967).

(68) V. A. Alessandrini and E. J. Squires, preprint ICTP/68/37(1968).

(69) P. D. B. Collins, R. C. Johnson and G. G. Ross, in preparation.

(70) C. H. Johnson and H. Steiner, UCRL 18001 (1967).

(71) W. Rarita, R. J. Riddell, C. H. Chiu and R. J. N. Phillips, Phys.Rev.165, 1615 (1968).

(72) V. Barger and D. Cline, Phys.Rev.Letters 19, 1504 (1967).

(73) V. Barger and D. Cline, Phys.Rev.Letters 20, 298 (1968).

(74) R. H. Dalitz, Oxford preprint of Irvine Conference talk, (1967).

(75) G. F. Chew and C. E. Jones, Phys.Rev.135, B.208 (1964).

(76) C. E. Jones and G. Tiktopoulos, J.Math.Phys. 7, 311 (1966).

(77) C. E. Jones, Nuovo Cim. 40, 761 (1965).

(78) D. Y. Wong, private communication to G. F. Chew, see ref.(75).

(79) C. E. Jones, Phys Rev. 135, B.214 (1964).

(80) P. D. B. Collins and V. L. Teplitz, Phys.Rev. 140, B.663 (1965).

(81) P. D. B. Collins, Phys.Rev. 142, 1163 (1965).

(82) G. F. Chew and V. L. Teplitz, Phys.Rev. 137, B139 (1965).

(83) G. F. Chew, Phys.Rev. 140, B1427 (1965).

(84) C. E. Jones, UCRL 10700 (1962); N. N. Khuri, Phys.Rev. 130, 429 (1963).

(85) R. G. Newton, "The Scattering of Waves and Particles", McGraw-Hill (N.Y.) (1966) § 17.3.1.

(86) A. Herglotz, Ber.Verh.Sächs.Akad.Wiss.Leipzig, Math.Natur. Kl., 63, 1 (1911).

(87) P. D. B. Collins, Phys.Rev. 157, 1432 (1967).

(88) J. Orear, Phys.Rev.Letters 12, 113 (1964); Phys.Letters 13, 190 (1964).

(89) N. F. Bali and S.-Y. Chiu, Phys.Rev. 153, 1579 (1967).

(90) P. D. B. Collins and R. C. Johnson, Phys.Rev. 169, 1222 (1968).

(91) B. Kayser, Berkeley preprint (1965), unpublished.

(92) G. Auberson and G. Wanders, NuovoCim. 46, 78 (1966).

(93) R. F. Sawyer, Phys.Rev. 142, 991 (1966).

(94) B. Kayser, Phys.Rev. 165, 1760 (1968).

(95) H. Bannerjee, Nuovo Cim. 50, 993 (1967).

(96) R. F. Dashen and S. C. Frautschi, Phys.Rev. 135, B1190 (1964); ibid. 137, 1318 (1965); R. F. Dashen, Phys.Rev. 135, B1196 (1964).

(97) M. Luming, Phys.Rev. 136, B1120 (1964).

(98) D. C. Teplitz and V. L. Teplitz, Phys.Rev. 136, B.142 (1965).

(99) N. F. Bali, Phys.Rev. 150, 1358 (1966).

(100) B. H. Bransden, P. G. Burke, J. W. Moffat, R. G. Moorhouse, and D. Morgan, Nuovo Cim. 30 297 (1963).

(101) P. G. Burke, CERN Conference report (1962), describes the numerical iteration of a single delta function.

(102) P. D. B. Collins, Phys.Rev. 139, B696 (1965).

(103) P. G. Burke and C. Tate, UCRL 10384 (1963).

(104) J. K. Finkelstein, Phys.Rev. 145, 1185 (1966).

(105) H. A. Bethe and R. Bacher, Rev.Mod.Phys. 8, 111 (1936).

(106) C. Eckhart, Phys.Rev. 35, 1303 (1930); V. Bargman, Rev.Mod.Phys. 21, 488 (1949).

(107) P. J. S. Watson, Ph.D. thesis, University of Durham, (1964) unpublished.

(108) D. Amati, S. Fubini and A. Stanghellini, Phys.Letters 1, 29 (1962).

(109) N. F. Bali, G. F. Chew, and S.-Y. Chiu, Phys.Rev. 150, 1352 (1966).

(110) P. D. B. Collins, Phys.Rev. 139, B696 (1965).

(111) P. D. B. Collins and R. C. Johnson, Durham preprint, to be published (1968).

(112) A. Ahmadzadeh and I. A. Sakmar, Phys.Letters 5, 145 (1963).

(113) G. F. Chew and V. L. Teplitz, Phys.Rev. 136, B1154 (1964).

(114) M. Roos and J. Pisut, CERN preprint Th885, unpublished (1968)

(115) F. Zachariasen, Phys.Rev.Letters 7, 112, 268(E) (1961)
L. A. P. Balazs, Phys.Rev. 128, 1939 (1962); ibid.129, 872 (1962)
F. Zachariasen and C. Zemach, Phys.Rev. 128, 849 (1962)
J. Fulco, G. L. Shaw and D. Wong, Phys.Rev. 137, B1242 (1965).

(116) S. Mandelstam, Nuovo Cim. 30, 1148 (1963).

(117) See ref. 5, and also E. J. Squires, Phys.Letters 26B, 461, 623(E), (1968).

(118) N. Cabibbo, J. J. J. Kokkedee, L. Horwitz and Y. Ne'eman, Nuovo Cim. 45, 275 (1966);
N. Cabibbo, L. Horwitz and Y. Ne'eman, Phys.Letters 22, 336 (1966);
Y. Srivastava, Phys.Rev.Letters 19, 47 (1967).

(119) K. Igi, Phys.Rev.Letters 9, 76 (1962).

(120) R. C. Johnson, Nucl.Phys. B5, 673 (1968); G. Hohler, to be published (1968);
M. G. Olsson, preprint, to be published (1968).

(121) E. J. Squires, Trieste preprint, subm. to Nuovo Cim. (1968).

(122) D. Cline, Nuovo Cim. 45, 750 (1966).

(123) M. N. Focacci et al.,Phys.Rev.Letters 17, 890 (1966).

(124) N. Levinson, Kgl.Danske Vid.Selsk.,Mat.-Fys.Medd 25, No. 9 (1949).

(125) S. Mandelstam, Tokyo Summer Lectures (1966); see also ref.5, p.264.

(126) R. V. Brower and J. Harte, UCRL 17613 (1967); S.-Y.Chiu and C. Tan, UCRL 17511 (1967).

(127) N. N. Khuri, Phys.Rev.Letters 18, 1094 (1967).

(128) C. E. Jones and V. L. Teplitz, Phys.Rev.Letters 19, 135 (1967).

(129) H. Goldberg, Phys.Rev.Letters 19, 1391 (1967).

(130) P. D. B. Collins, R. C. Johnson and E. J. Squires, Phys.Letters 26B, 223 (1968).

(131) J. D. Jackson, Nuovo Cim. 34, 1644 (1964).

(132) M. Gell-Mann, Phys.Letters 8,214, (1964); G.Zweig, CERN preprint, unpublished (1964).

(133) E. J. Squires, Edinburgh Summer School (1966).

(134) V. de Alfaro, S. Fubini, G. Furlan and C. Rossetti, Phys.Letters 21, 576 (1966).

(135) F. Calogero, J. M. Charap and E. J. Squires, Ann.Phys. (N.Y.) 25, 325 (1963).

(136) R. H. Dalitz, Les Houches Lectures (1965).

(137) T. F. Johnston et al., Phys.Rev.Letters 20, 1414 (1968).

(138) A. Kormanyos, A. D. Krisch and D. O'Fallon, Michigan preprint (1967).

(139) H. Baitke et al., Phys.Letters 24B, 118 (1967).